UNIVERSITÀ
DEGLI STUDI
DI PADOVA

University of Padova

PhD in Industrial Engineering

FABRICATION, CHARACTERIZATION, AND PERFORMANCE EVALUATION OF POROUS GEOPOLYMER COMPONENTS FOR SUSTAINABLE ENVIRONMENTAL APPLICATIONS

PhD Thesis

Author

Mattia Muracchioli

Supervisor

Prof. Paolo Colombo

Co-Supervisor

Prof. Giorgia Franchin

Padova, September 2023

Cycle XXXVI

To my dearest girlfriend **Francesca**,

From the very beginning, you have believed in me and encouraged me to pursue my dreams. Your love, patience, and understanding have been instrumental in my success. Your unwavering support and constant presence by my side have lifted me up during moments of self-doubt and provided me with the motivation to keep pushing forward. Your brilliance, intellect, and passion for knowledge have constantly challenged me to strive for excellence. This thesis is a testament to the love and joy you have brought into my life. Thank you for your unwavering belief in me and for being my guiding light.

To my loving **Mother**,

You have been my role model, my mentor, and my rock. Your selflessness, dedication, and sacrifices have paved the way for my educational pursuits. From the earliest days of my childhood, you instilled in me a thirst for knowledge, fostering a love for learning that continues to drive me today. Your endless encouragement, wise counsel, and constant reminders of the importance of education have shaped my character and molded me into the person I am today. This thesis is a tribute to your unwavering love, unwavering support, and unwavering belief in my abilities. Thank you for always being there for me, every step of the way.

To both of you, I am eternally grateful for your love, encouragement, and unwavering belief in me. You have been my guiding stars, lighting the path to success and filling my life with happiness and purpose. This thesis is dedicated to you, as a small token of my immense love and appreciation. May this work serve as a reflection of the profound impact you have had on my life and the gratitude I hold in my heart.

“There are people saying everything is possible.

That’s when I hit the brakes.

When people say: this is impossible,

that’s when I go full throttle.

I’m the moderator in a panel of optimists and pessimists.”

Martin van den Brink

Acknowledgements

I Am profoundly grateful for the support and opportunities I have received during the course of my Ph.D. journey, which has been a period of growth both professionally and personally. The following acknowledgements represent a small token of my gratitude to those who have contributed to this significant chapter of my life.

First, I wish to express my sincere appreciation to the Ministero dell'Università e della Ricerca (MUR) for the financial support through the PRIN 2017 project titled "Nanostructured Porous Ceramics for Environmental and Energy Applications" (project # 2017PMR932). This funding has been instrumental in facilitating the research presented in this thesis.

I am immensely grateful to Prof. Giovanna Menardi from the Department of Statistics at the University of Padova. Her invaluable assistance in statistical data analysis and model development, particularly in Chapter 4, has significantly enriched this work. Her expertise and insightful discussions have been a source of continuous inspiration.

My heartfelt thanks go to the research group at the University of Calabria, Dipartimento di Ingegneria Informatica, Modellistica, Elettronica e Sistemistica, led by Prof.

Flaviano Testa. Their meticulous efforts in carrying out the CO_2 adsorption tests, as detailed in Chapter 2 and Chapter 3, have been a cornerstone of this research project. The collaboration has not only advanced the scientific findings of this thesis but also provided a stimulating environment for intellectual exchange.

The six-month research stint at the University of Oulu, Finland, has been a rewarding and enriching experience. I am indebted to Prof. Tero Luukkonen for his supervision during my work on the development of geopolymer membranes in Chapter 4. His guidance, encouragement, and the constructive critiques have significantly contributed to the quality of this thesis.

I extend my deepest gratitude to my supervisor, Prof. Paolo Colombo, and my co-supervisor, Prof. Giorgia Franchin, from the Department of Industrial Engineering at the University of Padova. Their expertise, mentorship, and unwavering support have been instrumental in shaping this research. Prof. Colombo's visionary guidance and Prof. Franchin's meticulous attention to detail have not only enhanced the quality of this work but also nurtured my growth as a researcher.

I am also thankful to Prof. Enzo Menna from the Department of Chemistry at the University of Padova for his significant contribution to the clenbuterol adsorption test , as elaborated in Chapter 3. His expertise and guidance have been crucial in achieving the objectives of this particular aspect of the research.

I also wish to extend my gratitude to all the faculty members, colleagues, and staff who have made my time during the Ph.D. a memorable experience. Your camaraderie and support have made the challenging journey enjoyable and fulfilling.

Lastly, I dedicate this thesis to my family and friends, whose unwavering support and love have been my strength throughout this journey. Your belief in me has been the driving force behind my perseverance and achievements.

Thank you all for being part of this incredible journey.

Summary

In the face of escalating environmental challenges, the scientific community has been propelled into a relentless pursuit of sustainable and innovative solutions. Geopolymers, with their multifaceted applications and eco-friendly properties, have emerged as a beacon of hope in this quest.

Derived from alumino-silicate minerals reacting with aqueous solutions of alkali metal oxides or hydroxides, geopolymers offer a green alternative to traditional construction materials, notably Portland cement. Their inherent properties, such as high porosity, thermal stability, and chemical durability, position them as not only suitable for construction but also as potential candidates for a myriad of environmental applications. This includes the pressing issue of microplastic pollution in aquatic ecosystems, where geopolymer membranes have shown significant promise in adsorbing and mitigating these contaminants.

Furthermore, the integration of advanced technologies, like 3D printing through Robocasting, has unlocked new horizons for geopolymers. This technique facilitates the fabrication of tailored geopolymer structures, optimized for specific applications such as CO_2 adsorption and medical waste treatment. The remarkable success in these

domains underscores the versatility and potential of geopolymers in addressing a broad spectrum of environmental and health-related challenges.

The evolution in geopolymer technology has been significantly driven by inventive fabrication techniques aimed at augmenting the mechanical and microstructural attributes of geopolymers. Among these techniques, hot-pressing has emerged as a promising avenue, showcasing notable enhancements in geopolymer densification and mechanical robustness.

However, for geopolymers to transition from research laboratories to real-world applications, there's an imperative need for standardization in their manufacturing and testing processes. This ensures not only consistent quality but also fosters further research, innovation, and seamless integration into existing infrastructures.

The landscape of this research is vast, encompassing the exploration of geopolymers in various applications. However, our ambition is not limited to merely showcasing the versatility of geopolymers. The central aim of this study is to assertively position geopolymers as not just a viable alternative but as a superior contender against commercially available materials.

This thesis is organized into four chapters, each representing one of the four major works undertaken throughout my PhD journey.

The first chapter discusses the successful implementation of the High Shear Wet Granulation technique to fabricate geopolymer and composite granules tailored for carbon dioxide adsorption.

The second chapter delves into the effective utilization of the Robocasting technique to produce geopolymer and geopolymer-zeolite scaffolds for carbon dioxide adsorption, along with the application in adsorbing emerging pollutants such as clenbuterol.

The third chapter elaborates on the successful development of new geopolymer membranes designed for microplastic adsorption.

The final chapter marks the inaugural attempt to model the compressive strength behavior of geopolymers, considering a comprehensive range of variables that could

influence the compressive strength.

Through meticulous testing, in-depth characterization, and comprehensive performance evaluations, we have endeavored to benchmark geopolymers against industry standards. Our objective is to demonstrate that, when optimized and tailored for specific applications, geopolymers can not only meet but often exceed the performance metrics set by existing commercial materials. Moreover, by juxtaposing geopolymers with commercial materials, we aim to highlight their competitive edge, be it in terms of sustainability, efficiency, or cost-effectiveness. This research seeks to challenge the prevailing norms, advocating for a paradigm shift in material selection and application, with geopolymers at the forefront.

In essence, this study is not just an academic exploration but a clarion call to industries, policymakers, and stakeholders to recognize and harness the unparalleled potential of geopolymers in shaping a sustainable and eco-friendly future.

List of Conferences & Publications

Journals

Muracchioli, M., Menardi, G., D'Agostini, M., Franchin, G., & Colombo, P. (2023). Modeling the compressive strength of metakaolin-based geopolymers based on the statistical analysis of experimental data. Applied Clay Science, 242, 107020.

Conferences

1. CIS 2021 YOUNG RESERACHER: High Shear Granulation Of Geopolymer; Online
2. GEOPOLYMER CAMP 2021: High Shear Granulation Of Geopolymer, Saint-Quentin; France
3. LE NUOVE FRONTIERE DEI MATERIALI INNOVATI E GREEN NEL RESTAURO E NELL'EDILIZIA: High Shear Wet Granulation Of Geopolymer, Catania; Italy
4. CERAMICS IN EUROPE: Geopolymer's application for carbon dioxide adsorption, Krakow; Poland
5. ICACC 2023: Modeling the compressive strength of metakaolin-based geopolymers, Daytona; USA (Invited Talk)

Contents

1 High Shear Wet Granulation of Geopolymers for Carbon Dioxide Adsorption 1

1.1 Abstract 1

1.2 Introduction 2

1.2.1 High Shear Wet Granulation Process 6

1.2.2 Characterization 8

1.2.3 CO_2 adsorption tests 9

1.3 Results and Discussion 11

1.3.1 Screening phase 11

1.3.1.1 Compressive strength of monoliths 11

1.3.1.2 Rheology 12

1.3.1.3 Porosity 14

1.3.1.4 Multi-Objective Optimization 16

1.3.2 Optimization of the Liquid/Solid ratio 18

1.3.3 Characterization of the granules 19

1.3.3.1 Morphology and dimension of the granules 19

1.3.3.2 Evaluation of the percentage of zeolite 23

1.3.3.3 Compression strength of granules 24
1.3.3.4 BET analysis on granules 27
1.3.4 Adsorption tests results 28
1.4 Conclusions 32

2 Direct ink writing of Geopolymer and Geopolymer and Zeolite Components for Carbon Dioxide Capture and Medical Waste Disposal 34

2.1 Abstract 34
2.2 Introduction 35
2.3 Experimental 37
2.3.1 Ink Preparation 37
2.3.2 Direct Ink Writing 38
2.3.3 Scaffolds Geometry 40
2.3.4 Characterization 41
2.3.5 CO_2 adsorption tests 42
2.3.6 Clenbuterol adsorption test 43
2.4 Results and Discussion 44
2.4.1 BET analysis 44
2.4.2 SEM analysis 45
2.4.3 Permeability test 47
2.4.4 CO_2 adsorption 49
2.4.5 Clenbuterol adsorption 52
2.5 Conclusions 56

3 Optimization of Geopolymer Membrane Production for Enhanced Microplastic Adsorption 57

3.1 Abstract 57
3.2 Introduction 58
3.3 Experimental 62

3.3.1 Samples preparation 62
3.3.2 2.2 Characterization 63
3.3.3 Compressive strength 64
3.3.4 Permeability test 65
3.4 Results and Discussion 66
3.4.1 XRD 68
3.4.2 FTIR 69
3.4.3 Porosity 70
3.4.4 BET 71
3.4.5 SEM 72
3.4.6 Mechanical test 73
3.4.7 Permeability test 76
3.5 Conclusions 78

4 Modeling the compressive strength of metakaolin-based geopolymers 80

4.1 Abstract 81
4.2 Experimental 82
4.2.1 Design Of Experiment 82
4.2.2 Samples Preparation 84
4.2.3 Mechanical characterization 85
4.2.4 Data Analysis 85
4.3 Results and Discussion 87
4.3.1 Effect of curing and aging time 87
4.3.2 Effect of curing temperature 94
4.3.3 Effect of the SiO_2/Al_2O_3 molar ratio 98
4.3.4 Effect of the H_2O/Al_2O_3 molar ratio 101
4.3.5 Comprehensive Model 103
4.3.6 Model Limitations 107
4.3.7 Conclusions 107

Bibliography **111**

CHAPTER 1

High Shear Wet Granulation of Geopolymers for Carbon Dioxide Adsorption

1.1 Abstract

A novel approach for high-shear wet granulation has been proposed for a potassium based geopolymer, together with various functionalization approaches to enhance carbon dioxide (CO_2) adsorption. A geopolymer slurry was employed as the granulation liquid for geopolymer powder, and the optimization of the granulation process parameters, specifically the viscosity of the geopolymer slurry and the liquid-to-solid ratio, was carried out to maximize the granulation efficiency. Two types of granules were produced: geopolymer granules and geopolymer granules incorporating zeolites 13x. Additionally, a separate batch of geopolymer granules was functionalized with APTES (3-

aminopropyltriethoxysilane) using solution phase deposition, where the granules were directly dipped into an ethanol solution with two different APTES concentrations (10 and 20 wt%). The three different types of granules were then tested for carbon dioxide adsorption in a fluidized bed column system using two different air mixture concentrations and velocity. Finally, the results were compared with commercially available granules of pure zeolites 13x. The experimental findings demonstrated that high-shear wet granulation of geopolymer yielded well-formed and stable granules suitable for carbon dioxide capture applications. The optimization of process parameters led to improved granule formation, achieving maximum efficiency. The geopolymer granules exhibited considerable CO_2 adsorption capacity, which was further enhanced by the inclusion of zeolites 13x and the APTES functionalization. Comparatively, the geopolymer-based granules displayed comparable or even superior CO_2 adsorption capacities when compared to the benchmark zeolites 13x granules.

Keywords: Geopolymers, Granulation, CO_2 adsorption

1.2 Introduction

The urgent need to mitigate carbon dioxide (CO_2) emissions and combat climate change has spurred significant research efforts toward developing efficient carbon capture technologies. Among various strategies, the utilization of solid adsorbents for CO_2 capture has garnered significant attention due to its potential for large-scale implementation and cost-effectiveness (Samanta et al., 2011; Q. Wang et al., 2011). Geopolymer materials, with their unique properties including high porosity, thermal stability, and chemical durability (Davidovits, 2013; Duxson et al., 2007), have emerged as promising candidates for CO_2 adsorption applications (Boscherini et al., 2021b, 2021a; Minelli et al., 2016, 2018a, 2018b; Novais et al., 2020; Papa et al., 2019, 2023; Papa, Landi, Murri, et al., 2021; Papa, Landi, Natali Murri, et al., 2021).

In recent years, the technique of high-shear wet granulation has gained prominence

as a versatile method for producing granular materials with controlled properties and enhanced performance (Chevalier et al., 2009; Shanmugam, 2015). By utilizing a liquid binder or granulation liquid, this process facilitates the agglomeration of fine particles into larger, more manageable granules (Bansal et al., 2019; Kristensen & Schaefer, 1987a, 1987b). The successful implementation of high-shear wet granulation requires careful optimization of various process parameters to achieve maximum efficiency (Faure et al., 2001; Liu et al., 2021). In particular, the viscosity of the granulation liquid and the liquid-to-solid ratio play crucial roles in determining the granulation outcome (Dhenge et al., 2013). The optimization process aims at striking a balance between the granule size, strength, and porosity, ensuring favorable CO_2 adsorption characteristics.

High-shear granulation has already been proposed for the fabrication of geopolymer granules (Luukkonen et al., 2018, 2020). In those works, metakaolin was utilized as the powder batch while the granulation liquid comprised an alkaline solution. The straightforward control of this process was attributed to the rheology of the alkaline solution, which closely follows that of water. However, despite the process's apparent simplicity, obtaining a precise and homogeneous composition of the final granules presents a formidable challenge, as it is impossible to forecast exactly how much powder interacts with the liquid during granulation. The granulation process presented in this work, utilizes instead geopolymer powder that is milled to a dimension below 300 microns, and couples it with a geopolymer slurry of the same composition as the granulation liquid. This approach significantly enhances the compositional homogeneity of the resulting granules, strategically enabling to achieve the target geopolymer composition in all particles. Moreover, it also promotes a potentially effective route for the recycling of geopolymer materials, reinforcing its relevance in the context of sustainable materials management.

This novel granulation approach was employed to fabricate two distinct types of granules. The first type consisted of pure geopolymer granules; the second one incorporated, within the geopolymer matrix, zeolites 13x which are known for their exceptional

CO_2 adsorption properties (Konduru et al., 2007). This combination aimed at enhancing the CO_2 capture capacity of the pure geopolymer-based granules. Furthermore, to explore additional avenues for performance enhancement, a separate batch of pure geopolymer granules was functionalized with 3-aminopropyltriethoxysilane (APTES), a procedure well known and used in the literature (Miranda et al., 2020). APTES serves as a functionalizing agent, introducing amino groups onto the geopolymer surface to enhance its affinity for CO_2 molecules (Pokhrel et al., 2018). All the produced granules were then tested for CO_2 adsorption and the results compared with benchmark data for pure, commercially available 13x zeolite granules.

With this work we wish to propose a high-shear wet granulation process for the fabrication of geopolymer granules with controlled composition for CO_2 adsorption. The findings contribute to the development of advanced sorbent materials and technologies for efficient carbon capture and storage applications.

The preliminary screening phase entailed a comprehensive evaluation of various geopolymer blends to ascertain their suitability for the high-shear granulation process. This assessment also sought to determine which composition provides an optimal balance between slurry viscosity, mechanical characteristics and porosity of the resulting granules. Eight geopolymer mixtures were investigated; to manufacture the samples, metakaolin (Argical 1200s, Imerys, France) was mixed with an alkaline solution for 1 hour in a thermostatic bath at 0°C. The alkaline solution was obtained by dissolving potassium silicates (Kaslov 205 PQ Corporation) and potassium hydroxides (Sigma Aldrich) into distilled water. After that, the slurry was poured into cylindrical silicone molds of 14 mm in diameter and 20 mm in height and put in a sealed container at a constant 100% relative humidity (RH), achieved by placing a water container within the chamber and monitoring RH using a hygrometer, to proceed with the curing process at 40°C for one day. Afterwards, additional aging was carried out in a sealed container at a 75%RH for seven days, achieved by placing a supersaturated NaCl solution within the chamber and monitoring using a hygrometer. This combination of curing and ag-

ing processes was used because it was demonstrated to provide optimal mechanical properties for the geopolymer (Muracchioli et al., 2023). Table 1.1 summarized the geopolymer mixtures tested during this phase and their composition.

Table 1.1: *Geopolymer mixtures tested*

Sample Name	SiO_2/Al_2O_3	K_2O/Al_2O_3	H_2O/Al_2O_3
$GP_{2.4}H_{16}$	2.4	1	16
$GP_{2.4}H_{18}$	2.4	1	18
$GP_{2.4}H_{20}$	2.4	1	20
$GP_{2.4}H_{22}$	2.4	1	22
$GP_{2.4}H_{25}$	2.4	1	25
$GP_{2.5}K_{0.8}H_{18}$	2.5	0.8	18
$GP_{3.8}H_{16}$	3.8	1	16
$GP_{3.8}H_{25}$	3.8	1	25

In order to limit the number of experimental variables and reduce the collection of experimental data, the geopolymer composition was changed solely in terms of its Si/Al and H_2O/Al_2O_3 ratios, whereas the K_2O/Al_2O_3 ratio was always held constant at 1, except for sample $GP_{2.5}K_{0.8}H_{18}$. Of course, a K_2O/Al_2O_3 ratio of 1 corresponds to the composition at which the positive charge of the alkaline cation fully stabilizes the Al coordination from $[Al]^{VI}$ to $[Al]^{IV}$. This composition limits the material susceptibility to carbonation reactions by interaction with the atmosphere. Numerous scholarly contributions (Duxson, Provis, Lukey, Mallicoat, Kriven, & van Deventer, 2005; Muñiz-Villarreal et al., 2011) have documented the presence of unreacted metakaolin in final geopolymer specimens, implying that the ratio $K_2O/Al_2O_3 = 1$ may exceed one. This supposition is based on the premise that if not all metakaolin is fully dissolved, the resultant Al_2O_3 content in the solution could be reduced, thereby increasing the

K_2O/Al_2O_3 ratio in the geopolymer. This significant issue has been addressed by various other scholarly works, which have explored the efflorescence mechanism inherent in geopolymer materials (Simão et al., 2021); one proposed solution to this issue involves reducing the K_2O/Al_2O_3 ratio below 1. Subsequent Fourier Transform Infrared Spectroscopy (FT-IR) and boiling tests have provided evidence that the geopolymer network has been correctly formed for the mixture $GP_{2.5}K_{0.8}H_{18}$. Therefore, it merits serious consideration as a viable candidate for the preliminary screening phase.

1.2.1 High Shear Wet Granulation Process

The composition of the geopolymer powder used as the batch material for the high-shear wet granulation process was the best one identified during the screening phase ($GP_{3.8}H_{25}$, see later). Upon the completion of the aging period (see Section 2.1), the geopolymer monolith was subjected to milling via a rotational sphere mill and subsequently sieved to produce a powder with particle size less than 300 microns. A certain degree of heterogeneity in the dimension of the powder favors the production of granules with reduced void volume, consequently enhancing their mechanical properties (Herting & Kleinebudde, 2007). Pertaining to the granulation process, a high-shear granulator (Elrich EL1) was employed. Figure 1.1 shows the schematic representation of the granulation process.

In the granulation apparatus, the mechanism comprises a rotational component, the impeller, as well as a stationary segment, the chopper. The chopper's role is to facilitate the removal of residual powder adhered to the wall, which does not actively participate in the process, thus enhancing operational efficiency. In addition to the impeller, the granulator's body also performs a rotational movement; however, it moves in the opposite direction to the impeller. A precise quantity of the predetermined powder, weighing 100 grams, was loaded into the granulator, and a corresponding quantity of liquid possessing the same composition as the powder was introduced. This was executed while preserving a constant impeller rotational speed of 300 revolutions per minute (rpm).

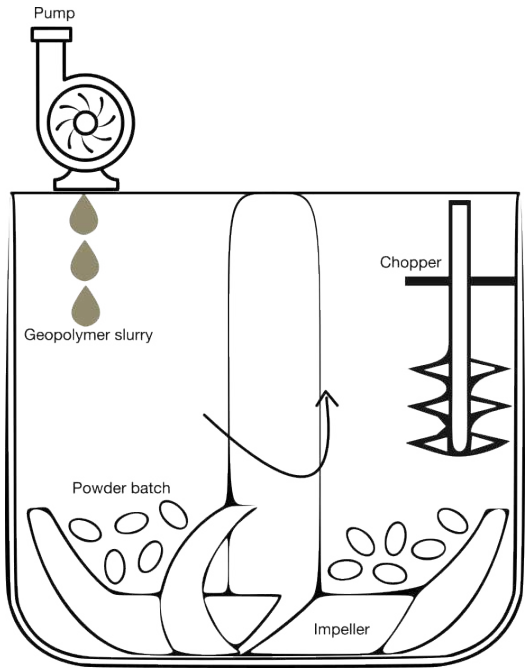

Figure 1.1: *Schematics of the high shear granulation process*

The addition of the binder material was achieved through the utilization of a Masterflex Easy-Load II pump, with the binder being introduced into the system from the top of the processing bowl. Upon completion of the liquid addition, the rotational speed was subsequently increased to 2000 rpm for a duration of two minutes. To streamline the process and maximize granulation efficacy, eight diverse Liquid/Solid ratios were investigated, ranging from 85 to 120 weight percentage in increments of 5. Following the completion of the granulation process, the resultant bulk material, composed of both granules and non-granulated powder, was subjected to the identical curing and aging treatment as outlined previously. After completion of the aging process, the aggregate material was subjected to a sieving procedure according to six dimensional classifications (> 2.8 mm, 2.8 - 1.4 mm, 1.4 - 0.8 mm, 0.8 – 0.6 mm, 0.6 – 0.4 mm, 0.4 – 0.3 mm). Composite granules, incorporating both geopolymer and zeolites 13x, were synthesized employing an identical methodological approach. The fabrication process relied on the exact compositional formulation of the geopolymer slurry, in conjunction with the same liquid-to-solid ratio (after the optimization studies) used during the production of the geopolymer granules. The sole variation introduced in the procedure was

the complete substitution of geopolymer powder with zeolite powder.

1.2.2 Characterization

A rotational rheometer (MCR 302, Anton Paar, Graz, A) equipped with a 50 mm diameter plate–plate geometry was used, with a set temperature of 20°C and a gap of 1 mm. All the eight mixtures were tested in a steady rate sweep with a shear rate increasing from 0.01 to 100 1/s.

The determination of the monoliths' compressive strength was carried out using a universal testing machine (Galdabini Quasar 25), operating at a crosshead velocity of 0.5 mm/min. Prior to testing, the compression surfaces of the specimens were subjected to a light sanding process. A total of 10 samples, representative of each experimental condition, were scrutinized.

To characterize the granules, identical parameters were employed, albeit using a more sensitive load cell with a maximum load capacity of 10N. The calculation of the stress field generated within a sphere under uniaxial compression applied at two points located at the extremes of a diameter is an established concept; it has been extensively studied, with significant contributions by Hiramatsu and Oka (Hiramatsu & Oka, 1966). They developed an understanding of the internal stress experienced by an isotropic linear elastic sphere with a radius, R, subject to symmetrically applied, evenly distributed radial loads over two equivalent spherical caps, centered along the compression axis, where the outer circle defines the contact radius, a. Hiramatsu and Oka demonstrated that the highest tensile stress is located along the compression axis, which is approximately 0.7 times the nominal stress, computed as $\sigma = \frac{F}{\pi \cdot r^2}$. Incorporating the analysis of Hiramatsu and Oka, the so-called "tensile strength" of particles undergoing uniaxial compression tests is determined as:

$$\sigma_T = k \cdot \frac{F_f}{\pi \cdot r^2} \tag{1.1}$$

where F_f symbolizes the peak (failure) load and k is a constant value. Experimen-

tal data (Jaeger, 1967)suggested that k ranges between 0.7 and 1.4; specifically, in our context, it was determined to be 0.9. The equivalent diameter was chosen to be the Sauter's diameter, defined as the diameter of a sphere exhibiting an identical Volume/-Surface Area ratio to that of the particles under investigation. The equivalent diameter value was determined employing a Mastersizer 2000. The strength data reported are the average of 10 measurements per each type of granule.

The bulk density of the monoliths was evaluated from mass and volume measurements. The apparent density of solid and ground geopolymers was measured by means of a helium pycnometer (AntoPaar Ultrapyc 3000). The total porosity of monoliths was therefore calculated as the ratio between their bulk and apparent density. The same procedure has been followed for the granule's characterization.

The specific surface area (SSA) of the granules was determined by multi-point Brunauer Emmett, Teller (BET) method with Quantachrome Autosorb iQ (Quantachrome Instruments, Boynton Beach, Florida), with a degassing temperature of 120°C for approximately 16 h under reduced pressure and analysis by N_2 adsorption at liquid nitrogen temperature.

The microstructure was assessed by means of a field emission scanning electron microscope (Sigma FESEM, Carl Zeiss). For a more comprehensive analysis of the interaction between geopolymer and zeolite 13x within the composite granules, X-ray diffractometry (XRD) (D8 Advance; Bruker Italia Srl, Milano, Italy) was used.

For a more comprehensive analysis of the interaction between geopolymer and zeolite 13x within the composite granules, X-ray diffractometry (XRD) (D8 Advance; Bruker Italia Srl, Milano, Italy) was used.

1.2.3 CO_2 adsorption tests

Figure 1.2 reports a visualization of the fluidized bed column system implemented for the carrying out of the carbon dioxide adsorption studies. The underpinning mechanisms of fluidization are centered around the elevation and suspension of particulate

matter. This is accomplished by forcing air or a different medium through a bed of particles within a confined space, thereby increasing the interaction interface between the solids and the gas (Hede, 2013; Suleiman et al., 2013; Teunou & Poncelet, 2002).

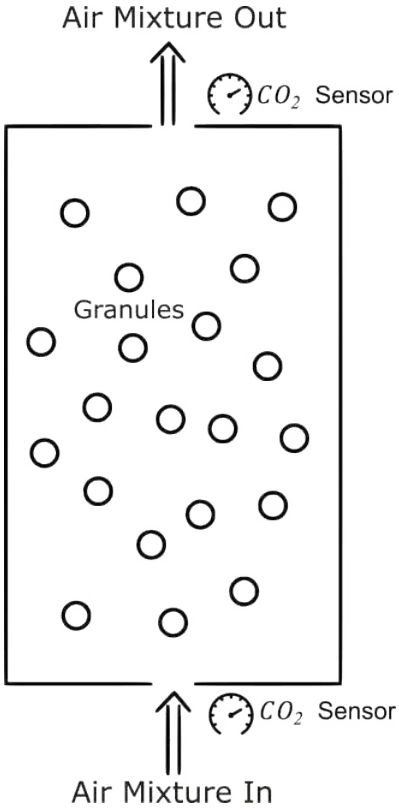

Figure 1.2: *Schematics of the fluidized bed column*

Within the parameters of our experimental design, we introduced into the column granules based on the most effective geopolymer composition (see section 1.2) and utilizing the optimal liquid-to-solid ratio (see section 1.2.1). Subsequently, an air mixture, containing two distinct carbon dioxide concentrations (10 and 20%), was introduced from the bottom of the column, under two different inlet velocities (5 and 12 cm/s). A sensor, strategically positioned at the top of the column, was utilized to quantify the concentration of air at the column's outlet. The data obtained from this experiment enabled to plot the back-through curves, which were then compared with the performance of zeolite 13x commercial pellets, serving as our benchmark.

1.3 Results and Discussion

1.3.1 Screening phase

1.3.1.1 Compressive strength of monoliths

Figure 1.3 reports the compressive strength results of the eight tested geopolymer mixtures, tested using the monoliths. Each mixture's median compressive strength, with its confidence interval visually represented by a blue box, was calculated with 95% confidence.

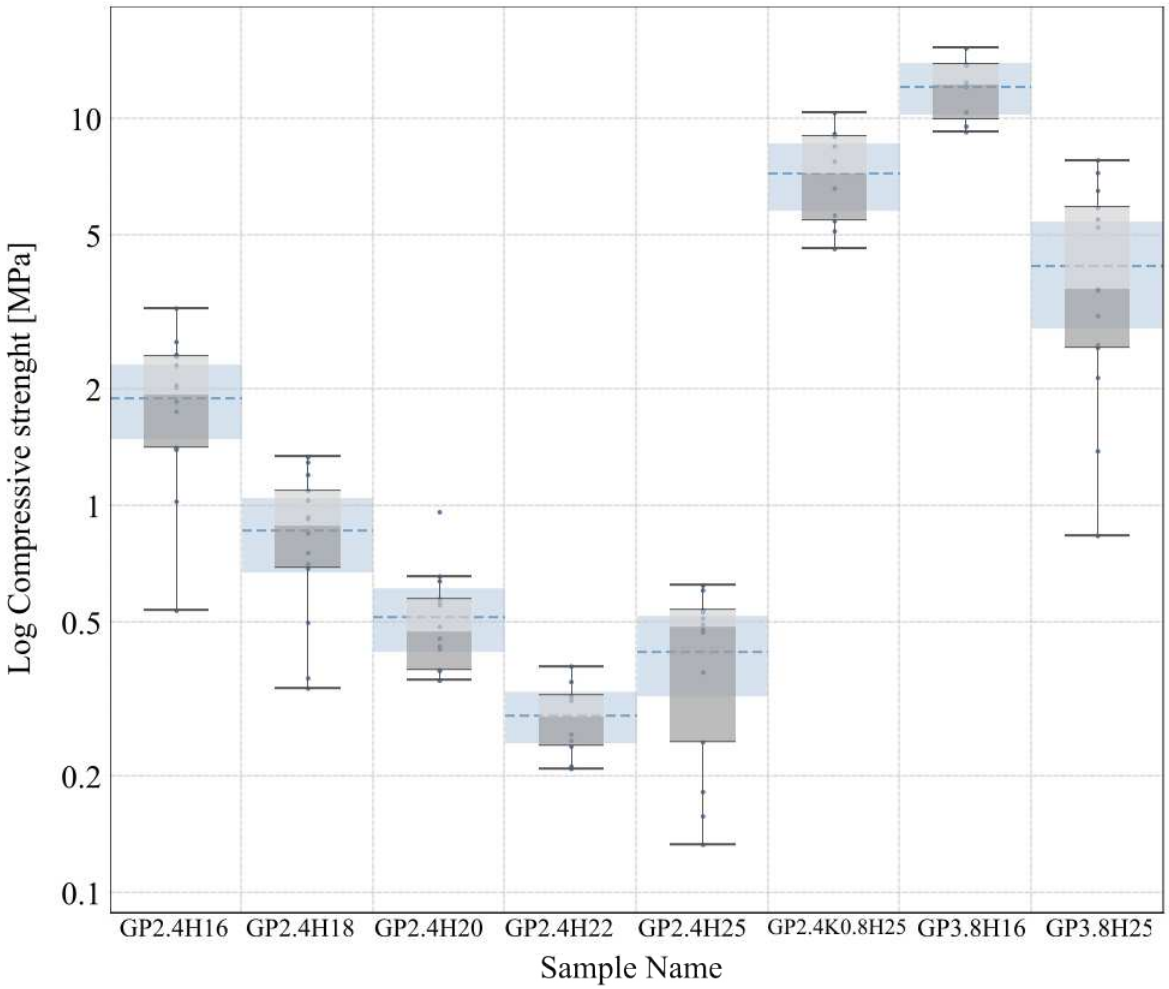

Figure 1.3: *Compression strength of geopolymer monoliths*

This visual aid assists in discerning genuine disparities across the different formulations. It is evident that sample $GP_{3.8}H_{16}$ possessed the highest compressive strength

value. Numerous studies (Duxson at al.,2005; Muracchioli et al., 2023) have demonstrated that increasing the SiO_2/Al_2O_3 ratio to 3.8 enhances the compressive strength, which aligns with the observed trends in our study. Knowing that the Al component of metakaolin tends to dissolve more easily than the Si component (Weng & Sagoe-Crentsil, 2007), we can assume that more $Al(OH)_4^-$ species are readily available for condensation with respect to $Si(OH)_4$ ones. This is particularly true for the systems with low values of the SiO_2/Al_2O_3 ratio: condensation is likely to have occurred between aluminate and silicate species, producing poly(sialate) polymer structures. With increasing Si content, the overall higher amount of silicate species promotes the reaction between them, resulting in oligomeric silicates; the dominance of the latter leads to better mechanical properties with increasing SiO_2/Al_2O_3ratio. Conversely, an increase in water content was observed to result in a reduction in the value of compressive strength; this trend is again in accordance with the literature (Ismail et al., 2011; Xie & Kayali, 2014). Increasing the water content (increasing the H_2O/Al_2O_3 molar ratio) increases the porosity of the final structure (Khale & Chaudhary, 2007), and pores act as a defect point and therefore a higher porosity significantly lowers the compression strength of the final product. A singular deviation is evident between samples $GP_{2.4}H_{25}$ and $GP_{2.4}K_{0.8}H_{25}$. Nonetheless, an examination of the confidence intervals for the mean values reveals an intersection. This overlap suggests that no substantial disparities exist between the two samples.

1.3.1.2 Rheology

The rheological data are shown in Figure 1.4. Generally, the geopolymer systems are characterized by a shear-thinning behavior with an initial yield stress, a finding which is congruent with existing literature (Romagnoli et al., 2012). Increasing the water content of the composition prompted a downward trend in the viscosity, because of the decrease in the solid content (Franchin et al., 2017).

A comparative evaluation of compositions with identical water content but different

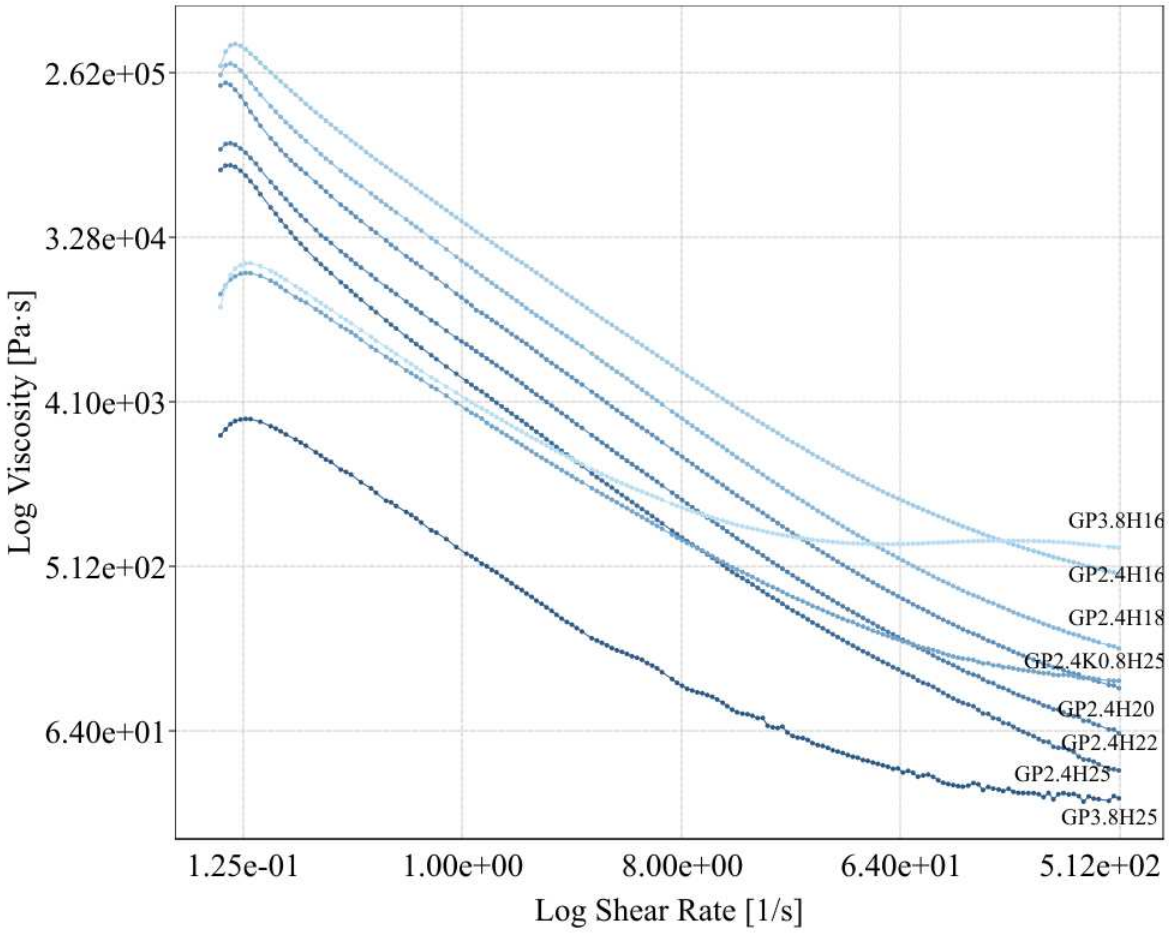

Figure 1.4: *Rheology of geopolymer mixtures*

silica-to-alumina ratios (i.e., $GP_{3.8}H_{16}$ and $GP_{2.4}H_{16}$), reveals distinct differences. In particular, the composition with the lower silica-to-alumina ratio exhibited a markedly higher yield stress, attributable to a higher solid content ratio (Rovnaník et al., 2018). However, these suspensions possessed a rather high viscosity, which can be represented using empirical models such as the Krieger-Dougherty relation. Its general form can be written as:

$$\eta = \eta_0 \cdot (1 - \frac{\phi}{\phi_{Max}})^n \tag{1.2}$$

with η_0 the solution viscosity, ϕ the packing fraction and ϕ_{Max} the dense packing fraction. Increasing the silica content increased the viscosity of the alkaline solution

employed in the formulation of the geopolymer slurry (η_0), thereby reducing the shear-thinning behavior and resulting in a higher viscosity value at elevated shear rates. This observation is equally applicable to the other direct comparison, i.e., between sample $GP_{2.4}H_{25}$ and $GP_{3.8}H_{25}$. However, in this particular instance, the difference in the initial yield stress is so pronounced that the shear rate range under consideration for our experiments does not adequately permit the variation in shear thinning behavior to significantly impact the final viscosity determination. Consequently, sample $GP_{3.8}H_{25}$ displayed a higher viscosity value when juxtaposed with its counterpart, sample $GP_{2.4}H_{16}$. The initial yield stress of sample $GP_{2.4}K_{0.8}H_{25}$ was similar to that of sample $GP_{3.8}H_{16}$ and lower than that of all other formulations with a silica-to-alumina ratio of 2.4. This phenomenon remains associated with the quantity of solid content, which is lesser in this context. However, the variation in shear thinning behavior at a medium shear rate continues to be ambiguous.

1.3.1.3 Porosity

Figure 1.5 reports the porosity data. The total porosity (TP) was computed employing the subsequent formula:

$$TP(\%) = \frac{\rho_{Powders} - \rho_{Geometric}}{\rho_{Powders}} \cdot 100 \tag{1.3}$$

where $\rho_{Powders}$ is the density of the powders obtained by grinding the geopolymer monoliths, as determined by pycnometry. $\rho_{Geometric}$ corresponds to the geometric density, computed utilizing the standard formula for density: mass/volume. The open porosity (OP) was estimated according to the formula:

$$OP(\%) = \frac{\rho_{Monolith} - \rho_{Geometric}}{\rho_{Monolith}} \cdot 100 \tag{1.4}$$

where $\rho_{Monolith}$ is the density of the entire monolith measure using the pycnometer.

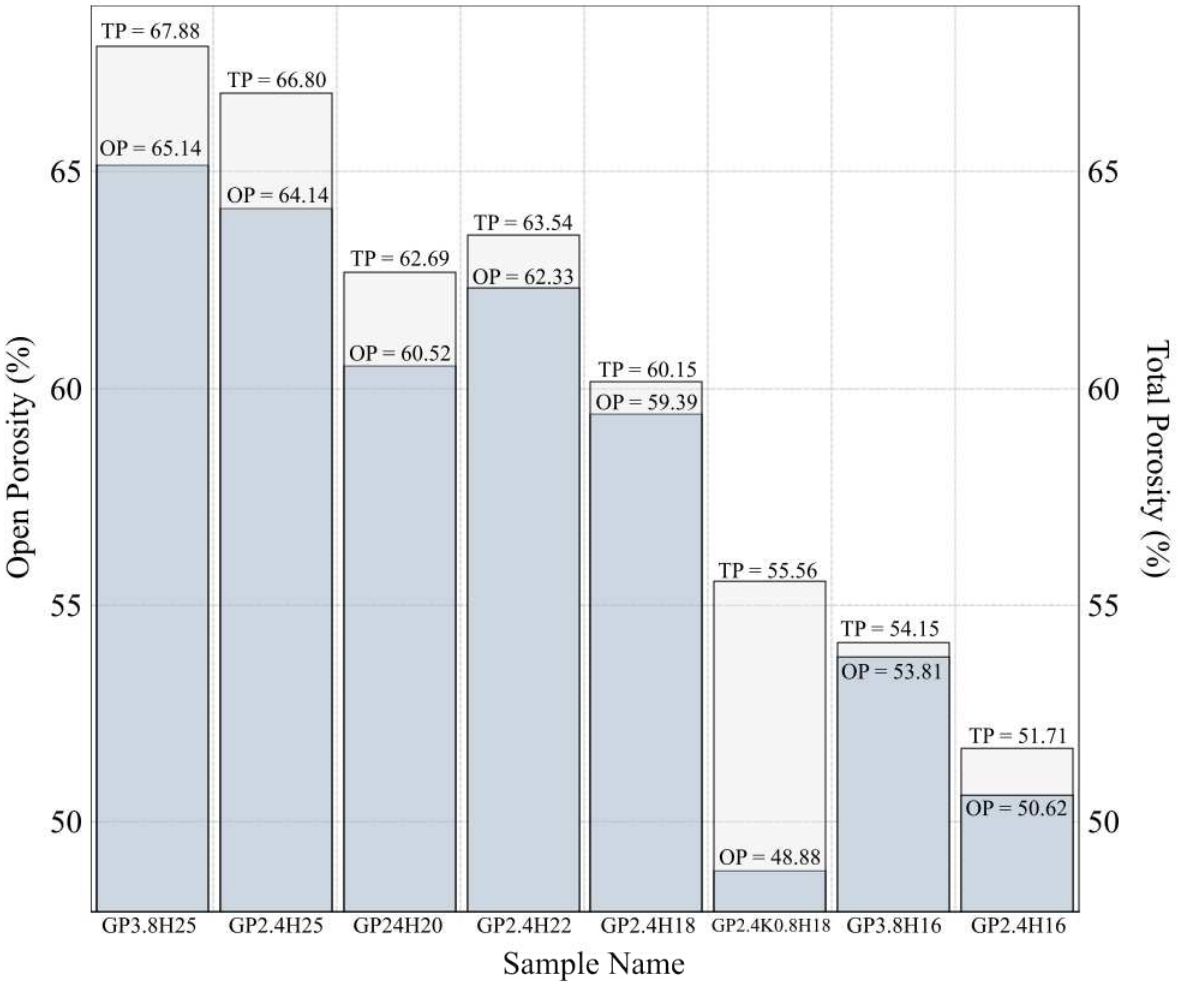

Figure 1.5: *Total (TP) and open (OP) porosity of geopolymer samples*

We can observe that an increase in the amount of water increased the total porosity of the samples, as expected. Moreover, at a constant water amount, the increase in the silica-to-alumina ratio increases the total porosity. Conversely, a reduction in the K_2O/Al_2O_3 ratio not only generates a decrease in total porosity, but the porous structure also appears less interconnected, as highlighted by the exceedingly low open porosity percentage. The underlying mechanisms driving this behavior remain ambiguous, necessitating more comprehensive analyses for a more precise understanding of the structural intricacies.

1.3.1.4 Multi-Objective Optimization

Prior to the optimization of the high-shear granulation process, it is imperative to determine what is the optimal balance between viscosity, compressive strength, and total porosity. As previously mentioned, the viscosity of the granulation liquid is a crucial parameter of the wet granulation process. The objective is to minimize this characteristic to ensure a uniform distribution of the liquid on the powder batch, thereby enhancing the efficiency of the process.

In our specific context, considering the targeted application, the goal was to concurrently minimize the viscosity of the formulation and maximize the total porosity and compressive strength of the granules. It should be noted, however, that maximizing the compressive strength is less critical, considering the forecasted use of the granules in a fluidized bed column system; in this application, the granules must solely be capable of withstanding their own weight.

To identify the optimal tradeoff, we carried out a multi-objective optimization (Caramia et al., 2020; Deb et al., 2016). This involved normalizing the values of viscosity, compressive strength, and total porosity to fall within a range of 0 to 1, using the following formula:

$$Poperty_{Norm} = \frac{Poperty_{Valuie} - PopertyValue_{Min}}{PopertyValue_{Max} - PopertyValue_{Min}} \tag{1.5}$$

In this context, the term "property" is used to denote either viscosity, compressive strength, or total porosity. The normalized form of these properties is referred to as $Poperty_{Norm}$. The specific value of the property under consideration for each mixture is termed 'Property Value', while $PopertyValue_{Max}$ and $PopertyValue_{Min}$ represent the maximum and minimum values of that property across all compositions under consideration, respectively. Given our aim to minimize viscosity, we subtracted the normalized viscosity values from 1 (1 -$Viscosity_{Norm}$. Subsequently, we computed a score for each formulation using the formula:

$$Score = \sum PopertyNorm \tag{1.6}$$

This score served as a measure of the optimal balance between the three properties under consideration; Fig. 1.6 shows the results of the score for each composition tested.

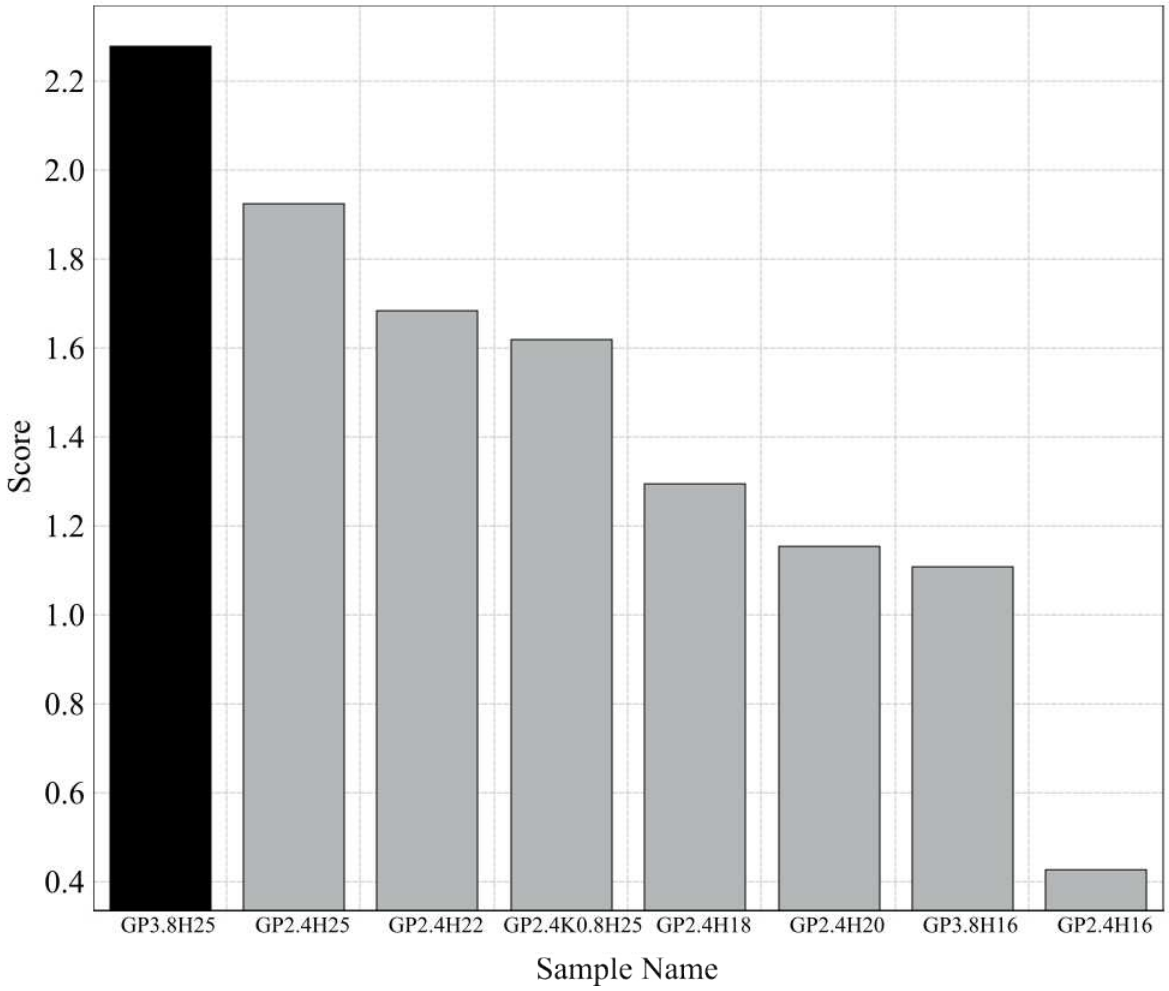

Figure 1.6: *Calculated score outcomes for each geopolymer composition*

Drawing upon the data presented in Figure 1.6, we can observe that the composition that obtained the best score was $GP_{3.8}H_{25}$. Consequently, subsequent optimization of the parameters for the high-shear wet granulation process was carried out using this specific composition for the geopolymer slurry employed as the granulation liquid.

1.3.2 Optimization of the Liquid/Solid ratio

Figure 1.7 shows the outcomes of the optimization procedure carried out for varying Liquid-to-Solid (L/S) ratios. The reported values were recalibrated to represent percentage distributions, rather than absolute mass values. Each L/S ratio is symbolized by a distinct bar, which collectively sum up to 100%, thereby underscoring the comprehensive nature of the data presentation.

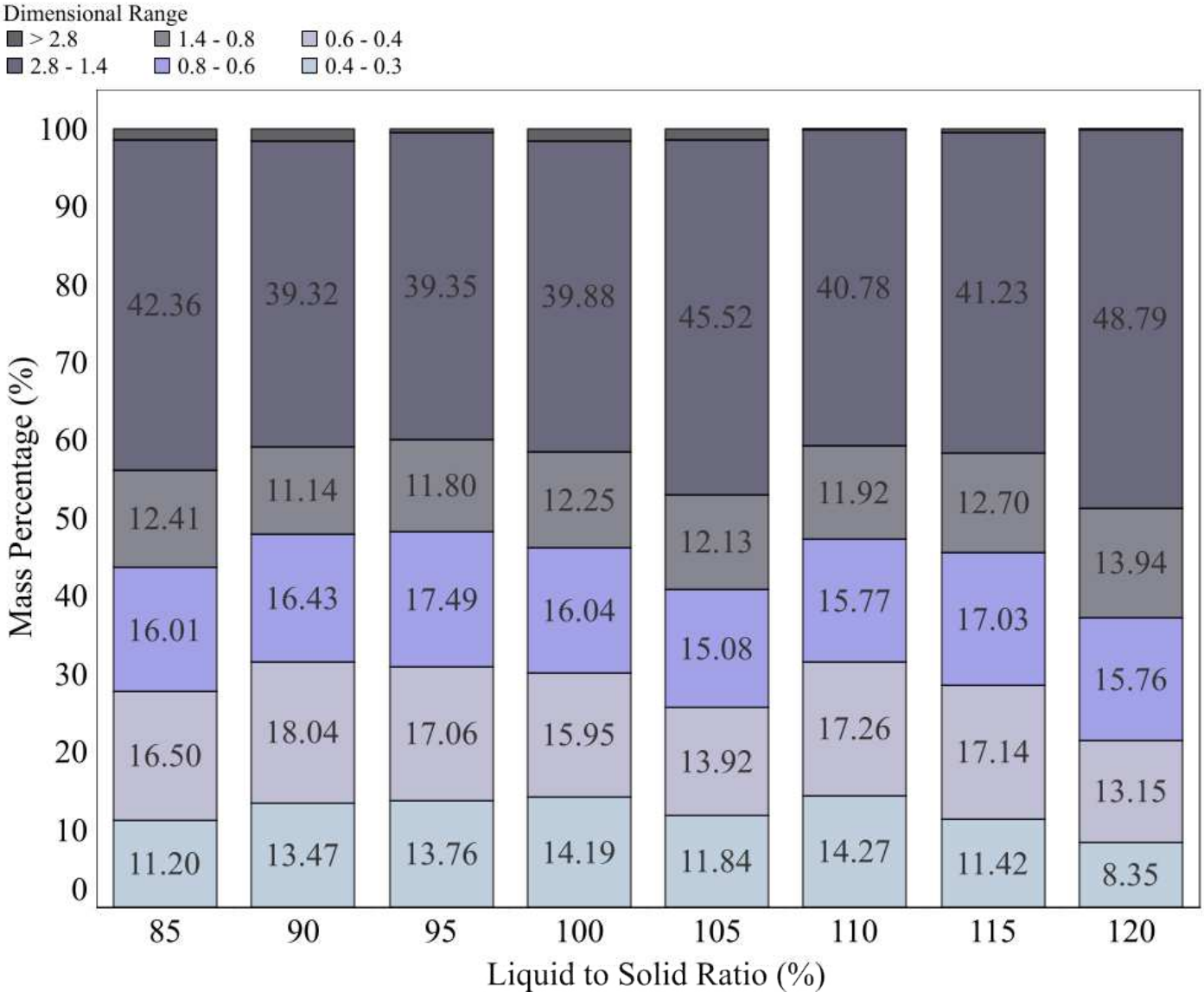

Figure 1.7: *Percentage distribution of mass across various dimensional ranges for each evaluated Liquid-to-Solid (L/S) ratio*

In general terms, two dimensional ranges - namely, greater than 2.8 mm (>2.8) and between 0.4 and 0.3 mm (0.4 - 0.3) - were deemed unsuitable, for the following reasons:

- particles with dimensions larger than 2.8 mm fail to guarantee an optimal functionality within the framework of a bed column system. These larger granules exhibit a decreased packing efficiency, thereby detrimentally influencing the overall efficacy of the bed in terms of carbon dioxide adsorption;
- conversely, particles with dimensions ranging between 0.4 and 0.3 mm are excessively small. Such small particles are responsible for generating a significant pressure drop within the adsorption system, which is also undesirable.

The adsorption tests for further analysis will be performed at two inlet velocities: 5 and 12 cm/s. According to Girimonte et.al (Girimonte et al., 2017a), these velocities are deemed the minimal thresholds ensuring fluidization for particles falling within the 0.4 - 0.5 and 0.7 - 0.8 mm ranges, respectively. As these particle sizes align with the intended application of our granules, the Liquid-to-Solid (L/S) ratio exhibiting the highest mass distribution percentage within these dimensional parameters was considered optimal.

In the context of our system, the optimal Liquid-to-Solid (L/S) ratio has been determined to be 115. This value has been selected for the fabrication of all granular materials - encompassing geopolymer, geopolymer + 13x, and zeolites + APTES.

1.3.3 Characterization of the granules

1.3.3.1 Morphology and dimension of the granules

In Figure 1.8 are shown representative images of the granules produced. SEM was used to confirm the occurrence of granulation. Figure 1.9 shows images of the original geopolymer powders as well as of the surface of granules with dimensions varying from 0.6 to 0.8 mm, which reveal that the granules were not hollow and that the particles from the initial powder were suitably encapsulated within the newly formulated geopolymer matrix, confirming successful granulation.

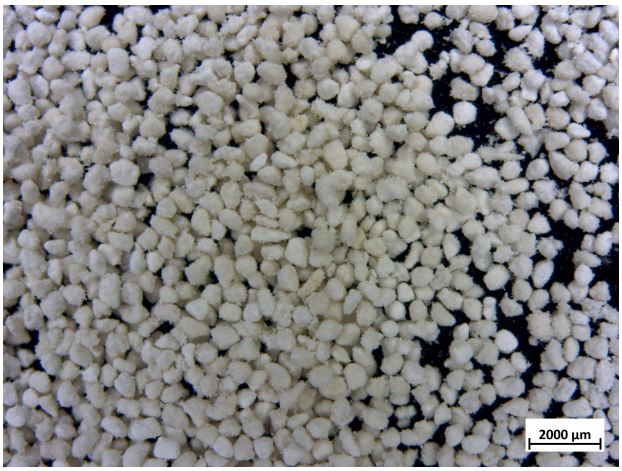

Figure 1.8: *Images of the geopolymer granules obtained*

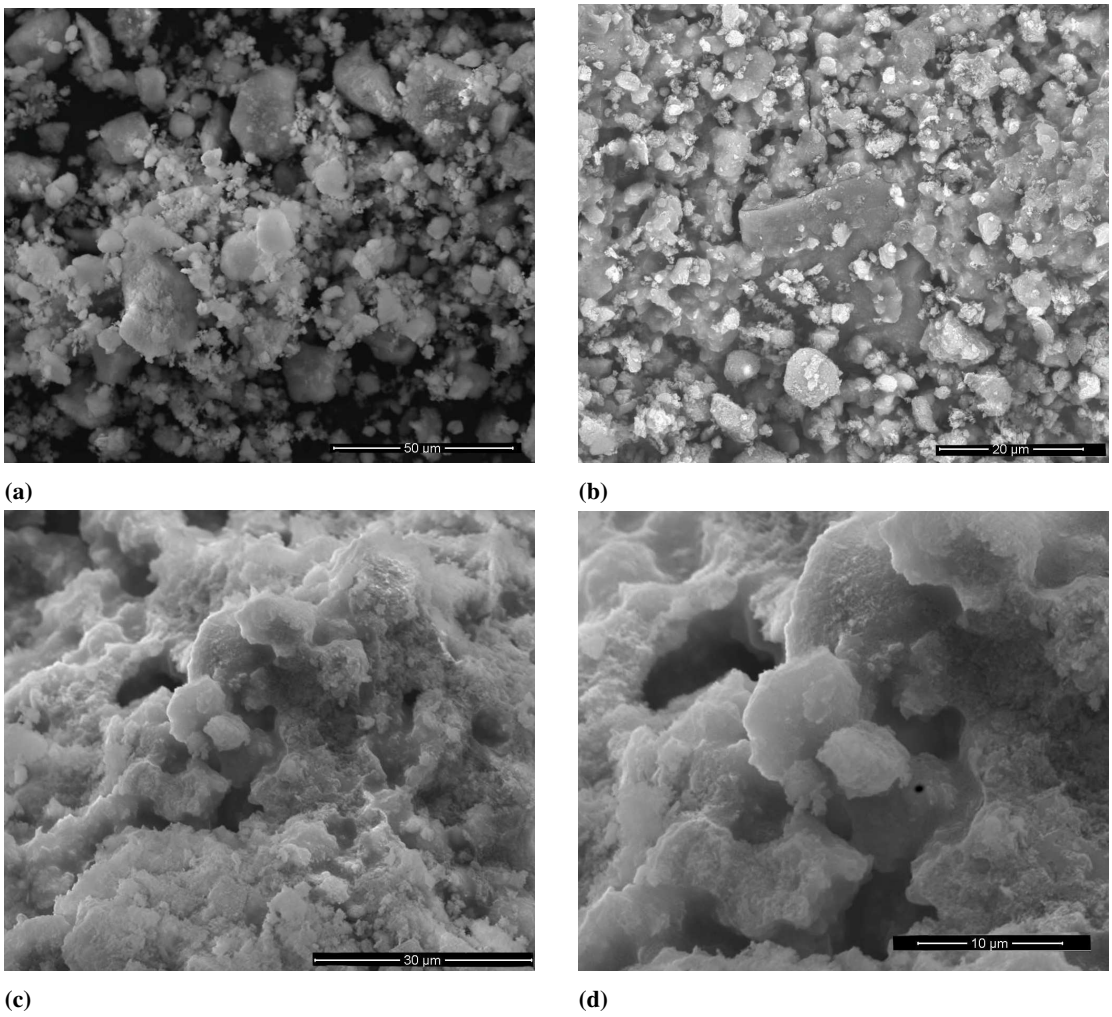

(a) **(b)**

(c) **(d)**

Figure 1.9: *SEM images of: (a) initial geopolymer powders; (b) external surface of a granule; (c) internal surface of a granule, and (d) detail of the internal structure of a geopolymer granule*

Figure 1.10 shows the SEM images of the granules produced using zeolite particles and a geopolymer liquid slurry (granules with dimensions varying from 0.6 to 0.8 mm). Analogously to the case of geopolymer granules, the initial zeolite powder appears to be effectively integrated within the newly formed geopolymer matrix. Interestingly, however, the zeolites predominantly locate themselves on the external surface of the granules, rather than internally.

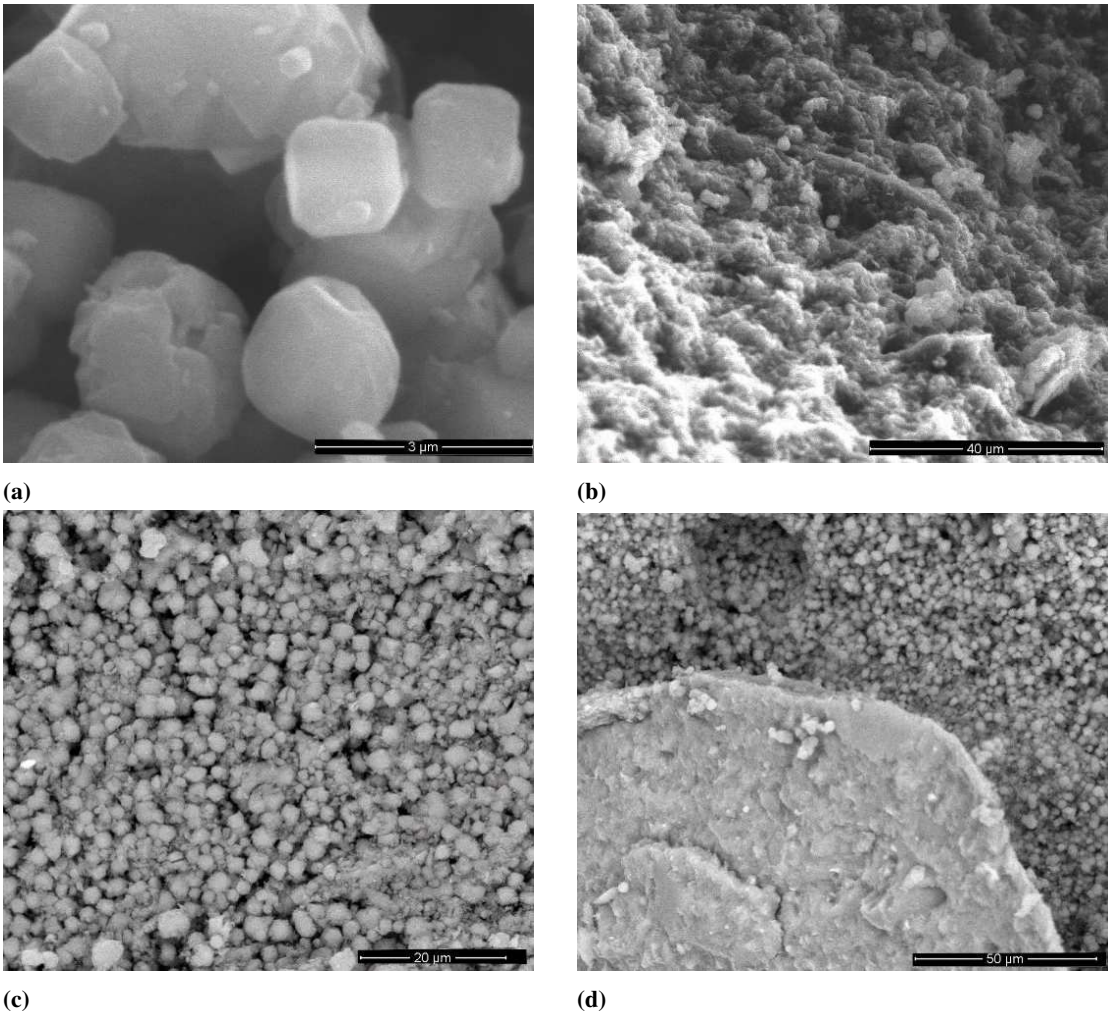

(a) **(b)**

(c) **(d)**

Figure 1.10: *SEM images of: (a) initial zeolite 13x powders, (b) external surface of a granule; (c) internal surface of a granule, and (d) detail showing simultaneously the internal and the external structure of a granule*

The observed predominance of zeolite distribution on the external surface of the granules may be correlated to the sub-optimal wettability of the zeolite powder batch. This could be attributed to several relevant factors, such as:

- contrast between hydrophilic/hydrophobic characteristics: zeolites, including 13x variant, are generally recognized for their hydrophilic properties, suggesting their strong attraction towards water (C. Wang et al., 2019). In contrast, geopolymers typically exhibit a hydrophobic behavior (Ruan et al., 2022). This mismatch in hydrophilic/hydrophobic properties could negatively affect their mutual interaction;

- surface roughness and porosity: zeolites are porous materials with a microscopically coarse surface texture (Wheatley et al., 2014). These characteristics can hamper the establishment of thorough contact between the zeolite and geopolymer surfaces;

- chemical dissimilarity: the pronounced alkaline environment formed by geopolymer precursors may result in the partial disintegration or alteration of zeolite 13x during the geopolymerization process, thereby exacerbating wettability issues.

However, having zeolites at the external surface is clearly advantageous, given the active role of zeolites in the adsorption process. By being on the external surface, the zeolites are directly exposed to carbon dioxide, thereby enhancing their active participation in adsorption.

For the granules comprised of geopolymer and APTES, further SEM analysis was deemed unnecessary as the deposition post-granulation would not alter the overall morphology of the granules.

The granules fabricated in this study are intended for carbon dioxide testing within a fluidized bed column system, as previously mentioned. Prior to the adsorption test, the dimension of each granule was characterized for their fluidization regime using a standard technique (Girimonte et al., 2017b). This investigation was conducted at room temperature and pressure, with dehumidified air serving as the fluidizing gas. Pressure drop and bed expansion curves were derived from the measurements of pressure and bed height during experiments conducted at both increasing and decreasing surface gas

velocities, yielding consistent results.

Taking into account the two selected inlet velocities, the granule dimensions required for minimum fluidization should range between 0.8 and 0.4 mm. Consequently, subsequent characterization tests were solely conducted on granules within these size ranges.

1.3.3.2 Evaluation of the percentage of zeolite

In order to quantify the amount of zeolites within the geopolymer-zeolite composite granules, an initial analysis of ten distinct zeolite concentrations in a geopolymeric matrix was conducted, employing X-ray diffractometry. The investigated concentrations ranged from 100 wt% zeolites and 0 wt% geopolymer to 10 wt% zeolites and 90 wt% geopolymer, adjusting at increments of 10 wt%. In Figure 1.11 are reported, as an example, the XRD patterns of zeolite 13x powders and sample $GP_{3.8}H_{25}$.

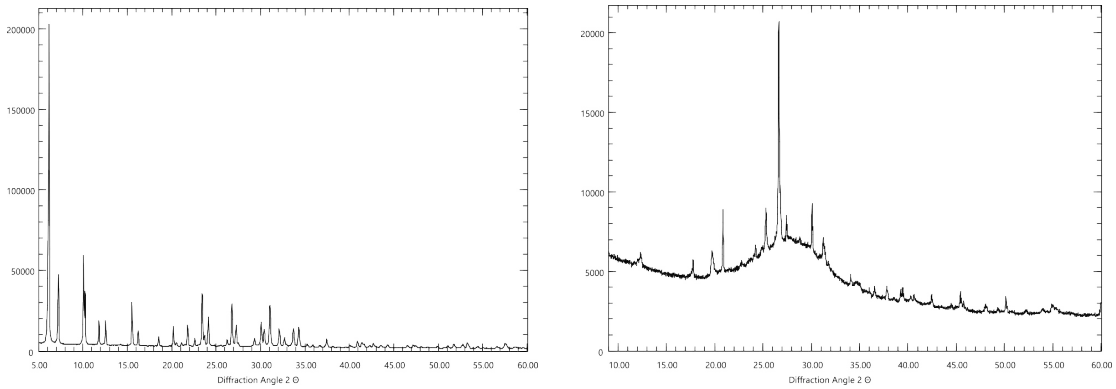

(a) **(b)**

Figure 1.11: *XRD patterns for: (a) zeolite 13x powders, and (b) sample $GP_{3.8}H_{25}$*

During each measurement, background noise was subtracted, as the increased geopolymer presence increased the interference due to the amorphous nature of geopolymer (see Fig.1.11b).

To normalize the gathered data, an initial analysis was carried out considering the standard deviation of the intensity values for each angle measured during the investigation. The aforementioned analysis revealed that the angle yielding the smallest standard deviation for intensity was 33.05493. Subsequently, all intensity values were standard-

ized using the following formula:

$$NewIntensity_i = \frac{Intensity_i}{Intesnity_{33.05493}} \cdot 100 \tag{1.7}$$

where $NewIntensity_i$ represents the standardized intensity value at angle I, $Intensity_i$ denotes the unstandardized intensity value at angle I, $Intesnity_{33.05493}$ corresponds to the value for the angle 33.05493, exhibiting near constant properties across varying compositions. A linear regression model was applied to the most prominent peak of the zeolite, which was the one located at 6.33°.

The equation derived from the linear regression analysis is as follows:

$$y = 55.29x - 315.33 \tag{1.8}$$

where x is the weight percentage of zeolite content, and y is the normalized intensity values of the principal peak of zeolite 13x. Subsequently, XRD analyses of geopolymer and zeolite granules in the dimensional ranges of 0.8 - 0.6 and 0.6 - 0.4 were performed. The obtained patterns were normalized using the aforementioned method, and the maximum peak values were incorporated into equation 1.8 to determine the zeolite content.

The weight percentage of zeolites in the granules was approximated to be around 20 wt% for both dimensional ranges analyzed.

1.3.3.3 Compression strength of granules

For an accurate dimensional characterization of the granules, enabling the determination of their compression strength according to Eq.1.1, it was necessary to assess the Sauter diameter. The results are reported in Table 1.2.

The weighted residual is a measure of the difference between the actual measured scattering pattern and the theoretical scattering pattern calculated by the instrument's software based on the estimated particle size distribution. The weighted residual is expressed as a percentage. A lower percentage indicates a better fit between the measured

Table 1.2: *Sauter Diameter measured using Mastersizer 2000*

Dimensional Range (mm)	Sauter Diameter (mm)	Weighted Residual (%)
0.8 - 0.6	0.766	11.018
0.6 - 0.4	0.424	8.966

and theoretical scattering patterns, suggesting that the estimated particle size distribution is a good representation of the actual particle sizes in the sample. In our case, the weighted residual was relatively low, suggesting that the estimated particle size distribution was a reasonably good fit to the actual particle sizes in our sample.

Figure 1.12 reports the compression strength data for the tests carried out on both the geopolymer granules and the composite granules of geopolymer and zeolite 13x.

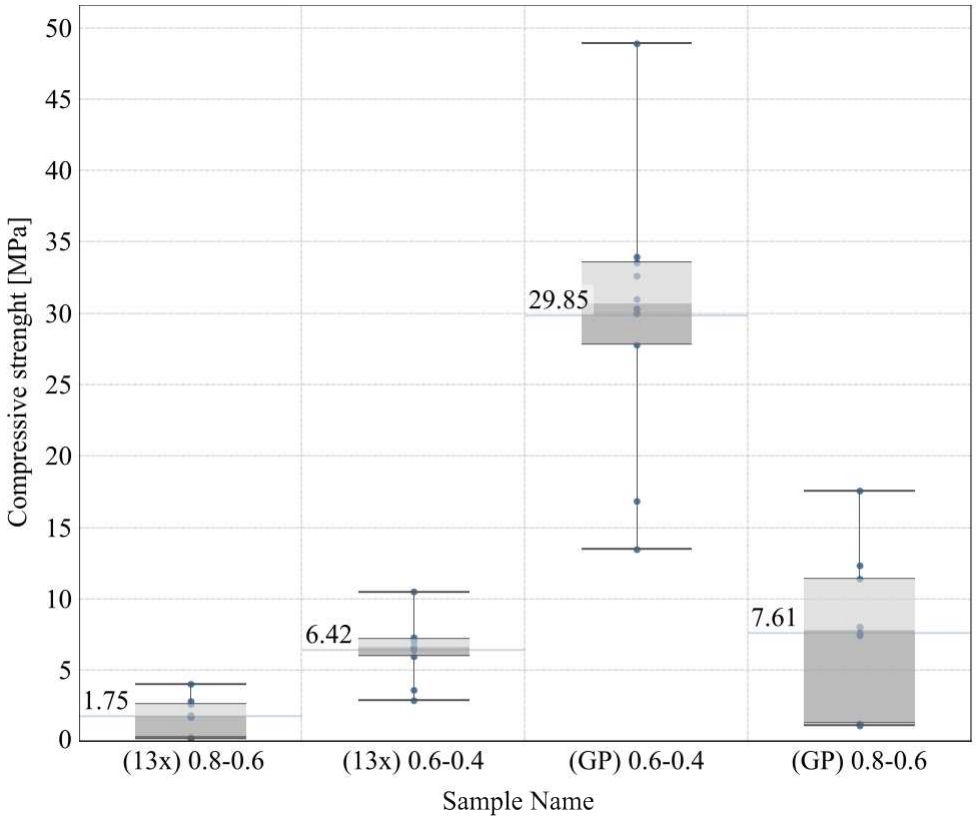

Figure 1.12: *Compression strength of the geopolymer and geopolymer + 13x granules for two dimensional ranges: 0.8-0.6 mm and 0.6-0.4 mm*

In all the cases, we can observe that granules with smaller dimensions exhibited greater compressive strength. This phenomenon can be attributed to the fact that smaller granules typically experience higher shear stress during the high shear granulation process, leading to a reduction in size (Han et al., 2019). Further research conducted by H Wang and colleagues (H. Wang et al., 2005) has indicated that the application of pressure to metakaolin-based geopolymers effectively eliminates most of the entrapped air, thereby enhancing the compressive strength of the matrix in its early stages. In the case of the geopolymer and zeolite composite granules, the characterization tests revealed a significant drop in the compressive strength values compare to standard geopolymer granules. This is further substantiated by the density values as outlined in Table 1.3, where it is distinctly observable that smaller granules exhibit a higher bulk density value, indicative of reduced porosity, as reflected in the Total Porosity value.

Table 1.3: *Bulk density Value and Total Porosity measure by helium pycnometer for the geopolymer granules produced*

Granules' dimension (mm)	Bulk Density (g/cm^3)	Total Porosity (%)
>2.8	0.95	75.49
2.8 - 1.4	1.06	73.68
1.4 - 0.8	1.12	69.98
0.8 - 0.6	1.17	67.83
0.6 - 0.4	1.22	67.6

There seems to be a clear correlation between the decrease in strength and the amount of zeolite present in the granules; indeed, a 20 wt% zeolite content corresponds to roughly a 20% reduction in compression strength. This may be attributed to the zeolite particles serving as points of defect within the geopolymeric matrix, consequently

diminishing the mechanical resistance of the granules. This implies a potential 1:1 relationship between the zeolite percentage and the granules' compressive strength.

1.3.3.4 BET analysis on granules

Table 1.4 reports the SSA data from BET analysis carried out on starting powders and all produced granules. Both geopolymer and geopolymer-zeolite granules exhibited a trend where smaller granules possessed a reduced surface area. This can be attributed to the lower porosity within these smaller granules, likely due to the increased shear stress they endure during the granulation process, as previously mentioned

Table 1.4: *SSA data for starting powders and geopolymer granules, geopolymer granules with zeolite 13x, and geopolymer granules functionalized with APTES.*

Sample Name	BET (m^2/g)
GP Powders	82.718
GP (0.8 - 0.6)	16.975
GP (0.6 - 0.4)	15.354
13x Powders	359.233
GP - 13x (0.8 - 0.6)	151.675
GP - 13x (0.6 - 0.4)	122.709
GP (10% APTES)	52.354
GP (20% APTES)	30.457

Considering the results for granules treated with APTES, a notable decrease in surface area value is observed with an increase in the APTES amount. This can be attributed to the partial occlusion of surface pores by the APTES continuous layer. However, this effect aligns well with the objectives of this study, as the intention was to

facilitate the interaction between APTES and carbon dioxide during the adsorption test, primarily on the external surface of the granules.

1.3.4 Adsorption tests results

The outcomes of the adsorption tests are described by what is commonly termed as "breakthrough curves". The evaluation of these breakthrough curves (see Figure 1.13) was carried out with the objective of determining:

- the Breakthrough Time (t_B): this denotes the period necessary for the concentration of CO_2 to attain 5% of the input concentration at the exit point of the adsorption column. On the breakthrough curve, this represents the point at which the C/Co ratio sees a significant rise from a virtually negligible value. This time marker represents the inability of the adsorbent to wholly absorb the incoming adsorbate, providing valuable insights into the effective operating duration of the adsorbent before requiring regeneration or replacement;

- the Saturation Time (t_s): this is representative of the moment when the adsorbent has reached its adsorption capacity, i.e., it cannot intake any more of the adsorbate. On the breakthrough curve, this corresponds to the time when the C/Co ratio reaches 1. At this point, the CO_2 concentration in the effluent mirrors that of the influent, suggesting that adsorption is no longer happening. This metric is crucial as it points to the maximum operational capacity of the adsorbent, thus indicating the overall duration for which an adsorbent can function before it is entirely spent and necessitates either regeneration or replacement;

- the quantity of CO_2 adsorbed per unit mass of the adsorbent mads (expressed as C/Co), computed via the integration of the breakthrough curves.

Due to the similar results for the granules sized 0.8 - 0.6 and 0.6 - 0.4, the results discussed further pertain exclusively to the granules within the 0.6 - 0.4 size range.

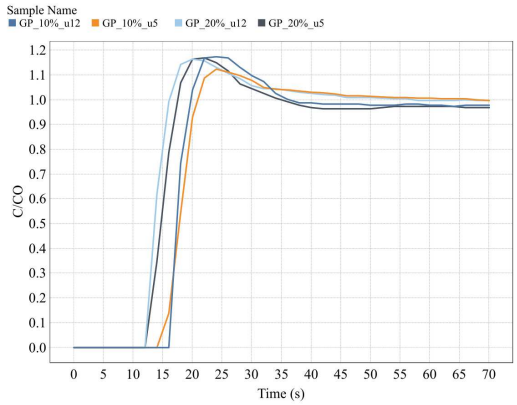

(a)

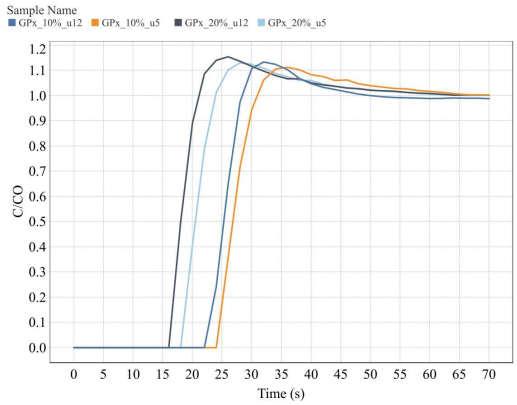

(b)

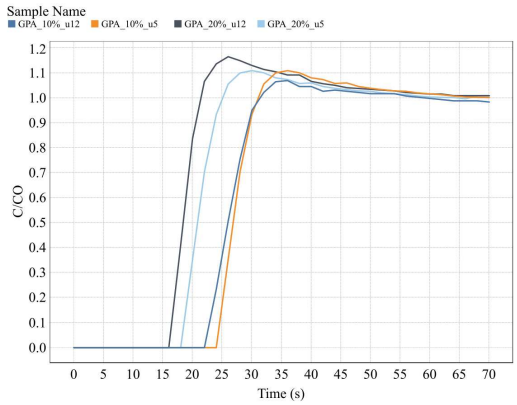

(c)

Figure 1.13: *Breakthrough curves of: (a) geopolymer granules, (b) geopolymer and zeolites 13x, (c) geopolymer and APTES (concentration of CO_2 = 10% and 20%; inlet velocity u =5 (u5) and u = 12 (u12))*

To facilitate a more streamlined interpretation of the curves, the most crucial parameters extracted from the curves of Fig.1.13 have been concisely aggregated in Table 1.5.

Table 1.5: *Breakthrough time (t_b), saturation time (t_s) and mass of carbon dioxide adsorbed (CO_2 adsorbed).*

Sample Name	t_b (s)	t_s (s)	CO_2 adsorbed (g)
13x_10% [u5]	50	56	15.2
13x_10% [u12]	48	55	17,7
13x_20% [u5]	46	54	19
13x_20% [u12]	43	56	33
GP_10% [u5]	16	24	6.2
GP_10% [u12]	12	22	7
GP_20% [u5]	14	24	7.7
GP_20% [u12]	9	22	9.75
GP(13x)_10% [u5]	24	29	8.36
GP(13x)_10% [u12]	22	27	10
GP(13x)_20% [u5]	18	28	10.5
GP(13x)_20% [u12]	16	29	19
GP(Aptes10)_10% [u5]	37	45	13.2
GP(Aptes10)_10% [u12]	33	43	16.5
GP(Aptes10)_20% [u5]	31	44	22
GP(Aptes10)_20% [u12]	26	45	33
GP(Aptes20)_10% [u5]	53	59	15.9
GP(Aptes20)_10% [u12]	49	60	29
GP(Aptes20)_20% [u5]	44	56	32
GP(Aptes20)_20% [u12]	41	55	37

In contrast to commercially available zeolite 13x granules, geopolymer granules exhibit a relatively lower adsorption capacity. This could be attributed to the proximity of t_b and t_s values in geopolymer granules, indicating a rapid saturation process. This phenomenon may be associated with the carbonation reaction mechanism that underlies carbon dioxide adsorption in geopolymer granules. In the natural carbonation process, atmospheric CO_2 undergoes an acid-base reaction with a hydroxide (Sani et al., 2016;

Zhang et al., 2014). However, in the context of geopolymers, efflorescence is primarily driven by the availability of Na^+ or K^+ and OH^- ions, according to the equations (for Na^+):

$$CO_2 + 2OH^- \rightarrow CO_3^{2-} + H_2O \tag{1.9}$$

$$2Na^+ + CO_3^{2-}CO_3^{2-} + xH_2O \rightarrow Na_2CO_3 \cdot xH_2O \tag{1.10}$$

The accumulation of carbonate product on the external surface of the granules appears to restrict the accessibility to the granules' porosity, thereby accelerating the saturation process.

In the context of geopolymer and zeolite granules, it is noteworthy that despite demonstrating a lower adsorption capacity, there is a 50% increase in efficiency with only a 20 wt% presence of zeolites in the matrix. In this situation, the zeolites, located solely on the granules' external surface, adsorb the carbon dioxide while the underlying geopolymer matrix serves as a storage medium. This process delays the saturation point for zeolites 13x, thereby enhancing the zeolite's overall adsorption capacity.

Regarding the functionalization of geopolymer granules with APTES achieved adsorption levels that met the benchmark set by pure zeolite 13x. Remarkably, granules functionalized with a 20% addition of APTES surpassed the adsorption capacity of the zeolite granules. The underlying mechanism of adsorption is elucidated in the subsequent reaction:

$$CO_2 + 2RNH_2 \longleftrightarrow RNHCO_2^- + RNH_3 \tag{1.11}$$

$$CO_2 + H_2O + RNH_2 \longleftrightarrow HCO_3 + RNH_3^+ \tag{1.12}$$

In this scenario, chemisorption emerges as the dominant mechanism for CO_2 up-

take. The integration of diverse amine-based basic components into porous solid sorbents has been identified as a significant factor in boosting their capture capacity. Specifically, the chemical interaction with CO_2 leads to the generation of carbamates and bicarbonates when CO_2 reacts with amine groups under anhydrous and hydrous conditions, respectively. The literature extensively documents the enhancement of CO_2 uptake by solid amine-based systems in the presence of H_2O, attributed to the formation of bicarbonates (Varghese & Karanikolos, 2020). Analogous to the case of composite granules (geopolymer + 13x), the geopolymer serves as a storage medium, prolonging the saturation time and thereby augmenting the total mass of carbon dioxide adsorbed into the matrix.

Although we are pioneers in employing this innovative granulation technique to fabricate geopolymer granules, drawing comparisons with existing literature proves to be challenging. Nonetheless, the observed trends align well with documented findings. It has been noted that geopolymer materials exhibit modest carbon dioxide adsorption capacity (Candamano et al., 2019; Papa, Minelli, Marchioni, Landi, Miccio, Natali Murri, et al., 2023). However, the functionalization of geopolymer with zeolite and APTES significantly enhances the adsorption capability of these materials, a finding that is well corroborated by existing literature (L. Han et al., 2022; Mahinpey et al., 2023).

1.4 Conclusions

In conclusion, this research has successfully demonstrated a novel approach to enhancing carbon dioxide (CO_2) adsorption through high-shear wet granulation of potassium-based geopolymer, optimization of process parameters, and the application of various functionalization techniques. Three types of granules were investigated: pure geopolymer, geopolymer incorporating zeolite 13x, and APTES-functionalized geopolymer, each subjected to CO_2 adsorption testing under varying conditions. The results revealed that the high-shear wet granulation of geopolymer resulted in well-formed and

stable granules, making them suitable for CO_2 capture applications. The optimization of process parameters, in particular the viscosity of the geopolymer slurry and the liquid-to-solid ratio, contributed to the efficient formation of granules. The geopolymer granules demonstrated a significant CO_2 adsorption capacity, which was further enhanced by the incorporation of zeolites 13x and the functionalization with APTES. Notably, the geopolymer-based granules with 20% of APTES functionalization exhibited CO_2 adsorption capacities that were either comparable to or exceeded that of the benchmark zeolites 13x granules. These findings underscore the potential of using functionalized geopolymer granules as effective adsorbents for CO_2 capture. Future research could explore other functionalization techniques and their impact on the adsorption capacity of geopolymers, contributing to the development of more efficient and sustainable solutions for CO_2 capture.

CHAPTER 2

Direct ink writing of Geopolymer and Geopolymer and Zeolite Components for Carbon Dioxide Capture and Medical Waste Disposal

2.1 Abstract

The escalating urgency to address carbon dioxide (CO_2) emissions and counteract climate change has intensified research into effective carbon capture solutions. Solid adsorbents, particularly geopolymer materials, have emerged as promising materials due to their inherent properties such as high porosity, thermal stability, and chemical durability, making them prime candidates for CO_2 adsorption. Concurrently, the multifaceted application of Clenbuterol (CLE), especially its residues in the environ-

ment, poses health risks, emphasizing the need for efficient pollutant removal methods. Among various techniques, adsorption separation, enabled by advanced absorbent materials, is particularly favorable for its effectiveness and energy efficiency. This study delves into the aqueous dissolution of Clenbuterol and the cationic exchange capacity of geopolymers, especially in adsorbing pollutants that protonate in water. Leveraging the potential of additive manufacturing, specifically the Direct Ink Writing (DIW) technique, this research explores the suitability of geopolymers for robocasting, emphasizing the fabrication of lattice structures tailored for specific applications. Evaluations of CO_2 adsorption capacities across different geometries and sample types, including a combination with Zeolite 13x, were also conducted to enhance CO_2 capture. Furthermore, a proof of concept is presented, showcasing the potential of geopolymer-based materials in medical waste treatment applications.

Keywords: Geopolymers; Robocasting; Medical Waste; CO_2 adsorption

2.2 Introduction

The urgent need to mitigate carbon dioxide (CO_2) emissions and combat climate change has spurred significant research efforts toward developing efficient carbon capture technologies. Among various strategies, the utilization of solid adsorbents for CO_2 capture has garnered significant attention due to its potential for large-scale implementation and cost-effectiveness (Samanta et al., 2011; Wang et al., 2011). Geopolymer materials, with their unique properties including high intrinsic meso-porosity, thermal stability, and chemical durability (Davidovits, 2013; Duxson et al., 2007), have emerged as promising candidates for CO_2 adsorption applications (Novais et al., 2020).

Clenbuterol (CLE) is a β_2-adrenergic agonist with diverse applications. While it's commonly incorporated as a feed supplement to recalibrate the metabolic pathways of nutrition, boosting protein synthesis, and minimizing fat accumulation (Degand et al., 1992) it has also found utility in the medical realm as a bronchodilator to manage

asthma and related respiratory ailments. However, residues of CLE in the environments, present significant health concerns. The presence of such residues in the human body, can lead to symptoms such as chronic intoxication, palpitations, and dizziness (Kang et al., 2016; Martinez-Navarro, 1990). Among the available approaches to eliminate environmental organic pollutants, methods like biodegradation (Allan et al., 2007) and photocatalysis (Yu et al., 2014) exist. However, adsorption separation stands out for its efficiency, purity assurance, and low energy consumption (Akpinar et al., 2019). This technique's success hinges on the advancement of suitable absorbent materials, emphasizing attributes such as an extensive surface area, rapid adsorption, lasting stability, and user-friendly recyclability.

The aqueous dissolution of Clenbuterol is governed by the following chemical reactions:

$$C_{12}H_{18}Cl_2N_2O + H_2O \longleftrightarrow C_{12}H_{18}Cl_2N_2OH^+ + OH^- \tag{2.1}$$

Geopolymers are recognized for their remarkable capacity to adsorb heavy metal ions through cation exchange (Ariffin et al., 2017; Cheng et al., 2012) . Owing to their inherent propensity for cationic exchange with the surrounding environment, there has been increasing interest in employing geopolymers for the adsorption of emerging pollutants, particularly those that undergo protonation upon immersion in water.

Additive manufacturing (AM) of ceramics is a very attractive field of research that has the potential to disruptively change the way complex shaped bodies are fabricated (Zocca et al., 2015). The Direct Ink Writing (DIW) technique was originally named Robocasting after Cesarano's patent (Cesarano III & Calvert, 2000) and is a layer by layer fabrication technique which involves the robotic deposition of a viscoelastic ink extruded through a fine nozzle. Central to the approach is the creation of an ink that can be extruded in filamentary form and can undergo rapid solidification to maintain the shape of such filaments even as they span gaps in the underlying layer(s). Evaporation of solvent can be employed as mean of rapid solidification for pastes with high solid loading, but there are limitations in terms of nozzle size (typically > 0.5 mm) in order

to prevent clogging.

It is well-established that geopolymers are materials aptly suited for production via robocasting (Botti et al., 2021; Franchin et al., 2017a) . The possibility of using geopolymers as ink in DIW for the fabrication of lattice structures makes this material even more interesting, precisely for enabling the a priori design of optimized structures as a function of the specific application (Bai et al., 2017; Franchin et al., 2017b; Panda et al., 2017; Zhong et al., 2017).

In evaluating the adsorption capacity for carbon dioxide, two geometries, linear and shifted, were examined for two sample types: Geopolymer and Geopolymer-13x. Zeolites 13x is well known for their exceptional CO_2 adsorption properties (Konduru et al., 2007); this combination aimed at enhancing the CO_2 capture capacity of the pure geopolymer.

For applications in medical waste treatment, only the linear geometry was evaluated using geopolymer-based materials. This assessment aims to provide a proof of concept for a novel application of geopolymer-based materials.

2.3 Experimental

2.3.1 Ink Preparation

In the formulation of the ink, a geopolymer composition with a SiO_2/Al_2O_3 ratio of 3.8 and an H_2O/Al_2O_3 ratio of 18 was utilized. The selection of a SiO_2 to Al_2O_3 ratio of 3.8 aligns with the observed peak in the mechanical strength of geopolymers, as well documented in the literature (Duxson et al., 2005; Vora & Dave, 2013). Furthermore, internal studies conducted by our research team on the surface area analysis of various geopolymer compositions revealed an optimal balance for the H_2O to Al_2O_3 ratio at 18. This specific ratio not only ensures a substantial porosity but also maintains smaller pore dimensions, resulting in a notably high surface area. To manufacture the inks, metakaolin (Argical 1200s, Imerys, France) was mixed with an alkaline solution for 1 hour in a thermostatic bath at 0°C. The alkaline solution was obtained by dissolv-

ing potassium silicates (Kaslov 205 PQ Corporation) and potassium hydroxides (Sigma Aldrich) into distilled water. A K_2O/Al_2O_3 ratio of 1 was selected. To optimize the rheological properties for robocasting compatibility, sodium bentonite (sourced from ClearOFF Minerals, UK) was incorporated into the mixture, to increase its pseudo-plasticity, in an amount of 5 wt%. For the geopolymer and zeolite 13x specimens, commercially available 13x (Sigma Aldrich) was employed. Given that the composite formulations comprise up to 60 wt% zeolites, the integration of a minor proportion of carbon methyl cellulose was deemed essential.

Carbon methyl cellulose plays a dual role, acting both as a dispersant (Park et al., 2023; Wellham et al., 1992) and as a water retention agent (Lavanya et al., 2011; Wu et al., 2021). Zeolites are well-documented for their significant water adsorption capacity (Bolis et al., 2006; Jänchen et al., 2004). This characteristic necessitates the use of a greater water quantity than typically required in standard geopolymer compositions. Excessive water can induce phase separation during the printing process. The incorporation of methylcellulose addresses this challenge. However, it is imperative to moderate its addition, as carbon methyl cellulose has been observed to decrease the overall surface area of the sample (Long et al., 2019). This is particularly crucial in carbon dioxide adsorption studies, where the surface area is a paramount property that must be preserved. Any reduction in this attribute is undesirable.

2.3.2 Direct Ink Writing

After mixing, the ink was transferred into a plastic syringe, which served as a cartridge for direct ink writing. Each syringe can contain up to 30 mm^3 of ink. The cartridges were mounted on a Delta printer (Delta Wasp 2040 Turbo, Wasproject, Massa Lombarda, IT) equipped with a pressurized vessel and an infinite screw for paste extrusion. The layer resolution of the printer is 50 μm. The system can mount the same kind of conical nozzles employed on the previous device; no difference was detected between samples printed with one or the other.

The ink was extruded at room temperature through the tip of a tapered capillary nozzle of size 0.84 mm (Nordson Italia S.p.a., Segrate, IT) to form a geopolymeric filament that was deposited onto a flexible polyimide substrate. The substrate was generally kept in air, but could also be immersed in a hydrophobic liquid (typically oil) to limit drying and clogging issues. Printing was carried out at ambient temperature.

The extrusion occurred at a predetermined flow rate and deposition speed . After patterning one layer, the nozzle was incrementally raised in the z-direction to generate the next layer. This process was repeated until the desired structure was formed. 3D periodic lattices composed of a simple tetragonal geometry, for example, could be assembled by patterning an array of parallel filaments in the x-y plane such that their orientation was orthogonal to the layers immediately above and below a given layer. Alternatively, the nozzle could be gradually raised in the z-direction as the print progresses to build objects in a spiral fashion. Solidification occurred in a sealed container at a constant 100% relative humidity (RH), achieved by placing a water container within the chamber and monitoring RH using a hygrometer, to proceed with the curing process at 40°C for one day. Afterwards, additional aging was carried out in a sealed container at a 75 %RH for seven days, achieved by placing a supersaturated NaCl solution within the chamber and monitoring using a hygrometer. This combination of curing and aging processes was used because it was demonstrated to provide optimal mechanical properties for the geopolymer (Muracchioli et al., 2023). The samples produced for the CO_2 adsorption test were printed through a nozzle with a diameter of 840 μm; the layer height was set at 600 μm to provide a small overlap between the layers and therefore better adhesion. Utilizing the specified parameters, two distinct geometries were fabricated:

- Linear Geometry: Characterized by its layering pattern, the initial layer is followed by a second layer extruded at a 90-degree angle. The third layer aligns precisely with the first, and this sequence continues until the desired sample height is attained;

- Shifted Geometry: While the first two layers mirror those of the linear geometry, the third layer exhibits a shift relative to the first, equivalent to half the strut diameter in the x-direction.

For the samples designated for clenbuterol adsorption, a singular geometry was fabricated. We opted for a more tortuous geometry, characterized by layers stacked at a 30-degree angle relative to one another.

2.3.3 Scaffolds Geometry

In this study, two distinct geometrical configurations are examined. The first, termed "Linear," is depicted in Fig.2.1a and Fig.2.1b. Conversely, the configuration named "Shifted" can be observed in Fig.2.1c and 2.1d.

For each geometry, the filament has a dimension of 0.84 mm. The primary distinction lies in the layer alignment: in the linear geometry, all layers are seamlessly superimposed, whereas in the shifted geometry, layers are offset by half a diameter. Consequently, the shifted geometry exhibits a more tortuous internal structure compared to its linear counterpart, increasing the pressure drop of the component but also the contact time between the fluid and the solid scaffold.

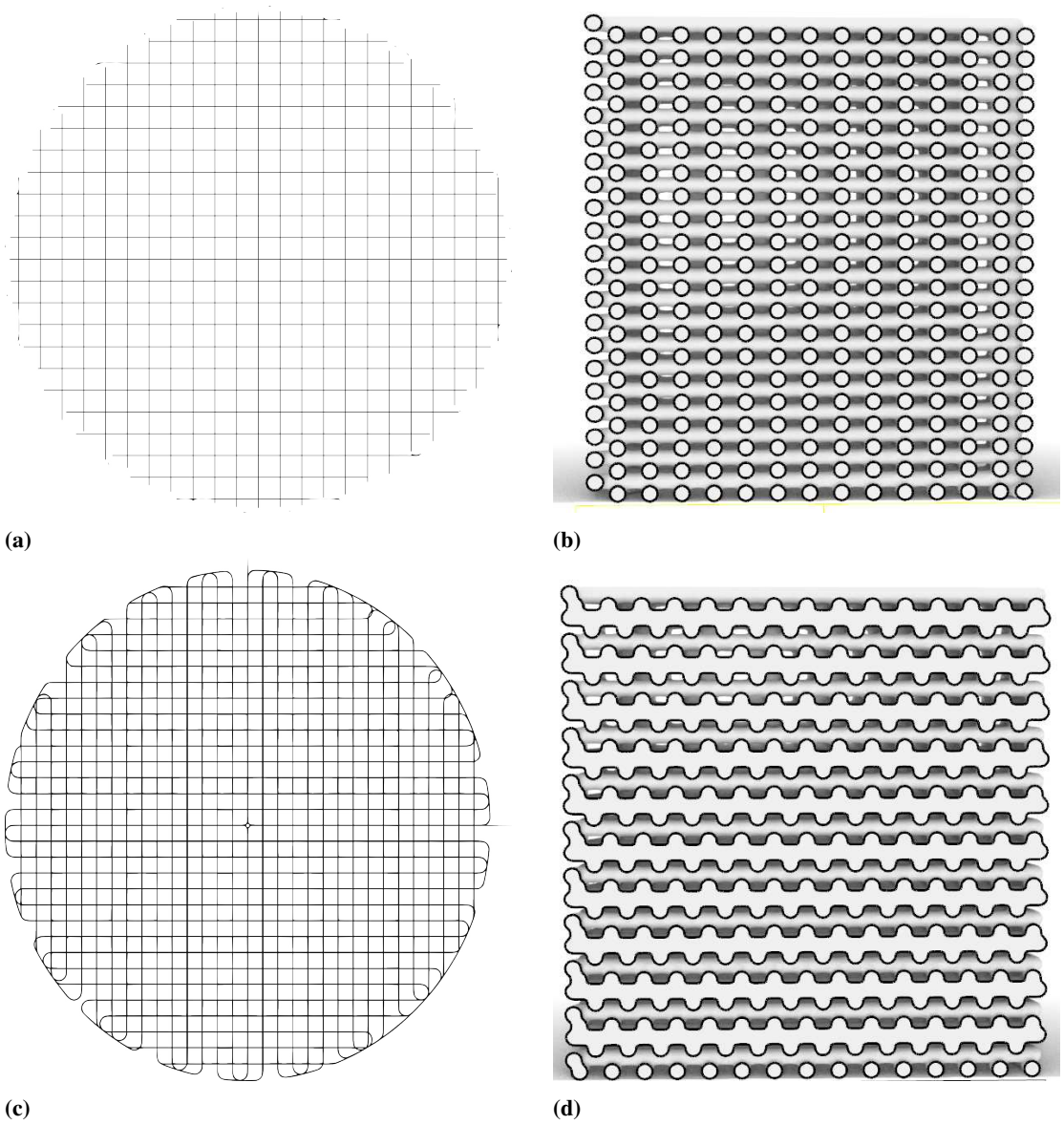

Figure 2.1: *Examined Geometry: (a) Linear Frontal Perspective, (b) Linear Cross-sectional View , (c) Shifted Frontal Perspective, (d) SHiftedCross-sectional View*

2.3.4 Characterization

The specific surface area (SSA) of the scaffolds curshed was determined by multi-point Brunauer, Emmett, Teller (BET) method with Quantachrome Autosorb iQ (Quantachrome Instruments, Boynton Beach, Florida), with a degassing temperature of 120°C for approximately 16 h under reduced pressure and analysis by N_2 adsorption at liquid nitrogen temperature.

The microstructure was assessed by means of a field emission scanning electron microscope (Sigma FESEM, Carl Zeiss).

Permeability tests were conducted on two distinct geometries: linear and shifted, both of which were utilized in the adsorption processes of carbon dioxide and clenbuterol. These tests were performed within a steel cylinder measuring 0.049 m in length and 0.02 m in diameter. Pressure sensors were strategically positioned at both the top and bottom of the cylinder. These sensors were interfaced with an Arduino system, which facilitated the conversion of analytical measurements into digital data. Subsequently, this digital data was processed and analyzed using Excel.

2.3.5 CO_2 adsorption tests

Figure 2.2 reports a visualization of the system implemented for the carrying out of the carbon dioxide adsorption studies.

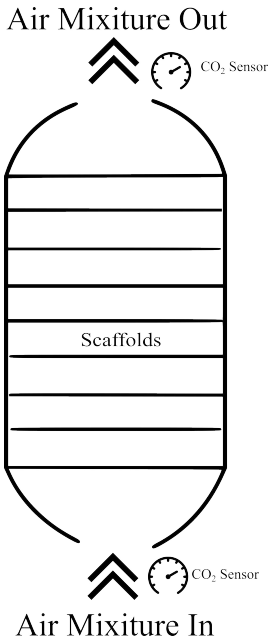

Figure 2.2: *CO_2 adsorption schema*

The Geopolymer and Geopolymer and Zeolites scaffolds with a diameter of 25 mm were introduced into the column. Subsequently, an air mixture, containing two distinct carbon dioxide concentrations (10 and 20%), was introduced from the bottom of the

column, under two different inlet velocities (5 and 12 cm/s). A sensor, strategically positioned at the top of the column, was utilized to quantify the concentration of air at the column's outlet. The data obtained from this experiment enabled to plot the back-through curves, which were then compared with the performance of granules analyzed in chapter 1.

2.3.6 Clenbuterol adsorption test

To study the adsorption kinetics, geopolymer specimens first underwent multiple rinses with deionized water. During these rinses, the pH of the resultant solution was consistently gauged using litmus paper until it stabilized at a pH level of 7. This step was imperative due to the inherent tendency of geopolymers in aqueous solutions to increase the pH. This phenomenon can be attributed to the availability of Na^+ or K^+ and OH^-. This availability is directly linked to the porous structure of the geopolymer and its ion exchange abilitiy (Longhi et al., 2019). When exposed to water, these alkali entities have a propensity to form hydroxide species, leading to an elevation in pH levels. An initial CLB (Sigma Aldrich) solution was formulated by taking a 5 ml sample of a 0.902 mM CLB solution in milliQ water and diluting it with an additional 20 ml of milliQ water. This resulted in a final volume of 25 ml, with a CLB concentration set at 50 mg/L (0.18 mM). For the adsorption assay, 3 g of geopolymer, equivalent to a single printed scaffold, was mixed with 20 ml of milliQ water and 5 ml of the aforementioned 0.902 mM CLB solution. This combination produced a 25 ml solution, preserving a CLB concentration of 50 mg/L (0.18 mM). The prepared solutions underwent agitation in an orbital shaker, operating at 150 rpm and maintained at 25°C. The adsorption trials were conducted at sequential timeframes of 5, 15, 30, 60 and 180 min. Following the agitation process, aliquots from these solutions were retrieved and subsequently subjected to HPLC-UV analysis. A supplementary set of experiments was undertaken using milliQ water, facilitated through a controlled-flow syringe pump. This involved a geopolymer, which was 3D printed with an altered compositional makeup. The sy-

ringe was primed with 20 mL of a CLB solution at a concentration of 50 mg/L in milliQ water. Notably, an initial 2 mL, considered as the dead volume, was systematically discarded. The subsequent elution process was calibrated to a flow rate of 0.1 ml/min, ensuring the collection of a 3 mL sample post the 30-minute mark. Sequential adsorption assays were carried out in milliQ water, wherein solution fractions were methodically extracted from the syringe at designated intervals of 10, 20, 30 min and 1 and 3 h, followed by their respective analyses.

For the evaluation of the adsorption isotherm, the geopolymer specimens underwent the same rinsing processes as the previous set of samples. Subsequently, an array of solutions was formulated, each with distinct pollutant concentrations: 20, 50, 100, 200, and 500 mg/L. These solutions were subjected to agitation in an orbital shaker for a span of 3 hours, operating at 150 rpm and maintained at 25°C. Subsequent to the agitation phase, aliquots from these solutions were retrieved and then subjected to HPLC-UV.

2.4 Results and Discussion

2.4.1 BET analysis

Table 2.1 presents the specific surface area (SSA) data, as determined by the BET analysis, for the pure zeolite 13x powder, two distinct optimized compositions of the geopolymer and zeolite ink, as well as the refined geopolymer ink in its pure form.

Table 2.1: *SSA data for zeolite 13x powders, Geopolymer ink and Geopolymer + 13x with 1 and 2 wt% addition of carbon methyl cellulose (CMC).*

Sample Name	BET (m^2/g)
13x Powders	359.23
GP SCaffolds	99.67
GP + 13x (1% CMC)	212.08
GP + 13x (2% CMC)	190.49

As described in Section 2.3.1, the formulation of ink with up to 60 wt% zeolites necessitates the inclusion of a modest amount of carboxymethyl cellulose (CMC). This serves dual purposes: acting as a dispersing agent and ensuring water retention to mitigate potential phase separation during the printing phase. Specifically, two ink compositions were optimized, subsequently printed, and their surface areas evaluated. It can be noticed in Table 1, that an increasing in the CMC concentration corresponded to a reduction in the specific surface area (SSA), as expected. This is suboptimal, as a greater surface area directly correlates with enhanced adsorption capacity of the materials. For carbon dioxide adsorption, the mechanism is predominantly physisorption (Minelli et al., 2018; Papa et al., 2021), making the accessibility of the matrix pores paramount to maximize the adsorption potential of our materials. Analogously, in the context of clenbuterol, existing literature has extensively elucidated that the adsorption mechanism of geopolymers, especially in the presence of cations, is predominantly governed by cation exchange (Franchin et al., 2020; Zhang et al., 2023). This accentuates the criticality of ensuring optimal pore accessibility. Given these insights, we resolved to fabricate all samples with a mere 1 wt% of CMC in the composition, despite this leading to a marginally more complex printing procedure. Reducing the CMC concentration implies that the mixing process must adhere to stringent controls to circumvent potential aggregate formation, which could obstruct the nozzle and compromise the printing process.

2.4.2 SEM analysis

Figure 2.3 shows the SEM micrographs of the fracture surfaces captured at diverse magnifications. At the lowest magnification, the filament exhibits a limited degree of closed porosity, a consequence of air bubbles becoming entrapped within the viscous inks. One method to mitigate the occurrence of these undesired air bubbles is through defoaming. However, given the swift initiation of polycondensation due to the heat generated by the mixer motor, defoaming isn't always feasible prior to printing. This makes

the presence of such closed porosity somewhat inevitable without the intervention of specialized apparatus. Predictably, upon closer inspection at elevated magnifications, the geopolymer matrix bears a visual resemblance to both the matrix of geopolymer granules and the overarching geopolymer structure. Notably, the lamellar formations, particularly evident in Fig.2.3c, are ascribed to the inclusion of bentonite, which is introduced to enhance the pseudoplastic behavior of the geopolymer, making it more suitable for 3D printing applications

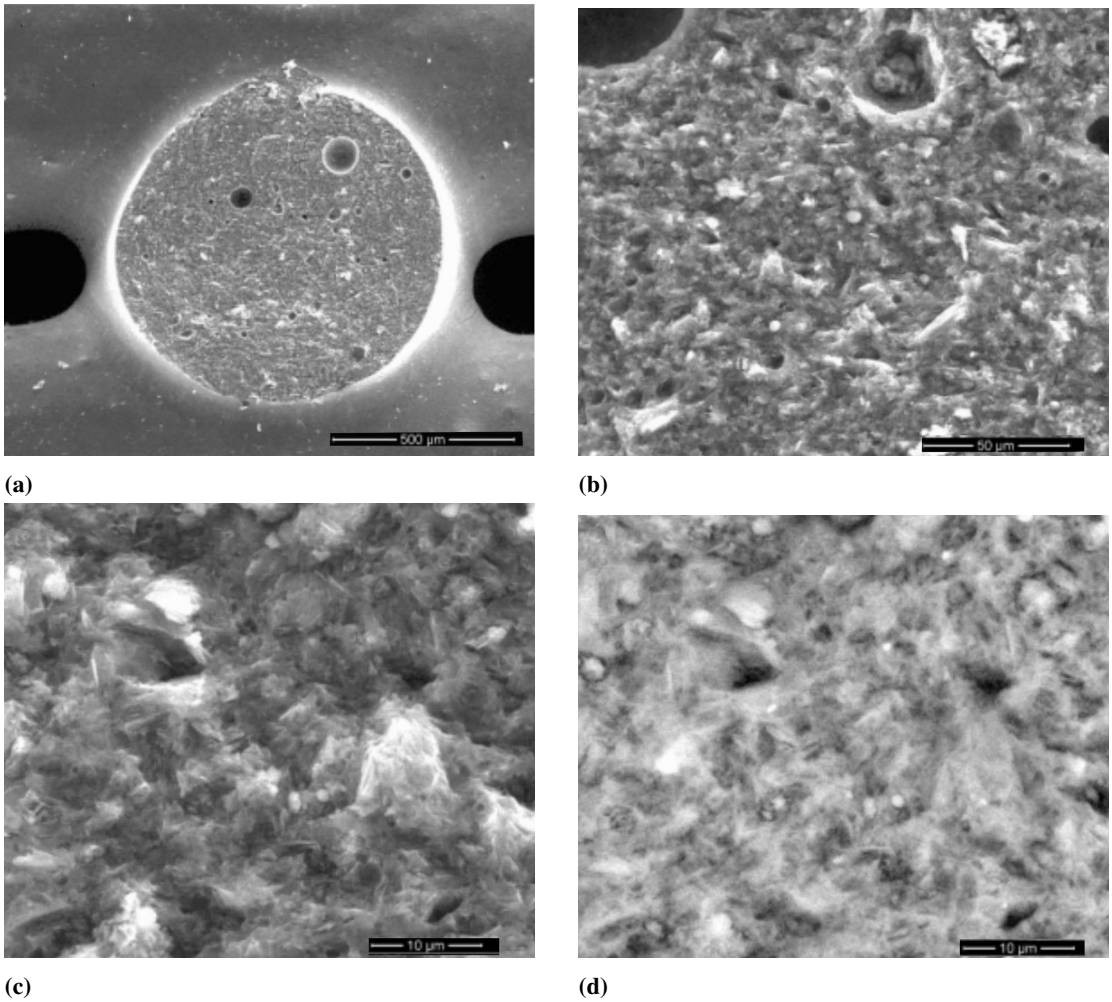

(a) **(b)**

(c) **(d)**

Figure 2.3: *SEM micrographs for GP13 showing the fracture surface of a filament at 100x magnification (a), 800x magnification (b), 2000x magnification (c) with associated BSE mode (d).*

Figure 2.4 displays the SEM micrographs of the combined geopolymer and zeolite scaffolds. Within Fig.2.4a, the zeolite 13x powder is shown, showcasing its characteristic cubic morphology. Echoing observations from the preceding figure, the fila-

ments exhibit closed porosity, a consequence of the inevitable entrapment of air bubbles within the ink, attributable to its high viscosity. Observations from Fig.2.4b and 2.4c distinctly highlight the zeolite (comprising 60 wt% by weight) as the predominant constituent within the filament's matrix. Nonetheless, the surrounding geopolymer matrix remains discernible, encapsulating the zeolite powder.

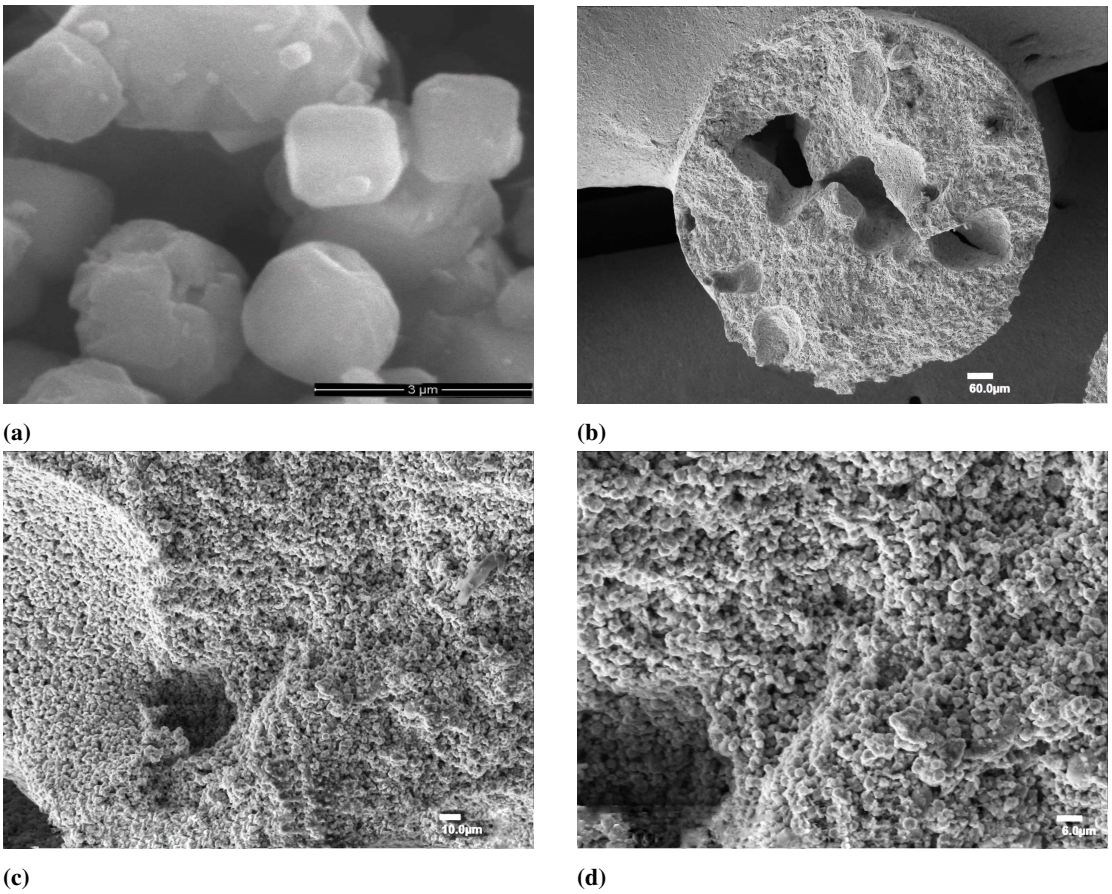

Figure 2.4: *SEM micrographs for (a) zeolite 13x initial powder and GP+13X showing the fracture surface of a filament at 100x magnification (b), 800x magnification (c), 2000x magnification (d). .*

2.4.3 Permeability test

In the realm of porous media, laminar fluid flow can be characterized by Darcy's law (Nield et al., 2017). This law is mathematically represented as:

$$\frac{\Delta P}{L} = \frac{\mu}{k_1} \cdot v_s \tag{2.2}$$

Within this framework, the pressure differential, ΔP, spanning a length L, is directly proportional to the fluid's velocity, denoted as v_s. This relationship is modulated by the dynamic viscosity, μ, and the intrinsic permeability of the porous medium, symbolized as k_1. However, at elevated velocities, it becomes imperative to account for the inertial effects stemming from turbulent flow. This necessitates the application of Forchheimer's equation.

$$\frac{\Delta P}{L} = \frac{\mu}{k_1} \cdot v_s + \frac{\rho}{k_2} \cdot v_s^2 \tag{2.3}$$

where ρ indicates the fluid density and k_2 represents the inertial permeability. Furthermore, in scenarios involving compressible flow, the pressure differential is expressed as:

$$\Delta P = \frac{P_{in}^2 - P_{out}^2}{2P_{out}} \tag{2.4}$$

Consequently, one can employ a polynomial regression to ascertain the two permeability coefficients that are intrinsically dependent on the structure (Erić et al., 2011). For the distinct geometries, namely linear and shifted, the coefficients k_1 and k_2 are comprehensively tabulated in Table 2.2.

Table 2.2: *k1 and k2 coefficients for the linear and shifted geometry*

Geometry	k_1	k_2
Linear	4.88E-09	3.59E-04
Shifted	2.52E-09	3.48E-04

Referring to Table 2.2, it is evident that the shifted geometry leads to a decreased permeability in comparison to its linear counterpart. This suggests that, under laminar flow regimes, the shifted geometry inherently possesses reduced permeability. Conversely, under turbulent conditions, it presents decreased flow resistance. It is pertinent to note that the CO_2 adsorption tests were conducted under laminar conditions. As illustrated in Figure 2.1d, the internal architecture of the shifted geometry is notably more

tortuous compared to that of the linear configuration. Given this structural intricacy, it is logical to infer that the shifted geometry would exhibit increased resistance leading to longer contact times between fluid and solid, potentially enhancing its carbon dioxide adsorption capacity. A detailed analysis and interpretation of this phenomenon will be articulated in the ensuing sections, which discuss the results of the carbon dioxide adsorption tests.

2.4.4 CO_2 adsorption

In this particular instance, the adsorption tests yielded what are termed as "breakthrough curves". An in-depth discussion on this topic is presented in Chapter 1, Section 1.3.4. Table 2.3 summarizes the CO_2 adsorption results for both geometries (linear and shifted) for both geopolymer matrix and geopolymer with 60 wt% of zeolite 13x.

Table 2.3: *Breakthrough time (t_b), saturation time (t_s) and mass of carbon dioxide adsorbed (CO_2 adsorbed).*

Sample Name	t_b (s)	t_s (s)	CO_2 adsorbed (g)
GP_linear_10% [u5]	13	23	6.82
GP_linear_10% [u12]	9	22	7.6
GP_linear_20% [u5]	14	24	8.18
GP_linear_20% [u12]	7	19	9.23
GP_Shifted_10% [u5]	13	23	8.28
GP_Shifted_10% [u12]	7	19	9.06
GP_Shifted_20% [u5]	12	22	9.77
GP_Shifted_20% [u12]	8	20	11.22
GP13x_linear_10% [u5]	43	55	31.75
GP13x_linear_10% [u12]	40	54	34.84
GP13x_linear_20% [u5]	45	59	40.05
GP13x_linear_20% [u12]	41	53	45
GP13x_Shifted_10% [u5]	46	59	41.87
GP13x_Shifted_10% [u12]	39	55	48.16
GP13x_Shifted_20% [u5]	47	66	49.84
GP13x_Shifted_20%[u12]	43	65	56

An analysis of the data presented in the table reveals a discernible influence of the geometry factor on both the geopolymer and the combined geopolymer-zeolite ma-

trix, culminating in an approximate 25% increase in CO_2 adsorption capacity for the shifted geometry. This observation is conceivably attributable to the permeability test outcomes, which indicate that the shifted geometry imposes greater resistance to fluid passage under laminar flow conditions. Such resistance increases the time of interaction between the air and the solid matrix, thereby enhancing the adsorption process. In the context of the geopolymer matrix, both t_b and t_s exhibited close values, suggesting a swift saturation process. This is probably linked to the carbonation reaction mechanism that takes place on the external surface, leading to pore obstruction and subsequently hindering the continuation of the physisorption mechanism. Further insights into this reaction can be found in Chapter 1, Section 1.3.4 of this thesis.

The incorporation of zeolite within the matrix consistently yields positive outcomes, as corroborated by the findings related to the geopolymer and zeolite granules delineated in Chapter 1. This integration amplifies the adsorption potential inherent to the geopolymer alone. Analogous to the granular scenario, the geopolymer matrix acts as a reservoir, prolonging the saturation point of the zeolite, thereby enhancing the zeolite's overall efficacy.

For a comprehensive juxtaposition of the printed structures and granules, Figure 2.5 selectively showcases the most optimal outcomes observed for both granular and scaffold configurations.

In the presented figure, the label "gr" denotes granules, whereas those without this label represent 3D-printed structures. The symbol "x" refers to samples made of geopolymer and zeolite, while "Ax" signifies APTES functionalization, with "x" indicating the APTES quantity as elaborated in Chapter 1. Notably, when considering solely the geopolymer matrix, both granules and 3D-printed structures exhibit nearly similar results. However, the geometry factor's influence slightly enhances the CO_2 adsorption capacity in the 3D-printed structures. A significant improvement in performance is evident when examining the combined geopolymer and zeolite matrix. It's crucial to recognize that the zeolite content in the 3D-printed structure (60 wt%) substantially

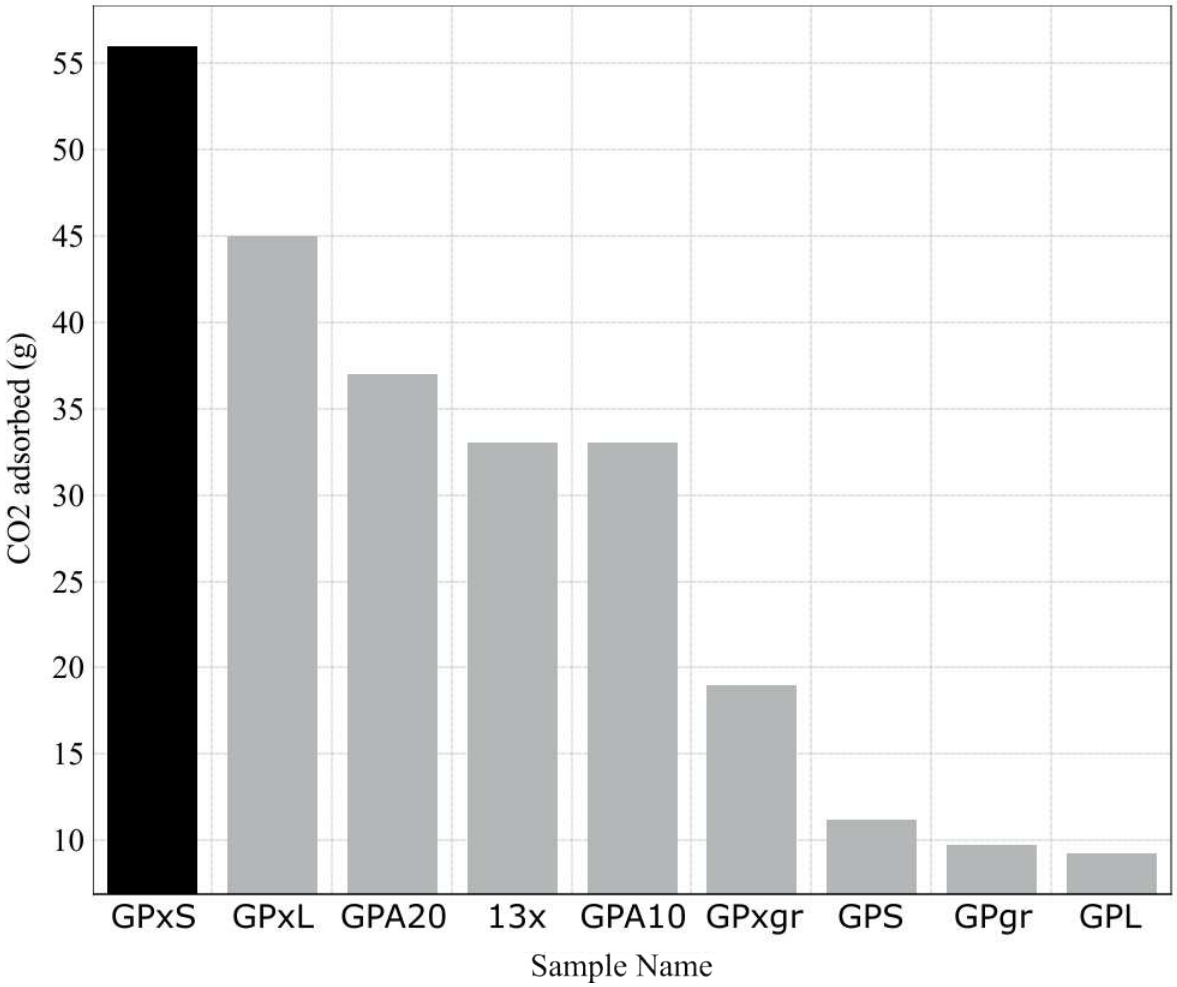

Figure 2.5: *Comparative illustration of CO_2 adsorption capacity between 3D-printed structures and granules.*

exceeds that in the granules (20 wt%), explaining the former's enhanced adsorption capability. This underscores that, in the DIW process, controlling the zeolite content (and other additives) in the matrix is more manageable since it's not process-dependent; the powders are simply mixed with the geopolymer. In contrast, granulation is heavily process-dependent, as discussed in Chapter 1, particularly when addressing powder wettability.

Observing the 13x, which acts as a benchmark, it is clear that both linear and shifted geometries for the geopolymer and 13x matrix surpass the benchmark values. This underscores the potential of these materials and the associated process for commercial applications in carbon dioxide adsorption.

2.4.5 Clenbuterol adsorption

Figure 2.6 presents the clenbuterol adsorption outcomes for the 3D geopolymer scaffolds featuring the shifted geometry, juxtaposed against the benchmark—commercially available activated carbon (PAC).

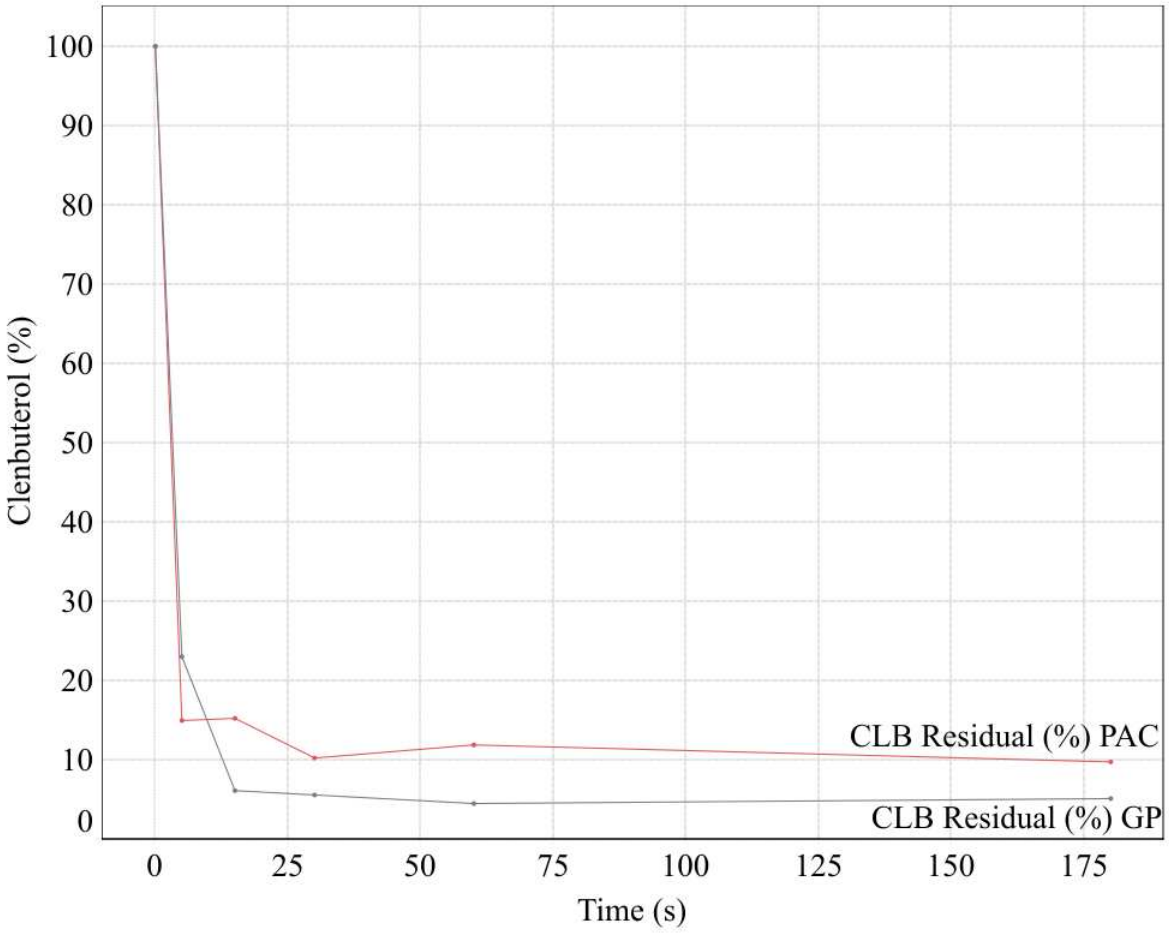

Figure 2.6: *Comparative analysis of clenbuterol adsorption in milli-Q water between Geopolymer with shifted geometry and commercially available activated carbon pellets (PAC).*

Figure 2.6 illustrates that, initially (within the first 5 seconds), PAC demonstrates a marginally superior adsorption efficiency. Specifically, the clenbuterol percentage decreased to 15% for PAC, whereas it reached 23.5% for the geopolymer structure. Nevertheless, post this initial phase, the geopolymer showcases a superior overall adsorption capability, reducing clenbuterol levels to approximately 5%, whereas PAC does not drop below 10%. Within the initial 3 hours, the geopolymer exhibits a peak clen-

buterol adsorption of 47.5 mg/L, corresponding to an adsorption efficiency of approximately 95%. These findings are particularly remarkable given the cost-effectiveness of geopolymers (priced at 1 euro per kilogram). Utilizing a DIW methodology, these geopolymers can be printed and molded into a vast array of geometries, rendering them suitable for a plethora of systems. The adsorption behavior of clenbuterol in our 3D printed geopolymer samples, when interpreted through the lens of a second-order kinetic model, offers several pivotal insights. The model suggests that the rate of clenbuterol adsorption is closely tied to the square of the number of unoccupied sites on the geopolymer surface. This could potentially indicate interactions between two clenbuterol molecules or between clenbuterol and specific active sites on the geopolymer during the adsorption process (Akpen et al., 2018). The mathematical representation of the second-order kinetic model is provided below:

$$\frac{t}{q_t} = \frac{1}{k_2 q_e^2} + \frac{t}{q_e} \tag{2.5}$$

Where:

- t is the time of adsorption
- q_t is the amount of solute adsorbed at time t
- k_2 is the second-order rate constant of adsorption
- q_e is the equilibrium adsorption capacity, i.e., the amount of solute adsorbed at equilibrium

To visually demonstrate the alignment of our data with the second-order kinetics, a graphical representation of the adsorption behavior is depicted:

This graph underscores the fit of our experimental data to the second-order kinetic model, emphasizing the chemisorptive nature of the adsorption process (An, 2011). While the second-order model aptly describes our observed data, it's essential to approach this interpretation with caution. The fit to this model doesn't exclusively confirm

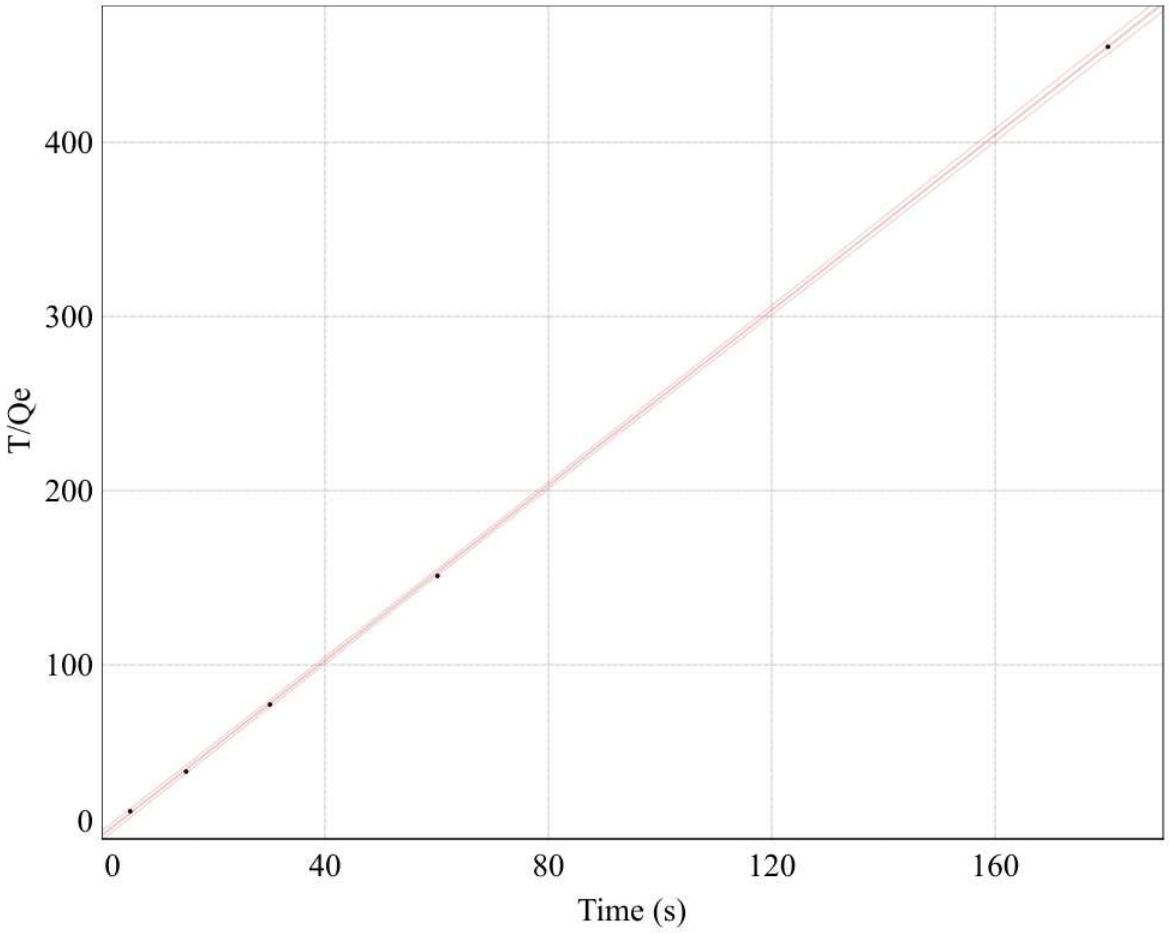

Figure 2.7: *Graphical representation of clenbuterol adsorption data aligned with the second-order kinetic model*

a chemisorptive process, and other kinetic models and experimental evidence should be considered when interpreting the underlying mechanism. Of practical significance, the geopolymer's congruence with the pseudo-second-order model might be attributed to diffusion-based mechanisms, especially given the unique 3D printed structure of the samples. This suggests that the geopolymer's structure plays a pivotal role in enhancing clenbuterol adsorption, offering potential avenues for further optimization (Hubbe et al., 2019).

Figure 2.8 presents the clenbuterol adsorption outcomes under flow conditions in the syringe. This methodology is designed to simulate a real-world continuous flow process scenario.

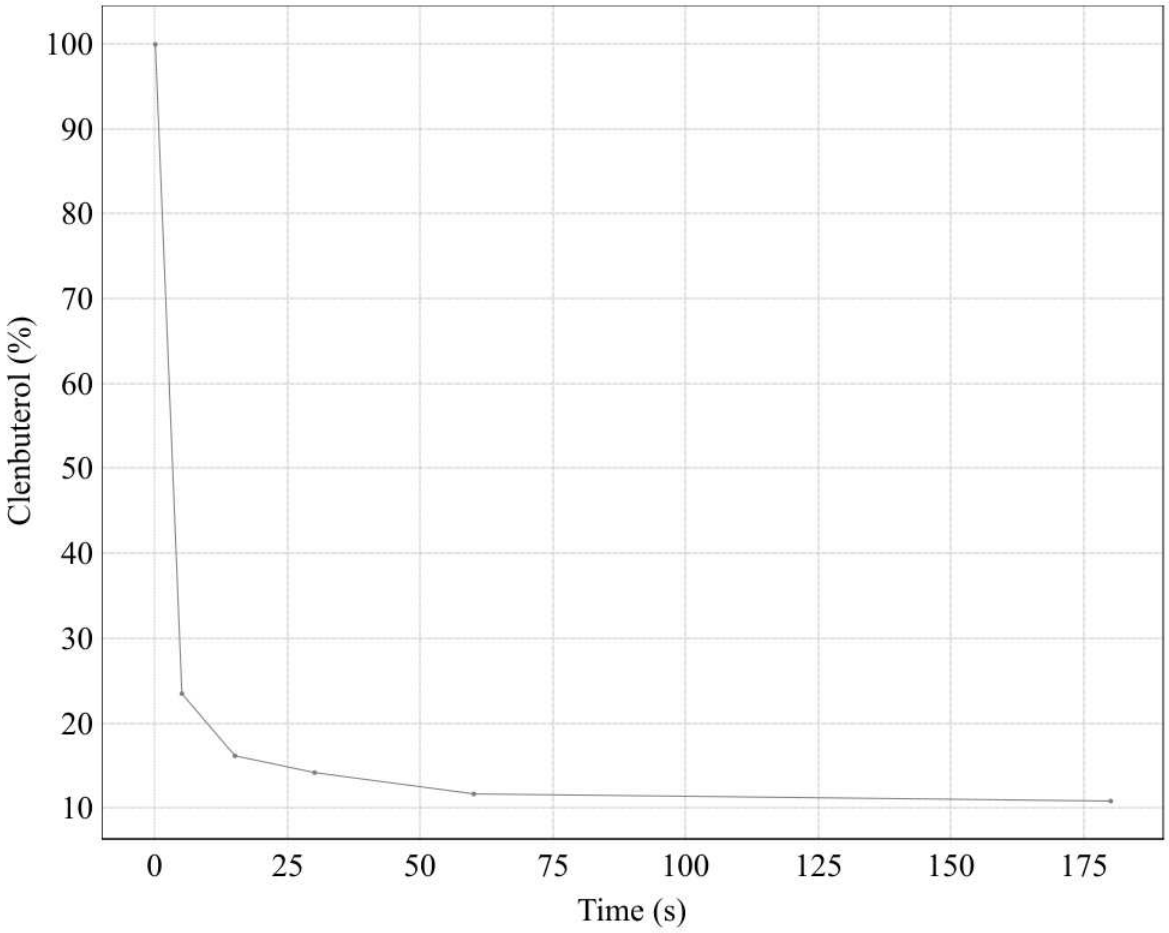

Figure 2.8: *Adsorption data of clenbuterol on geopolymer scaffolds under regulated continuous flow conditions.*

In this instance as well, the geopolymer demonstrates notable adsorption potential, achieving up to 87.4% clenbuterol adsorption in a span of 30 minutes, corresponding to an adsorption rate of 46mg/L.

Extended tests were conducted over durations up to 24 hours. Over these prolonged periods, a marginal increase in clenbuterol concentrations was observed. This rise is likely attributed to residual alkali from the sample's washing pretreatment. This alkali surplus may elevate the solution's pH, prompting the release of clenbuterol from the geopolymer matrix (refer to the chemical reaction 2.1). Notably, this phenomenon was absent in continuous flow tests. Addressing this issue might involve more thorough hot water rinsing of the sample to ensure deeper cleaning. Alternatively, adjusting the

geopolymer's chemical formulation to have an alkali deficit (K_20/Al_2O_3 <1) could be beneficial. As previously documented, this approach effectively mitigated geopolymer efflorescence (Simão et al., 2021), a condition known to arise from excessive alkali presence (refer to Chapter 1).

2.5 Conclusions

In summary, this study effectively employed the Direct Ink Writing (DIW) method to fabricate both geopolymer and geopolymer-zeolite structures, exploring two distinct geometries: linear and shifted. The findings underscore the significant influence of geometry on performance, with enhancements observed up to 25%. The DIW technique offers superior control over the zeolite content in the composition, in contrast to the granulation method where zeolite incorporation within the geopolymer matrix is heavily process dependent. Notably, geopolymers containing 60%wt of 13x showcased exceptional carbon dioxide adsorption capacities, outperforming standard 13x granules. Specifically, the shifted geometry recorded a carbon dioxide adsorption rate 40% higher than the benchmark. These outcomes hold substantial promise for the successful commercialization of such products. However, a primary challenge remains scaling up the DIW process for industrial applications.

In the context of clenbuterol adsorption tests, the obtained results highlighted a remarkable adsorption capability, surpassing the benchmark set by activated carbon pellets (PAC). Additionally, flow-controlled continuous tests, which emulate real-world scenarios, further affirmed the potential and promise of geopolymers in such applications. Future research endeavors will focus on refining the sample's geometry to further harness the material's inherent high adsorption capacity. Concurrently, efforts will be directed towards optimizing the sample's pretreatment to mitigate leaching, potentially achievable through compositional adjustments.

CHAPTER 3

Optimization of Geopolymer Membrane Production for Enhanced Microplastic Adsorption

3.1 Abstract

A groundbreaking use of geopolymer for microplastic adsorption has been explored. Leveraging a warm press technique, geopolymer membranes were fabricated in less than 30 minutes. This study investigated the effects of process parameters such as pressure and temperature on the membrane properties. Membrane characterization was conducted using the Ball on Three Balls test (BRB) to assess compressive strength, and mercury porosimetry was used for evaluating surface area, pore volume, and total porosity. Following these analyses, two optimal combinations of pressure and temperature were identified that offered a balance between porosity, surface area, and compres-

sive strength. Membranes produced under these conditions were subjected to microfiltration tests with pure water. The study further explored the impact of fluid pressure and temperature on permeability. Preliminary data suggest that our membranes perform optimally at 10 bar and 50°C. Current tests are assessing the size of microplastic particles these membranes can intercept, aiming to establish the potential of these materials, manufactured via this approach, to address the pressing environmental issue of microplastic pollution in contemporary society.

Keywords: Geopolymers; Membranes; Microplastics

3.2 Introduction

Microplastics, polymeric particles with sizes ranging from 1 μm to 5 mm, are either of primary or secondary origin and can have regular or irregular shapes (Frias & Nash, 2019; Prata, 2018). These small plastic fragments are often detrimental to aquatic life. Primary microplastics are found in many personal care and cosmetic products, while secondary ones originate from various sources, including the degradation of larger plastic debris into smaller pieces (Li et al., 2018). Microbeads from facial cleansers, toothpaste, and the numerous microplastic fibers released during washing are frequently discharged directly into wastewater (Cheung & Fok, 2017; Fendall & Sewell, 2009; Murphy et al., 2016a; Sun et al., 2019a; Ziajahromi et al., 2017a). These microplastics are collected in wastewater treatment plants (WWTPs), and untreated wastewater effluent has been identified as a significant source of microplastics in aquatic environments (Ali et al., 2021; Murphy et al., 2016b; Sun et al., 2019b; Ziajahromi et al., 2017b).

Given the vast quantities of microplastics produced, especially from activities like laundry where a single wash can release up to 236,000 microfibers, it's estimated that around 2.2 × 1018 synthetic fibers are introduced into aquatic systems annually, even after WWTP processes (Belzagui et al., 2019; Galvão et al., 2020; Napper & Thompson, 2016), primarily because conventional WWTPs aren't designed to retain microplastic

fibers (Talvitie et al., 2017a; Wu et al., 2021). Recent research suggests that mitigation should occur before these fibers even reach the WWTPs (Belzagui et al., 2020; Gavigan et al., 2020; Lv et al., 2019). Commercial devices, both in-drum and external filters, have been developed to capture microplastic fibers during laundry cycles, with efficiencies ranging from 21% to 87% (McIlwraith et al., 2019; Napper et al., 2020).

Studies have shown that membrane bioreactor (MBR) processes, especially those using polymeric microfiltration (MF) membranes with a nominal pore size of 0.4 μm, achieve the highest microplastic removal rate of 99.9% in full-scale WWTPs (Sun et al., 2019c; Talvitie et al., 2017b). However, the use of polymeric membranes can lead to secondary microplastic contamination due to the shedding of fibers from the membrane itself (Ding et al., 2021; Huang et al., 2020). As a result, alternative durable membrane materials, such as ceramic membranes, have gained popularity. These membranes offer higher water permeance, lower fouling propensity, and are increasingly used in various industrial wastewater treatments (Cha, Boo, & Park, 2022; Cha, Boo, Song, et al., 2022; Cha et al., 2020; Jeong et al., 2017; Kim & Park, 2022; Lee et al., 2022) .

The advancement in geopolymer technology has been significantly propelled by innovative fabrication techniques aimed at enhancing the mechanical and microstructural properties of geopolymers. Among these techniques, hot-pressing has emerged as a promising method, demonstrating substantial improvements in geopolymer densification and mechanical robustness.

In a pioneering study by Ranjbar et al. (Ranjbar et al., 2017) , the hot-pressing technique was utilized to fabricate fly ash-based geopolymer, achieving an impressive compressive strength of 134 MPa under optimized conditions of temperature, pressure, and duration. The study highlighted the crucial role of induced pressure in augmenting the mechanical attributes of the geopolymer. Similarly, another investigation by Ranjbar et al. (Ranjbar et al., 2018) elucidated the dual effects of temperature and curing time on the kinetics and mechanical properties of VA-based hot-pressing geopolymer. The findings revealed a notable improvement in the dissolution trends of aluminosilicates

with the increment in temperature and curing time, thereby accelerating the geopolymerization kinetics.

Furthermore, the study by Ranjbar et al. (Ranjbar et al., 2020a) explored the geopolymerization kinetics, microstructure, and mechanical performance under varying conditions of pressure and heat. The hot-pressing technique was shown to not only reduce the size and volume of porosity but also change the continuous pore network to a closed one, promoting higher geopolymer gel formation and accelerating polycondensation. On the other hand, Živica, Balkovic, and Drabik (Živica et al., 2011) delved into the effects of a low liquid/solid (l/s) ratio and pressure compaction on the properties of hardened metakaolin geopolymer paste, showcasing a highly dense nano- or near-nano-pore structure with a high degree of homogeneity and strength.

The collective insights from these studies underscore the transformative potential of the hot-pressing technique in geopolymer technology. The technique not only holds promise for enhancing the mechanical performance of geopolymers but also opens new frontiers in the development of geopolymer-based membranes and other innovative applications. The convergence of the hot-pressing technique with sustainable raw materials further accentuates its significance in the broader narrative of sustainable material technology.

In the 1970s, Davidovits (Davidovits, 1989, 2011) pioneered the concept of geopolymers, describing them as semicrystalline three-dimensional aluminosilicate materials. These innovative materials can be synthesized from various aluminosilicate sources, such as metakaolin, fly ash, or slag, when combined with an aqueous solution containing specific reactive agents. Their unique attributes, including low thermal conductivity, robust mechanical properties, and exceptional high-temperature stability, have garnered significant attention. Geopolymers, as ceramic materials, can be broadly categorized into two groups: purely inorganic and those containing organic components. These materials have significantly influenced both industrial and research sectors globally over the past 50 years or so. Their adaptability to diverse compositions suggests

their potential to pave the way for environmentally sustainable solutions. In the realm of civil engineering, for instance, geopolymer cement has emerged as a viable alternative to conventional Portland cement, offering not only similar functional benefits but also some enhanced properties. In particular, when compared with Ordinary Portland Cement (OPC) concrete, geopolymer concrete exhibits superior durability, especially under chemical assaults, a testament to its inherent chemical stability. This resilience suggests a promising trajectory for the development and adoption of geopolymer binder technologies in the future.

Today, the environmental applications of geopolymers have become a focal point of research and development. As amorphous aluminosilicates, these materials have demonstrated significant potential in addressing various environmental challenges. Their ability to adsorb noxious gases, effectively filtering out contaminants such as CO, CO_2, and NOX (Hassan et al., 2019), underscores their role in pollution control. Furthermore, the adaptability of geopolymers in waste management, particularly in the utilization of industrial byproducts like fly ash and steel slag, highlights their contribution to sustainable waste reduction and resource optimization. Their inherent properties, combined with their eco-friendly nature and low-energy manufacturing process, position geopolymers as promising materials for a range of environmental solutions, offering a sustainable alternative to more traditional approaches in the domain.

In this study, we introduce a novel method of geopolymer fabrication using hot pressing, offering a significant advantage in terms of production time, by enabling the creation of geopolymer membranes in under 30 minutes. The inherent porous matrix of geopolymers, combined with the ability to fine-tune this porosity through process parameters such as pressure, temperature, and composition, identifies geopolymers as a promising, cost-effective, and environmentally friendly alternative to plastic membranes for microplastic adsorption.

3.3 Experimental

3.3.1 Samples preparation

In this research, Metakaolin (Imerys, Argical 1200s) was combined with a sodium-based alkaline solution, comprising 13 wt% NaOH (VWR Chemicals) and 87%wt Na-Silicate (Supelco), to formulate a geopolymer mixture. This mixture consisted of 62 wt% Metakaolin and 38%wt of the aforementioned alkaline solution. The molar ratios were:

- SiO_2/Al_2O_3 = 3.1
- Na_2O/Al_2O_3 = 1
- H_2O/Al_2O_3= 4.86

The selection of this particular composition was influenced by prior experiments conducted by the research group at the University of Oulu, led by Prof. Tero Luukkonen. Their investigations aimed to ascertain the optimal geopolymer composition for warm pressing manufacturing processes, and this composition was identified as the most suitable. Due to time limitations, the decision was made to utilize this established composition for the current study.

The chosen liquid-to-solid ratio ensured that the geopolymer slurry remained contained within the mold under applied pressure. However, the relatively dry nature of the mixture posed challenges for conventional mixing techniques. For instance, utilizing a mechanical mixer, as employed for sample preparation in other chapters, proved to be unfeasible. Consequently, the mixing process was conducted manually, albeit with a consistent time allocation of 15 minutes for each preparation. Efforts were made to maintain a uniform mixing approach for every slurry, although some degree of human error was inevitable.

Following the preparation of the geopolymer mixture, it was transferred into a cylindrical steel mold with a diameter of 75 mm. Subsequently, the mold was positioned be-

tween the steel plates of a press (LABECON 300). Utilizing the integrated software of the press, the desired temperature and pressure settings for the plates were configured. For temperatures exceeding ambient levels, it was ensured that the plates attained the specified temperature before placing the steel mold within the press.

Due to time constraints, an in-depth examination of the effect of pressure duration was not conducted. Instead, a fixed pressure duration of 30 minutes was adopted, as recommended by the research group from the University of Oulu. In their prior investigations concerning the optimal geopolymer composition for this process, the group had determined that a 30-minute duration was sufficient to complete the geopolymerization process effectively.

3 samples were fabricated under varying temperature and pressure conditions. A comprehensive summary of all the tested conditions is presented in Table 3.1.

Table 3.1: *Summary of Temperature and Pressure Conditions Employed for Geopolymer Membrane Preparation*

Temperature (°C)	Ambient	75	150	250
Pressure (kN)	67	133	200	266

3.3.2 2.2 Characterization

Mercury porosimetry (Thermoquest, porosimeter 2000) was used for the determination of the specific surface area (SSA), Total Porosity (TP), Bulk Density, Apparent density and Averege Pore radius.

The microstructure was assessed by means of a field emission scanning electron microscope (Sigma FESEM, Carl Zeiss).

XRD (Rigaku SmartLab 9kW) and FTIR (Jasco FTIR6200) analyses confirmed the geopolymerization process's success. Notably, as seen in Figure 3.c, increasing the pressure decreased total porosity and reduced pore sizes, with larger pores for the 150°C samples. Mechanical tests indicated stronger samples at lower temperatures due to reduced pore sizes.

3.3.3 Compressive strength

Conventional strength tests primarily elucidate the failure behavior of materials under simplistic stress scenarios, typically uniaxial stresses. However, in real-world applications, mechanical loading often induces multiaxial stresses, necessitating the early development of experimental methods to assess strength and deformation behavior under such conditions (refer to ref.1 for an overview). Notable among these methods are the Ring-on-Ring Test (ROT) and the Balls on 3 Balls Test (B3B). While most strength tests demand high-quality specimen surfaces, the B3B test is an exception.

The Ring-on-Ring Test (ROT) operates on a principle where a disk-shaped specimen is supported by a ring and subjected to load by a concentric ring of smaller diameter (as illustrated in Figure3.1).

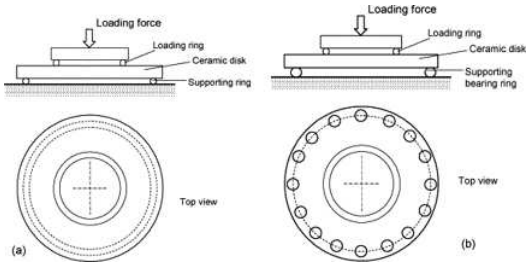

Figure 3.1: *Ring-on-Ring Test Schema*

This setup ideally engenders a well-defined stress state within the inner ring, contingent upon ideal loading conditions. However, achieving this requires highly plane parallel disk-shaped specimens; otherwise, a three-point contact between the ring and specimen may ensue, leading to undefined supporting conditions. An alternative adaptation is the Ball-on-3-Balls (B3B) configuration, where the outer ring is substituted with three balls, establishing statically well-defined conditions (Börger et al., 2002a; Godfrey & John, 1986). A schema of this test is given in Figure 3.2

Through this modification, the test aims to address the challenges associated with specimen alignment and surface quality, thereby providing a more accurate assessment of material behavior under multiaxial stress conditions. Through this innovative test methods, a more accurate representation of material behavior under multiaxial stress

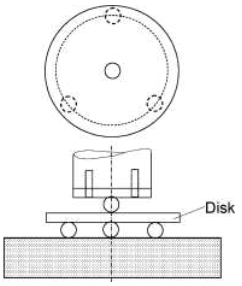

Figure 3.2: *Ball-on-3-balls (B3B) Test Schema*

conditions, akin to practical scenarios, can be achieved. The test was carried out in speed control at at 0.5 mm/s using a universal testing machine (Galdabini Quasar 25).

3.3.4 Permeability test

The permeability assessments were conducted utilizing a laboratory-scale P28 cross-flow membrane apparatus (CM-CELFA Membrantrenntechnik AG, Switzerland) as depicted in Figure 3.3.

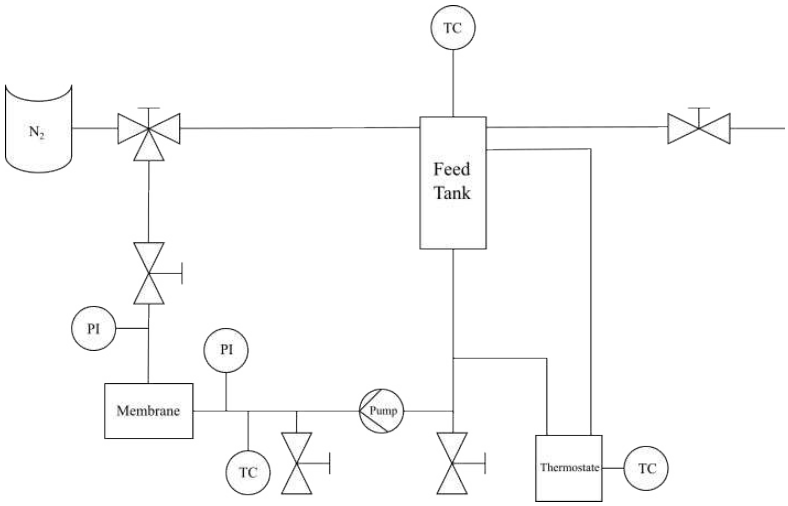

Figure 3.3: *FlowChart Schema of the permeability test conducted*

The effective membrane surface area measures 2.8 × 10-3 m2, with a maximum feed volume capacity of 500 mL. The apparatus functions in a batch operation mode, wherein the retentate is redirected to the feed tank, while the permeate is systematically extracted from the system. Temperature regulation of the feed solution was achieved through a Lauda Ecoline Staredition E 103 thermostatic unit. The circulation of the

feed stream was facilitated by a Scherzinger 3000 3B/M gear pump, integrated with a frequency converter. Fluid pressure modulation was accomplished utilizing liquid nitrogen. Each experimental run lasted for approximately 1 hour. Sample collections were carried out from the initial feed solution, intermittently (every minute) from the feed and permeate throughout the experiment, and subsequently from the residual feed solution post-experiment. The mass of the samples was quantified, and the permeate flux (J) was calculated utilizing the subsequent equation:

$$J = \frac{Volume_{Fluid}}{A \cdot t} \tag{3.1}$$

where:

- J is the flux (L/m^2h^{-1}) through the membrane
- The volume of the fluid (m^3), representing the collected permeate (in this instance, water), was ascertained by measuring its mass and subsequently dividing the mass value by the water's density value at the specific temperature at which the tests were conducted.
- The effective surface area of the membrane, denoted as A (m^2), was 0.0028.
- The variable t (h) represents the sampling time. In this study, given that samples were taken every minute, a value of 0.017 was utilized for t.

3.4 Results and Discussion

Prior to presenting the results of the characterization tests conducted, it is noteworthy to mention that it was not possible to achieve a successful production of membranes at 250°C for any given pressure. This was due to the severe damage sustained by the membranes at the conclusion of the process, if not their complete disintegration into pieces.

This phenomenon may be clarified by understanding that geopolymerization is a thermally activated reaction (Muñiz-Villarreal et al., 2011), which undergoes a poly-

condensation phase accompanied by water elimination (Khale & Chaudhary, 2007), subsequently leading to the formation of the characteristic porous matrix of geopolymeric materials. However, if the reaction proceeds too rapidly, the swift elimination of water could compromise the internal structure leading to the formation of cracks, thereby rendering the production of membranes under such conditions unfeasible.

The production of membranes at ambient temperature also proved to be unfeasible. This was attributed to the incomplete geopolymerization of the membrane by the end of the process, which resulted in membranes that lacked sufficient strength to be removed from the mould intact.

Conversely, membranes fabricated at 75 and 150 degrees Celsius were successfully prepared (refer to Figure 3.4a). Subsequent analysis was conducted using optical microscopy (Figure 3.4b) to identify any undetectable damage that might impact further characterization tests. No such damage was observed, hence the results for all characterization tests were exclusively performed on membranes produced at 75 and 150°C.

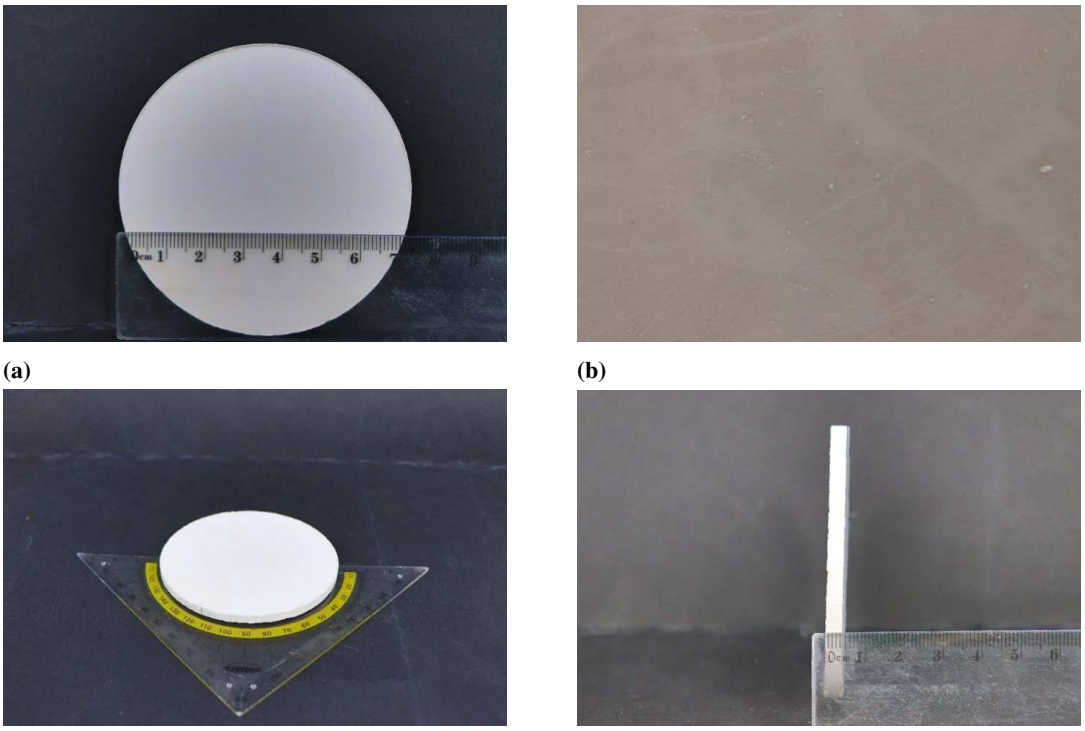

Figure 3.4: *Examination of the Fabricated Membranes: (a) Top-down View of the Membranes, (b) Optical Imagery of the Top Surface, (c) angular view and (d) thickness view*

3.4.1 XRD

Figure 3.5 illustrates the X-ray diffraction (XRD) analyses of the membranes fabricated at temperatures of 75 and 150°C under pressures of 67 and 266 kN. It is pertinent to mention that the results observed under intermediate pressure conditions (133 and 200 kN) are largely analogous, hence, for the sake of clarity, only the boundary conditions for each membrane are reported herein. The characteristic amorphous hump of the geopolymer is evident, with a notable peak around 32°, attributable to Anatase, a common occurrence in geopolymers (Muñiz-Villarreal et al., 2011; Wang et al., 2005).

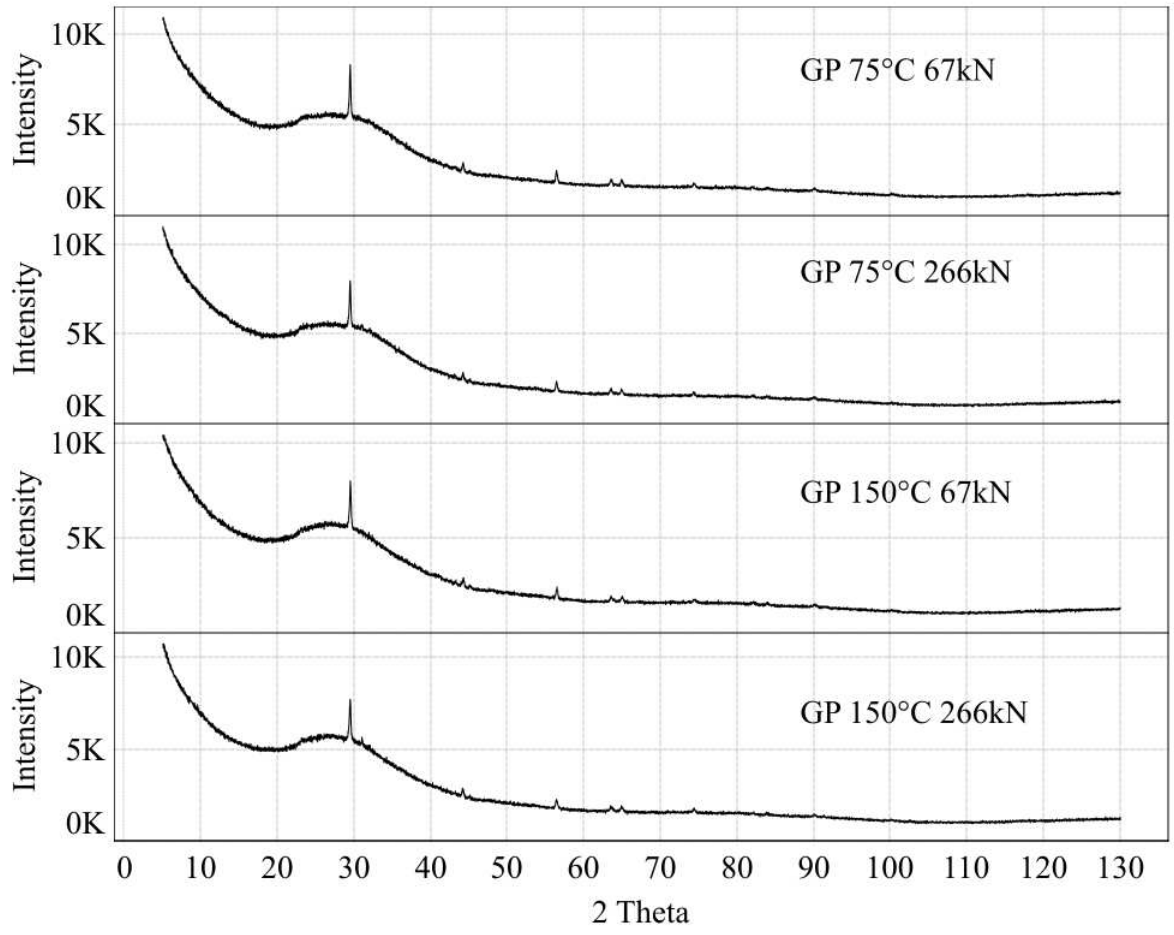

Figure 3.5: *XRD analysis of the membranes produced at 150 and 75 °C for pressure of 67 and 266kN*

3.4.2 FTIR

The most distinctive band is observed between 1500 and 1000 cm^{-1}, attributed to the asymmetric stretching of "X-O" bonds (where X denotes Si or Al), prevalent in the gel of hydrated sodium aluminosilicate. The prominence of this band primarily arises from the amorphous nature of the material, alongside the short-range ordering of Si and Al tetrahedra. Additionally, geopolymer materials often exhibit minor bands between 600 and 450 cm-1, associated with the bonds found in metakaolin (predominantly quartz). Another band, situated between 3400 and 3600 cm^{-1}, typically corresponds to the bonds present during geopolymer hydration, i.e., relating to water molecules within the material and in the NASH gel. These graphs align well with FTIR analyses documented in literature (Casarez et al.,2014), thereby confirming the realization of the geopolymerization reaction. To further substantiate this, a boiling test, a standard assay for evaluating the presence of a three-dimensional geopolymer network (Alloul et al., 2023; Matalkah et al., 2017; Seiffarth et al., 2013), was conducted, entailing the immersion of geopolymeric samples in hot water for a minimum of several hours. For a material to qualify as a geopolymer, the samples must endure this test unscathed. All tested membranes withstood the test, thereby confirming their geopolymeric nature.

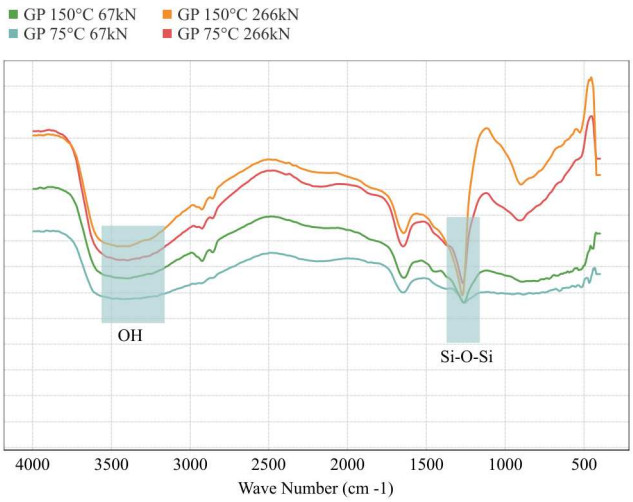

Figure 3.6: *FTIR analys results for membranes produced at 75 and 150°C and pressure of 67 and 266kN*

3.4.3 Porosity

Figure 3.7 shows the total porosity (%) and average pore radius (Å) for the tested membranes. We can observe that increasing the pressure for membranes fabricated at both 75 and 150°C results in a decrease in the average pore radius and total porosity. This phenomenon could potentially be ascribed to the enhanced densification of the materials, possibly owing to the consolidation of larger pores into smaller ones, under elevated pressure. This observation aligns with findings reported in other scholarly works (Ranjbar et al., 2020b). Concerning the temperature's influence, an increase in temperature results in an increase in both the average pore radius and total porosity. This is plausible given that, as previously noted, the geopolymerization reaction is thermally activated and undergoes polycondensation; hence, the additional energy supplied to the reactions expedites water expulsion from the matrix, culminating in larger pores.

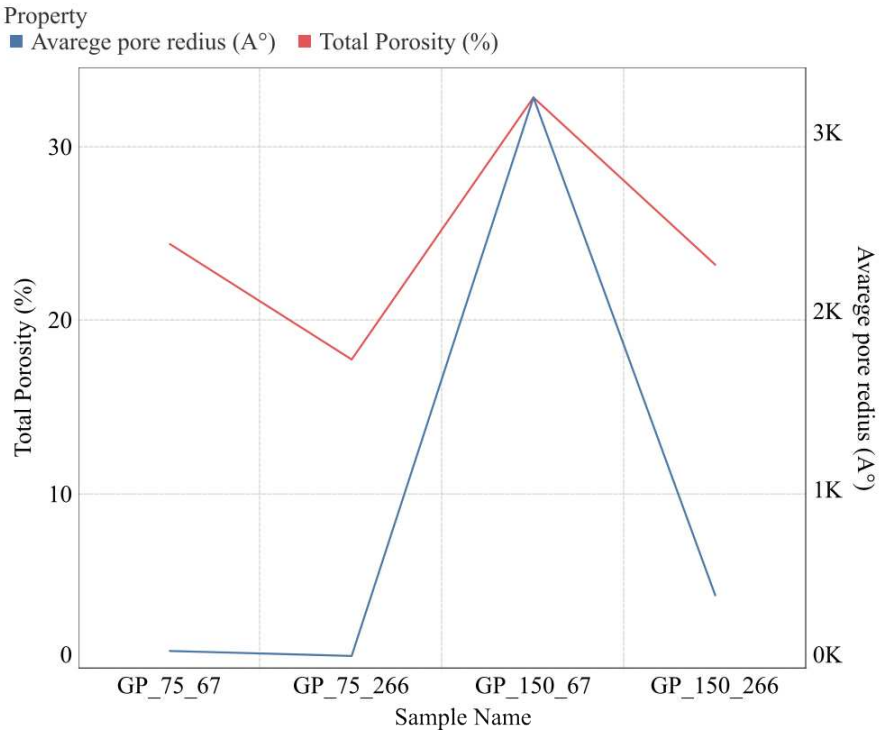

Figure 3.7: *Total Porosity (%) and Average pore radius (A°) for membranes produced at 75 and 150°C for pressure of 67 and 266kN*

3.4.4 BET

Figure 3.8 reports the Specific Surface Area (SSA) values of the examined membranes. In light of the observations from Figure 8, these results were somewhat anticipated. Specifically, both membranes fabricated at 75°C exhibited significantly higher SSA values, correlating with the smaller average pore radius observed. Intriguingly, an increase in pressure appears to adversely impact the SSA; however, the variance among membranes produced at identical temperatures cannot be definitively attributed to this factor due to the systematic errors inherent in the analysis. Consequently, the observed differences among membranes produced at the same temperature fall within the error margin of the analysis and therefore they should be regarded as nearly equivalent. This assertion is substantiated for membranes produced at 75°C, as their average pore radius values were markedly similar. On the other hand, membranes produced at 150°C display a more pronounced difference in average pore radius, yet the increased dimensions of the pores make the results of the BET analysis less accurate (Sing, 2001; Tan et al., 2012).

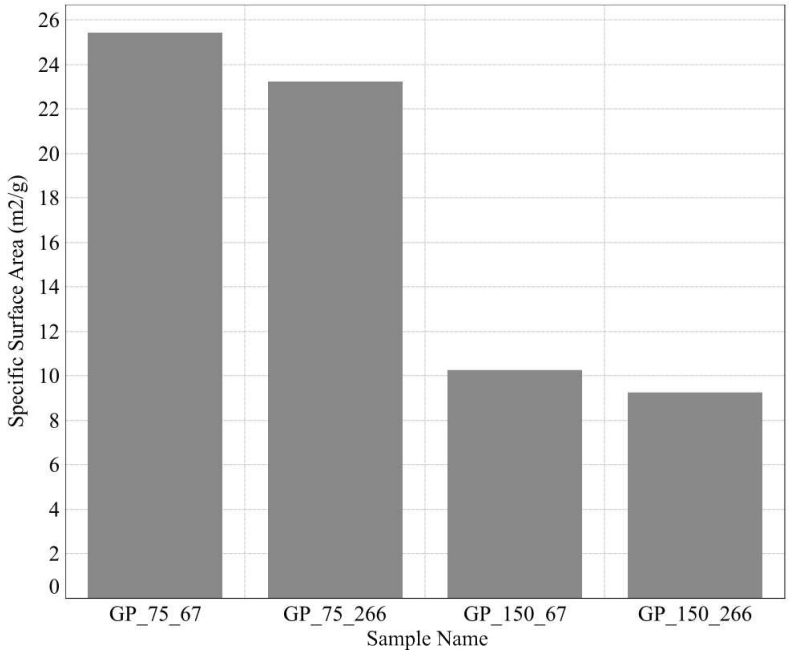

Figure 3.8: *Specific Surface Area (SSA) for the membranes produced at 75 and 150°C and 67 and 266kN*

3.4.5 SEM

Figure 3.9 presents the Scanning Electron Microscopy (SEM) images of the membranes fabricated at 75 and 150°C under pressures of 67 and 266 kN. We can observe that all the produced membranes exhibit a highly comparable microstructure, typical of geopolymers. This further corroborates the successful occurring of the geopolymer reaction.

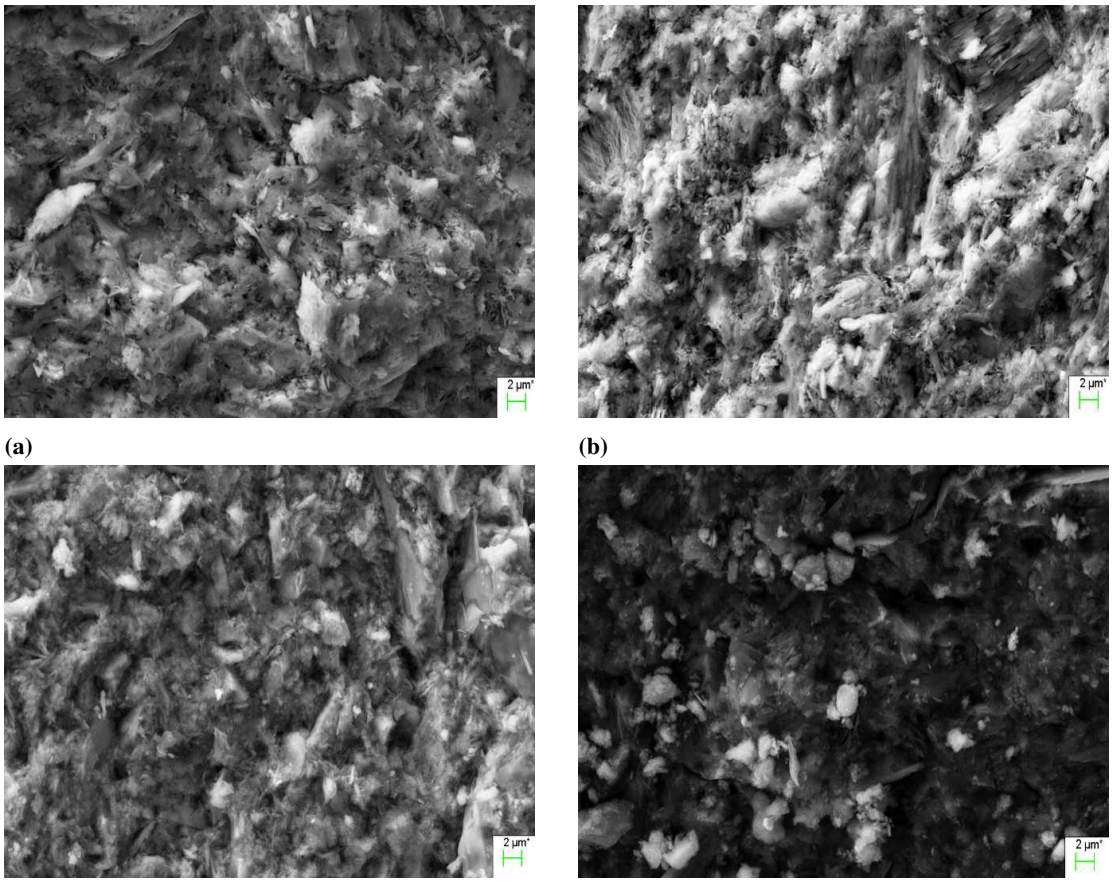

(a) **(b)**

(c) **(d)**

Figure 3.9: *SEM images of the membrane produce at (a) 75°C and 67KN, (b) 75°C and 266KN, (c) 150°C and 67KN and (d) 150°C and 266kN*

3.4.6 Mechanical test

The stress σ_{max} is given by:

$$\sigma_{max} = f(\alpha, \beta, \nu) \cdot \frac{F}{t^2} \tag{3.2}$$

where:

- F is the applied force
- t is the thickness of the disc
- f is a dimensionless factor namely the dimensionless maximum tensile stress which only depends on:
- $\alpha = \frac{t}{R}$ where R is the radius of the disk
- $\beta = \frac{R_a}{R}$ where R_a is the radius of the support
- ν is the poisson ratio of the geopolymer which was taken as 0.14 (Chouksey et al., 2022)

Figure 3.10 illustrates the stress field experienced by the samples throughout the testing phase.

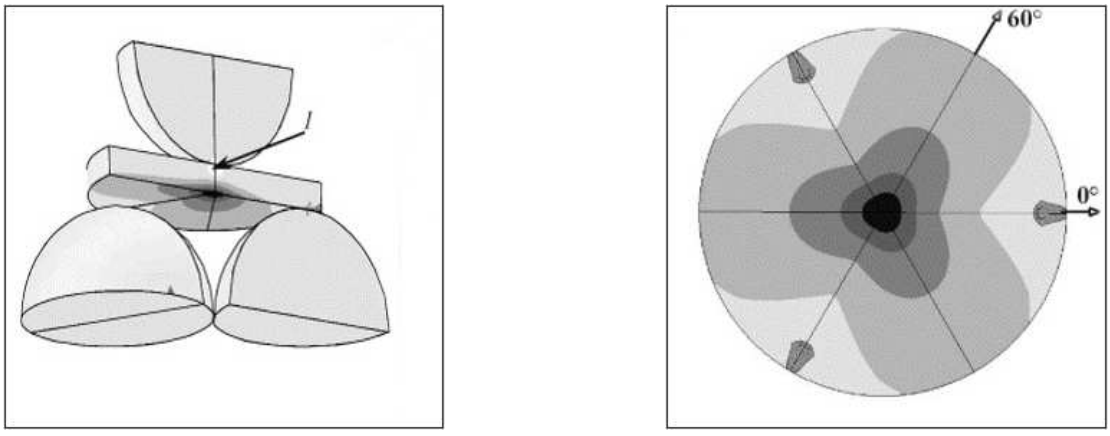

(a) **(b)**

Figure 3.10: *Stress distribution on the discs during the B3B test.*

As shown in Figure 3.10, the contact points between the supporting balls and the disc form an equilateral triangle. Consequently, the radius Ra can be determined using the following equation:

$$R_a = \frac{2\sqrt{3}}{3} \cdot R_b \tag{3.3}$$

where R_b is the radius of the balls, in our case 10 mm. Table 3.2 reports the values of the variables responsible for evaluating the factor f.

Table 3.2: *Value of the variables responsible for the adimensional factor f*

Variable	Value
α	0.08
β	0.31

According to Börger et.al (Börger et al., 2002b) these value range of α and β correspond to a value of f = 2.1. Utilizing this in Equation 3.2, calculations were carried out to determine the value of f = 2.1 for the tested membranes. The results are reported in Figure 3.11.

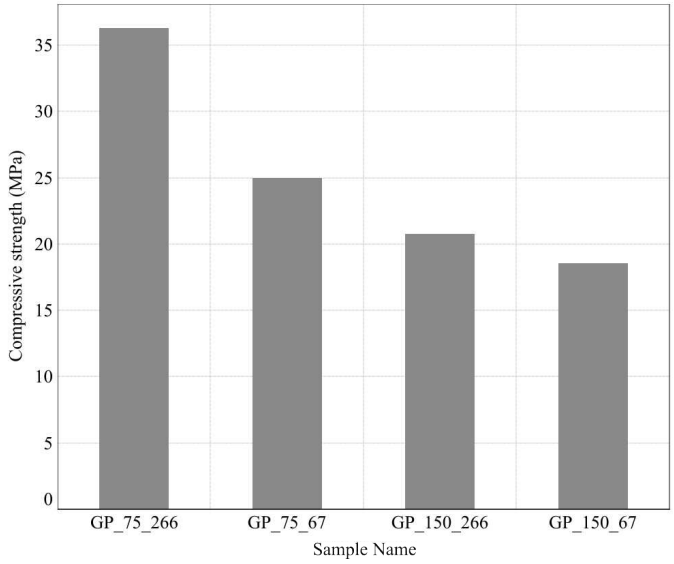

Figure 3.11: *Calculated Stress for the B3B test performed on the membranes*

It can be observed from the data pertaining to membranes produced at 75°C and 150°C, that an increase in pressure correspondingly led to an increase in strength. This phenomenon can be clarified by referring to Figure 3.7, which demonstrates a reduction in pore dimensions with the increase of pressure during the hot-pressing procedure. Given that pores serve as defect points, which mitigate the resistance of the samples, the presence of smaller pores is indeed advantageous for increasing the mechanical resistance of the sample. It is also noteworthy that heightened pressure results in a decline in overall porosity (%), effectively diminishing defect sites within the sample, thereby strengthening its mechanical attributes. A similar trend is observed with the increment in temperature, which induces the formation of substantially larger pores within the structure, further decreasing the sample's resistance.

In assessing the reliability of the test, the sample should fracture into three pieces as a criterion for validation. Observing Figure 3.12a, a similar fracturing pattern is discernible in our experiment, corroborating the stipulated criteria. Ideally, the fracture should initiate on the tensioned plane beneath the ball, thereby exhibiting a tri-symmetrical pattern. However, as depicted in Figure 3.12b, the precise manifestation of the three-fold fracturing was not consistently observed across all tests

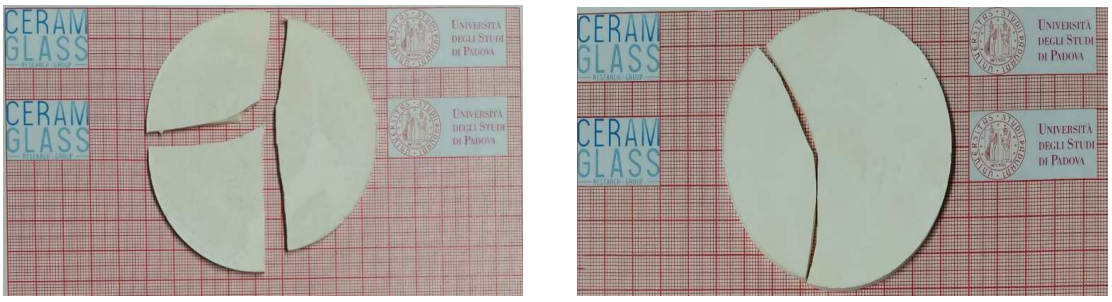

(a) **(b)**

Figure 3.12: *Depiction of fracture patterns observed during the B3B test. (a) Tripartite fracture, (b) Bipartite fracture*

3.4.7 Permeability test

The water flux values were obtained utilizing Equation 3.1. Each measurement was replicated 2 - 3 times, and two membranes for each specified condition were examined to validate the repeatability of the findings. Pursuant to the conditions delineated in Table 3.1, preliminary testing was conducted to establish the range for pressure and temperature required to achieve a certain level of permeation through the membrane. The lower threshold for pressure was designated at 4 bar, while the temperature was set at 50°C, given that there was an absence of flux through the membrane at pressures lower than the established limit. The correlation between the permeate flux J and the pressure P is elucidated in Figure 3.13.

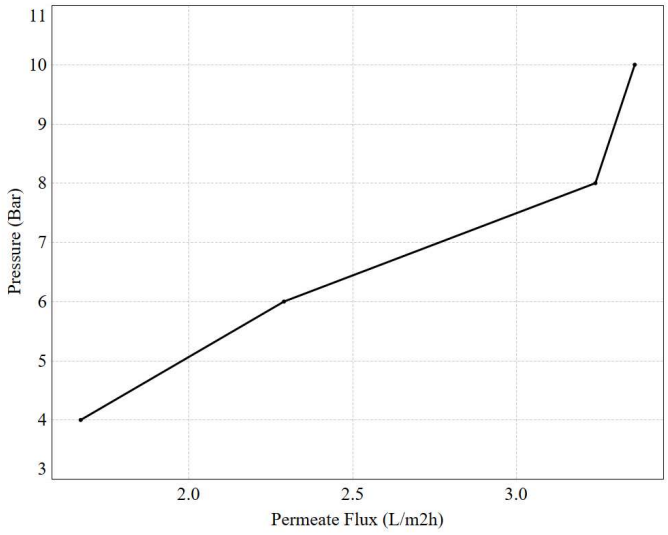

Figure 3.13: *Permeate Flux Vs Pressure for a Temperature of the fluid (water) of 50°C*

It is discernible that there exists a positive correlation between pressure and permeate flux, a phenomenon that aligns with expectations. Elevated pressure levels exert a force on the fluid, propelling water through the open porosity of the membranes. This boost to water permeation through the membrane correspondingly increases the permeate flux.

In order to assess the impact of temperature on the permeability of the membranes, the fluid pressure was maintained at 4 bar; this lower pressure value was chosen to

mitigate the influence of pressure on the permeate flux across the membranes. Subsequently, the fluid temperature was elevated to match the conditions outlined in Table 3.1. It is noteworthy that, prior to measuring the volume of water traversing the membrane over a one-minute interval, a three-minute pause was observed post temperature stabilization, to ensure a more accurate measurement. This procedure was repeated thrice, and two membranes were tested for consistency. Figure 3.14 shows the relationship between the permeate flux J and the fluid temperature.

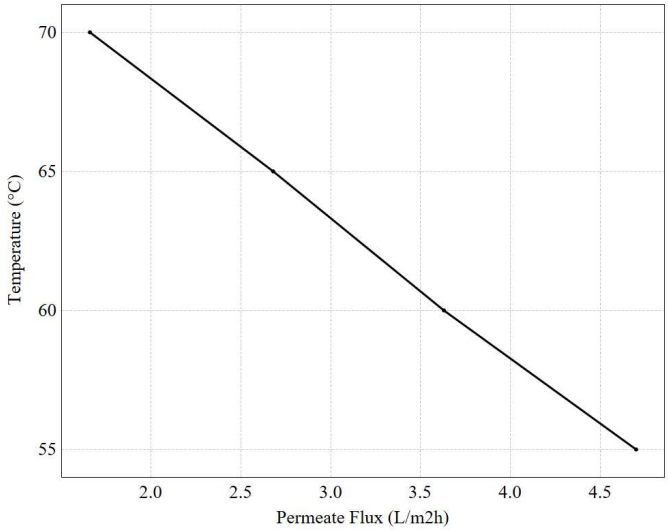

Figure 3.14: *Permeate Flux Vs Pressure for a Temperature of the fluid (water) of 50°C*

It can be observed that increasing the fluid temperature adversely affects the permeability, which was unexpected. Initially, it was hypothesized that a higher fluid temperature would result in reduced viscosity, thus facilitating the passage of water through the membranes. However, the decline in permeate flux with increased temperature could potentially be attributed to some erosion of the membranes, which might obstruct the porosity, thereby decreasing the permeability. Notably, the collected water exhibited a certain degree of turbidity, likely due to particulate matter from the membrane. Despite this erosion, there was no discernible impact on the membrane's resistance or integrity. Post-experiment examination of the membranes revealed no indications of cracking or any other forms of damage. This study aimed to determine

the optimal conditions for carrying out microplastic adsorption tests using the specified membranes. The favorable condition was determined to be maintaining the fluid pressure at 10 bar while keeping the fluid temperature at 50°C; these conditions are compatible with hydraulic fracturing in oil and gas extraction, where high-pressure water is utilized . Similarly, ammonia synthesis (Akay & Zhang, 2017), and wastewater treatment processes (Akarsu et al., 2021). Currently, experiments concerning the cut-off properties of these membranes are being conducted by the research group at the Oulu department, produced utilizing the identified process conditions. Specifically, the group is evaluating the adsorption capabilities of these membranes concerning PEG 35000 and PEO (100k, 200k, and 600k) through Total Organic Carbon (TOC) analysis. The results of these investigations are expected to be made available in the near future.

3.5 Conclusions

In this study, we aimed to introduce a novel application for geopolymer membranes, manufactured employing the warm pressing technique. Specifically, we successfully optimized and produced geopolymer membranes within a timeframe of under 30 minutes. Two temperature settings, 75°C and 150°C, were found to be conducive for the production of these geopolymer membranes at various pressures (67, 133, 200, and 266 kN). All produced membranes were characterized using XRD and FTIR analysis, together with the boiling test, to evaluate the occurrence of the actual geopolymerization reaction, confirming the presence of the three-dimensional geopolymer network.

Utilizing mercury porosimetry, we observed that increasing the pressure yielded membranes with reduced total porosity (%) and smaller pore dimensions, whereas an increase in temperature had the opposite effect, increasing the average pore dimensions. The total porosity and average pore dimensions directly impacted the mechanical properties of the membranes as measured by the B3B test; specifically, larger pores (obtained in higher temperature and lower pressure conditions) adversely affected the mechanical properties of the membranes. The specific surface area (SSA) values also

followed a similar trend, wherein membranes with smaller pores exhibited higher SSA values.

Moreover, we successfully identified the optimal conditions, in terms of pressure and temperature, to achieve higher permeability with these membranes. The most favorable condition was established at a pressure of 10 bar and a fluid temperature of 50°C. Based on these findings, cut-off experiments are currently underway to ascertain the minimum particle size these membranes can filter. This study serves as a precursor to determining the applicability of these membranes in addressing the critical issue of water pollution, thereby contributing towards combating this hazardous phenomenon.

CHAPTER 4

Modeling the compressive strength of metakaolin-based geopolymers

Publication

The chapter herein encapsulates work that has been disseminated in the well-regarded journal, Applied Clay Science. The referenced publication can be accessed through the provided Qrcode. The paper is entitled: "Modeling the compressive strength of metakaolin-based geopolymers based on the statistical analysis of experimental data."

4.1 Abstract

The relationship between the compressive strength of metakaolin-based geopolymer samples and different processing conditions has been investigated for both potassium and sodium based geopolymer systems. Cubic geopolymer samples were prepared by mixing the slurry for 1 hour in a thermostatic bath at 0°C. More than 1200 samples have been tested to gather enough data to carry out a meaningful statistical analysis. All the data evaluation and model development have been carried out extensively using R. The variation of curing and aging time, curing temperature, SiO_2/Al_2O_3 and H_2O/Al_2O_3 molar ratios has been accounted for via the application of statistical models whose reliability has been suitably checked. Curing has been performed in a sealed container at 100% relative humidity. Aging has been conducted in a climate chamber kept at 75% of relative humidity using an oversaturated solution of NaCl. Curing time has proved a positive relationship with compressive strength while aging time does not show evidence of any significant effect. Curing temperature negatively affects compressive strength. Increasing the SiO_2/Al_2O_3 molar ratio results in an increase of the compressive strength within a certain range of values for the ratio; however, above a threshold (3.8 for the potassium-based and 3.4 for the sodium-based geopolymer system) the mechanical properties decrease. The H_2O/Al_2O_3 molar ratio displayed an inverse proportionality with the compressive strength except for the sodium-based geopolymer, where the mechanical properties initially increased. A further comprehensive and statistically sound model has been proposed that allows us to predict the strength of geopolymer samples as a function of process variables and their composition, ranging in a rather wide set of values.

4.2 Experimental

4.2.1 Design Of Experiment

All the experiments were conducted on both potassium- and sodium-based geopolymers, as they are both extensively used and possess different properties. The compressive strength of the geopolymers was evaluated for varying conditions alleged to affect their microstructure and performance, namely the curing and aging time, curing temperature, silica to alumina ratio and water to alumina ratio (Hardjito et al., 2004; Moradikhou and Esparham, 2020). In order to limit the number of experimental variables and curb the collection of experimental data, the geopolymer composition was changed solely in terms of SiO_2/Al_2O_3 ratio and H_2O/Al_2O_3ratio, whereas the Na_2O or K_2O/Al_2O_3 ratio was always held constant at 1; this corresponds to the composition at which the positive charge of the alkaline cation fully stabilizes the Al coordination from $[Al]^{VI}$ to $[Al]^{IV}$ while limiting the material susceptivity to carbonation reactions. In natural carbonation, atmospheric CO_2 reacts with hydroxide, i.e., an acid-base reaction is established (Zhang et al., 2014; Sani et al., 2016). However, in geopolymeric materials, the main driving factor to efflorescence in geopolymeric materials is the availability of Na^+ or K^+ and OH^- as shown in the following equations (for Na^+):

$$CO_2 + 2OH^- \rightarrow CO_3^{2-} + H_2O \tag{4.1}$$

$$2Na^+ + CO_3^{2-} + xH_2O \rightarrow Na_2CO_3 \cdot xH_2O \tag{4.2}$$

Thus, the efflorescence development potential observed by the total alkalinity value of the samples leachate may be due to the alkalinity resulting from the hydroxide (OH^-) and carbonate (CO_3^{2-}) ions. Excessive efflorescence and, consequently, leaching and carbonation on the surface and inside the pores can reduce geopolymers' compressive and tensile strength. L. Simão et al. (Simão et al., 2021) studied a new approach to controlling the efflorescence in geopolymeric material. In their work, they

studied, in particular, different Na_2O/Al_2O_3 ratios concluding that a value of about 1 showed a higher compressive strength value. Nevertheless, the number of factors and possible combinations that could be considered limits the possibility for a straightforward evaluation of the relationship between the compressive strength and the whole set of conditions and precludes the prediction of geopolymer performance. Hence, a factorial design of experiments approach was followed in this investigation for a wide, yet specific selection of conditions. Experimental conditions for each considered varying factor were selected based on the analysis of a wide range of papers reporting different processing conditions and resulting material's characteristics, and cover the widest range considered appropriate for typical geopolymer materials (Ismail I. et al., 2011; Timakul et al., 2015; Verma et al., 2022). Additionally, a pilot set of experiments was carried out to tune the geopolymer composition and the curing temperature to provide the lowest strength variability. The resulting design of the experiments is summarized in Table 4.1 and in the following detailed.

The effect of curing and aging time on the compression strength was evaluated on geopolymer samples of composition $K/Na_2O \cdot 3.4SiO_2 \cdot Al_2O_3 \cdot 18H_2O$ cured at 40°C for C days and aged afterward for A days, with (C, A) varying in the set {1, 7, 28}x{0, 7, 21, 28, 56}. The effect of curing temperature on the compression strength was evaluated on geopolymer samples of composition $K/Na_2O \cdot 3.4SiO_2 \cdot Al_2O_3 \cdot 18H_2O$ cured for 1 day at T degrees (°C) and aged for 7 days at room temperature, with T varying in the set {25, 40, 50, 60, 75, 90}. Curing and aging time conditions were selected in the pilot experiments as the ones providing the lowest standard deviation values, besides being the most suited in term of general processing approach and times. The effect of the SiO_2/Al_2O_3 molar ratio on the compression strength was evaluated on geopolymer samples with ratio selected in the set {2.6, 3.0, 3.4, 3.8, 4.2}, cured at 40°C for 1 day and aged for 7 days. The H_2O/Al_2O_3 ratio was kept at 18, as this value provides geopolymer systems with a rheology suitable for a variety of processing methodologies, including casting. The effect of the H_2O/Al_2O_3 ratio on the compression strength was

evaluated on geopolymer samples with ratio selected in the set {11, 13, 15, 18, 20, 22, 25}, cured at 40°C for 1 day and aged for 7 days; the SiO_2/Al_2O_3 ratio was kept at 3.4.

Table 4.1: *Design of Experiments: tested variables and conditions*

Variable	Conditions						
Curing (days)	1	7	28				
Aging (days)	0	7	21	28	56		
Curing temperature (°C)	25	40	50	60	75	90	
Si/Al ratio	2.6	3.0	3.4	3.8	4.2		
H2O/Al2O3 ratio	11	13	15	18	20	22	25

4.2.2 Samples Preparation

To manufacture the samples, metakaolin (Argical 1200s, Imerys, France) was mixed with an alkaline solution for 1 hour in a thermostatic bath at 0°C; The primary purpose of the thermostatic bath is to slow down the geopolymeric reaction that is taking place while mixing to better asses the influence of curing time on the compressive strength. The alkaline solution was obtained by dissolving sodium (SS2942 Ingessil Italy) or potassium silicates (Kaslov 205 PQ Corporation) and sodium or potassium hydroxides (Sigma Aldrich) into distilled water. After that, the slurry was poured into 10x10x10 mm^3 silicone molds to obtain the samples shown in Fig 4.1.

The choice of relatively small molds serves the purpose of enabling the production of a great number of specimens while limiting the volumes of material to be processed. This way, each set of specimens can be produced in a single batch, assuring better homogeneity among the set. The molds were placed in a sealed container at a constant 100% relative humidity (RH), achieved by placing a water container within the chamber and monitoring RH using a hygrometer, to proceed with the curing process in different conditions placing the samples in the oven. Curing refers to the time (days) that geopolymer samples remain in the aforementioned conditions inside the silicone

Figure 4.1: *Geopolymer Cubic Samples*

mold in a sealed container. After curing, the samples are removed from the mold and placed in a climate chamber at a constant 75% RH, achieved by placing a supersaturated NaCl solution within the chamber (which acts as water regulator) and monitoring using a hygrometer. The duration of this second step is referred to as aging time (days). The relatively high value of RH maintained during aging is motivated by preliminary tests showing a tendency to crack for geopolymer samples aged otherwise. For all conditions studied in this work, boiling tests and FT-IR analyses were conducted to assess the complete consolidation of materials (especially for low curing and aging times).

4.2.3 Mechanical characterization

The compressive strength was measured using a universal testing machine (Galdabini Quasar 25) with a crosshead speed 0.5 mm/min; the compression surfaces of the samples were lightly sanded before testing, and 20 samples for each condition were analyzed.

4.2.4 Data Analysis

The statistical analysis has been conducted on the collected data using the R software for statistical computing (R Core Team, 2020), an open-source environment available

under the GNU General Public License, primarily written in C, Fortran and R itself. The relationships between the compressive strength and composition, curing temperature, curing and aging conditions were preliminary explored by means of box and whiskers plots - boxplots -, widespread graphical tools that summarize an empirical distribution by building a box delimited by its first and third quartile and cut by its median as a measure of central tendency. The box is then possibly provided by whiskers extending to the spread of the data, and by outliers which are individually plotted. Results of the exploratory data analysis, discussed in the following section, suggested a broad adequacy of linear models with polynomial trends and Analysis of Covariance (ANCOVA) to evaluate significant effects of composition, curing temperature, curing and aging conditions. ANCOVA refers to regression problems to model the expected variation of continuous responses as a function of both qualitative (as the alkaline cation on which the geopolymer formulation is based upon) and quantitative predictors (e.g., the SiO_2/Al_2O_3 molar ratio and the H_2O/Al_2O_3 ratio), possibly interacting among them. To evaluate the effect of the considered experimental factors ceteris paribus, model specification also accounted for possible random variations in the experimental conditions, such as the sample geometric density or its volume, and kept it in the resulting model whenever resulted significant. A general formulation of the considered models to explain the expected variation of the compressive strength $E(\sigma)$ for varying experimental factors F on sodium or potassium geopolymer is the following:

$$E(\sigma) = \begin{cases} \beta_0 + \beta_1 F + ... + \beta_k F^k \; Alkaline\, Cation\, K \\ \\ \gamma_0 + \gamma_1 F + ... + \gamma_k F^k \; Alkaline\, Cation\, Na \end{cases} \tag{4.3}$$

Details on the estimated models for the different experiments, along with the associated residuals analysis and indexes of goodness of fit are illustrated in the next section. The samples were labelled as: KCxAy or NaCxAy, where:

- K and Na identify the alkaline cation on which the geopolymer formulation is

based on;

- x, expressed in days, is the curing time (curing temperature was kept constant at 40°C;
- y, expressed in days, is the aging time.

4.3 Results and Discussion

4.3.1 Effect of curing and aging time

Fig 4.2 reports the mechanical test results for all the selected curing and aging conditions. Due to the difference in behavior between these two types of geopolymer, the conditional distributions of compressive strength vs curing were analyzed, depending on the amount of aging and of curing.

Fig 4.3 show the empirical distribution of compressive strength vs aging time for different curing times.

Fig 4.4 show the empirical distribution of compressive strength vs curing time for different aging times.

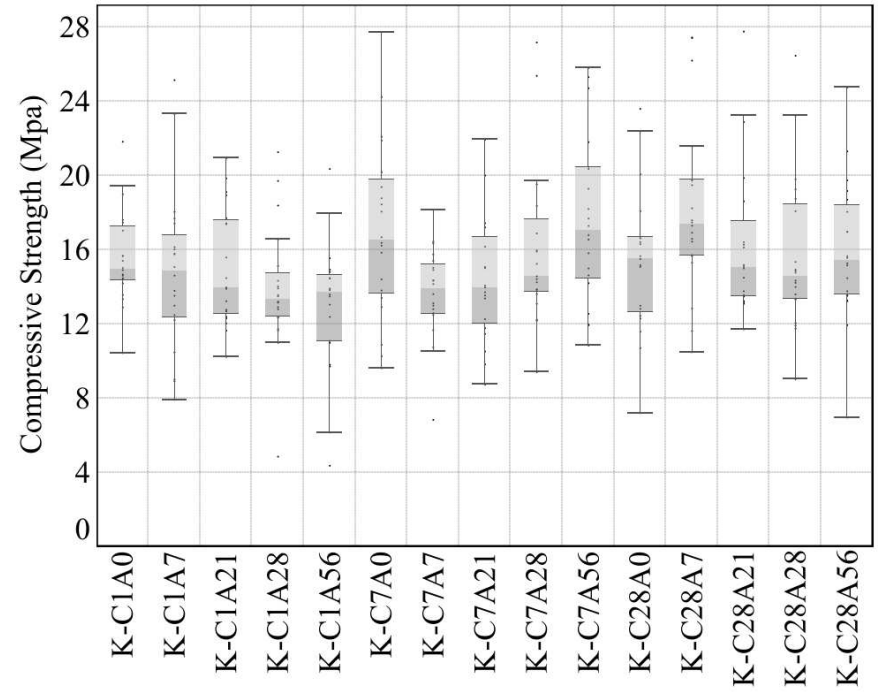

(a)

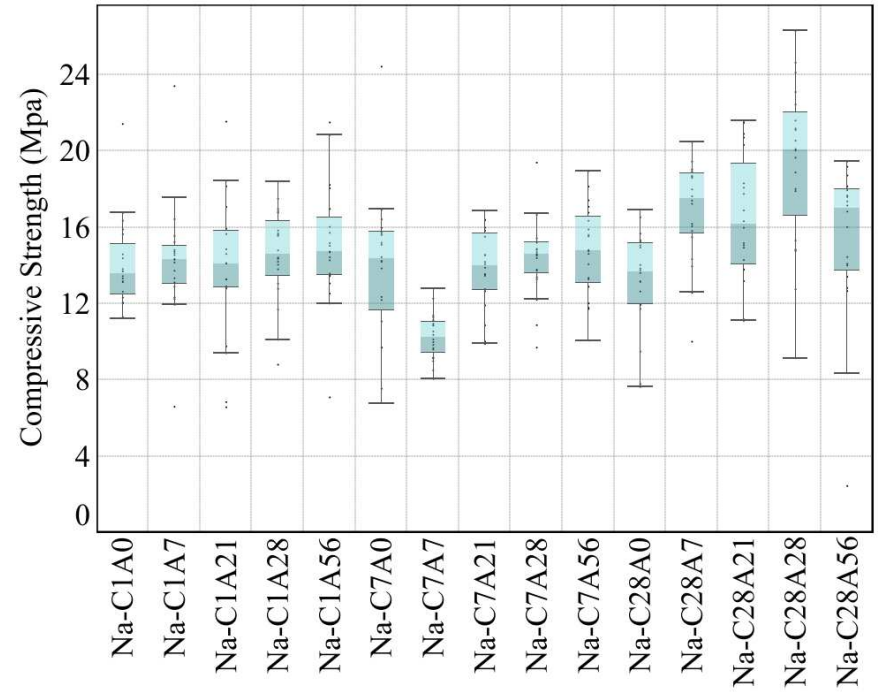

(b)

Figure 4.2: *Overview of the effect of curing time (at fixed curing temperature = 40°C) and aging conditions on compression strength. a) Potassium-based geopolymer, b) Sodium-based geopolymer*

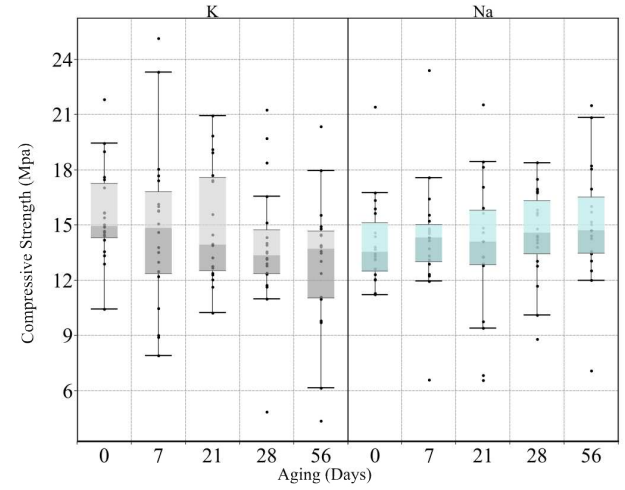

(a)

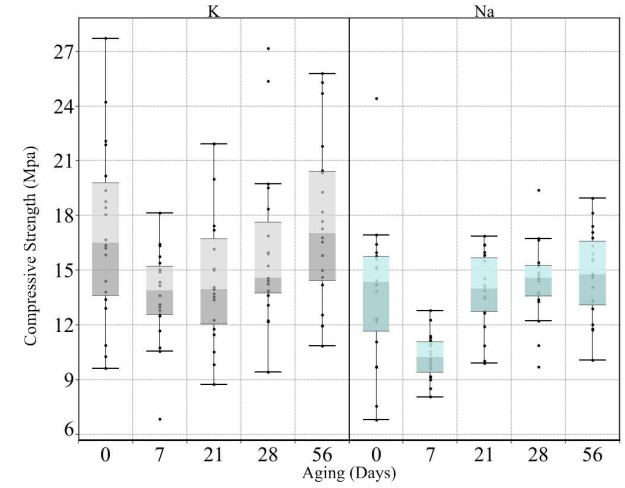

(b)

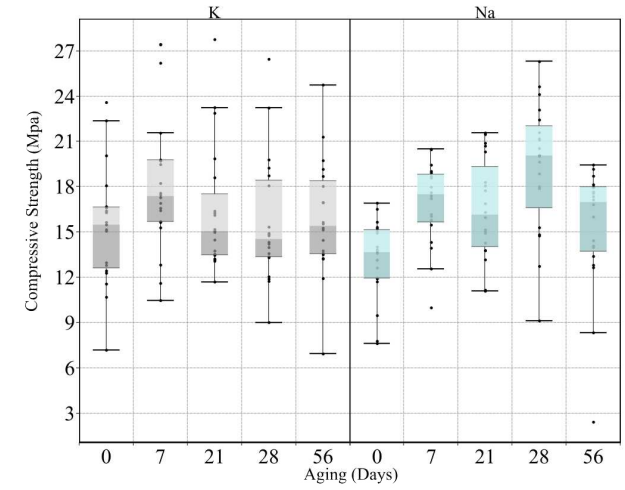

(c)

Figure 4.3: *Empirical distribution of compressive strength vs curing age (at fixed curing temperature = 40°C) for curing times 1 day (a), 7 days (b), 21 days (c)*

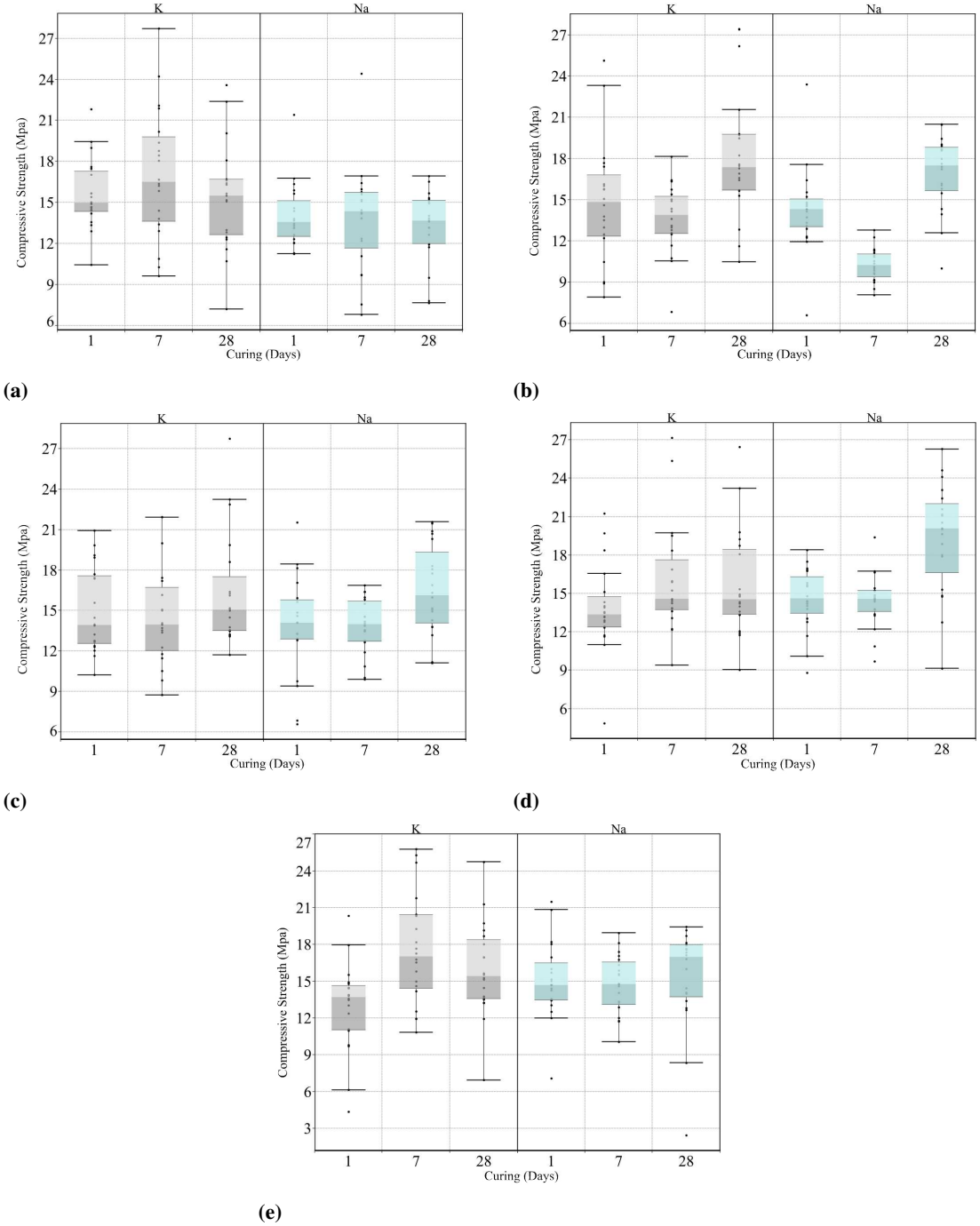

Figure 4.4: *Empirical distribution of compressive strength vs curing time (at fixed curing temperature = 40°C) for aging times 0 days (a), 7 days (b), 21 days (c), 28 days (d), 56 days (e)*

As a general remark, potassium geopolymers show a broadly higher compressive strength. A positive linear association between compressive strength and curing time appears, yet possibly of different intensity in potassium- and sodium-based geopolymer samples. The relationship between compressive strength and aging time appears less evident and of interest for sodium geopolymers only. The above considerations suggest the formulation of the following model:

$$E(\sigma) = \begin{cases} \beta_0 + \beta_1 C + \beta_2 A \; Alkaline \; Cation \; K \\ \\ \gamma_0 + \gamma_1 C + \gamma_2 A \; Alkaline \; Cation \; Na \end{cases} \tag{4.4}$$

where C is the curing time and A is the aging time. The estimated parameters, along with their standard errors and significance are summarized in Table 4.2; their analysis validates and strengthens our previous, qualitative findings.

Table 4.2: *Estimates, standard errors and level of significance of parameters in Eq. 1; F statistics, R2, DF (Degree of Freedom). Significance levels: 0 '***', 0.001 '**', '× ' 1*

Parameter	Estimate (standard error)	Significance
β_2	14.98 (0.39)	***
γ_0	-2.00 (0.55)	***
β_1	0.06 (0.02)	**
γ_1	0.09 (0.02)	***
β_2	-0.01 (0.01)	
γ_2	0.03 (0.01)	**
$R^2 = 0.07$; F-statistic: 9.424 on 5 and 590 DF ***		

On average, a higher compressive strength of potassium geopolymers than sodium-based ones, amounting to about 2 MPa, is confirmed and significant in accordance with previous reports (Lizcano et al., 2012). The drop in strength observed for both potassium and sodium-based geopolymers at 7 days of curing and 7 days of aging still needs to be fully understood, but it is most likely related to the stage of pore refinement reached by the material. After 1 day of curing, the polycondensation reactions are still far from being completed (Sagoe-Crentsil & Weng, 2007) and little water is expected to be produced. After 7 days of curing, however, there might already be considerable water coalescence (Archez, et al., 2021); while its effect cannot be appreciated at 0 days of aging, the subsequent evaporation in the following 7 days generate large pores that limit the strength of the material. With additional aging time, the microstructure continues to develop, and the material shows an increase in its strength. After 28 days of curing, the reactions are mostly completed, and the subsequent aging has a lower influence. This hypothesis will need to be validated with further investigation on the materials' porosity; however, the combination of 7 days of curing and 7 days of aging can be deemed undesirable for both material systems studied here.

Curing time has a slight, yet fully significant, effect on increasing the expected compressive strength in both potassium- and sodium-based geopolymers, quantifiable in an average increase of 0.06 and 0.14 MPa for each additional day of curing, respectively. The slight increase in strength could be explained by the fact that the temperature accelerates the geopolymerization reaction. Keeping the samples at 40°C for longer times forces the reactions towards the product, helping to consume all the reagents and therefore resulting in the development of a more complete geopolymer network. The greater concentration of Si-O-Si bonds with respect to Si-O-Al bonds can be held responsible for higher values for the compressive strength (Jong and Gordon, 1980). This trend is in agreement with previous experiments carried out considering similar conditions (Rangan et.al, 2010).

Aging time has a slight positive effect on sodium geopolymers quantifiable in an

average increase of about 0.03 MPa for each additional day of aging; conversely, it does not result in significantly affecting potassium-based geopolymers. The result can be explained considering by the fact that the geopolymerization reaction rate for the Na-based geopolymer is slower (Botti et al., 2021).

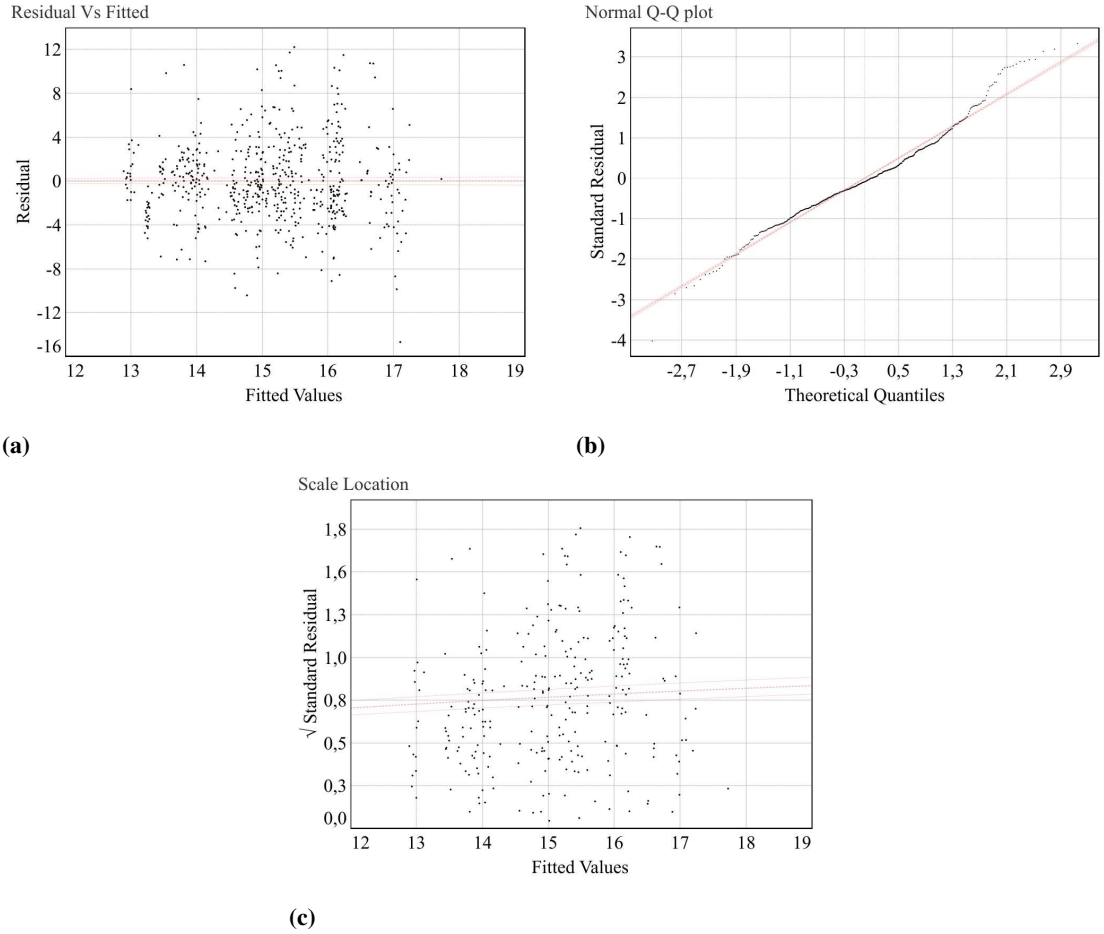

Figure 4.5: *Residual analysis of the estimated model in Eq.4.4*

In Fig.4.5a, model residuals are plotted versus the predicted values of the compressive strength, according to the estimated model; while residuals are comprehensively high, the plot does not show any trend, thus suggesting an overall correct model specification; the normal quantile-quantile plot (Fig.4.5b) compares the empirical quantiles of the residuals with the theoretical quantiles of a normal density. Except for some data at the tail of the distribution, which depart from the general trend, the linearity of the points indicates that model errors comply with Gaussianity, hence the whole inference

about the model, relying on such assumption, can be considered reliable. Furthermore, the scale- location plot (Fig.4.5c) does not present any trend, hence does not show violations of the hypothesis of homoscedasticity of the error term and guarantees the efficiency of the estimates. Besides a general adequacy and reliability of the estimated model, the value of the R^2 indicates that curing and aging time can explain about the 8% only of the variability of compressive strength, hence requiring inclusion of further experimental factors in the model.

4.3.2 Effect of curing temperature

Fig. 4.6 shows the empirical distribution of compressive strength vs curing temperature.

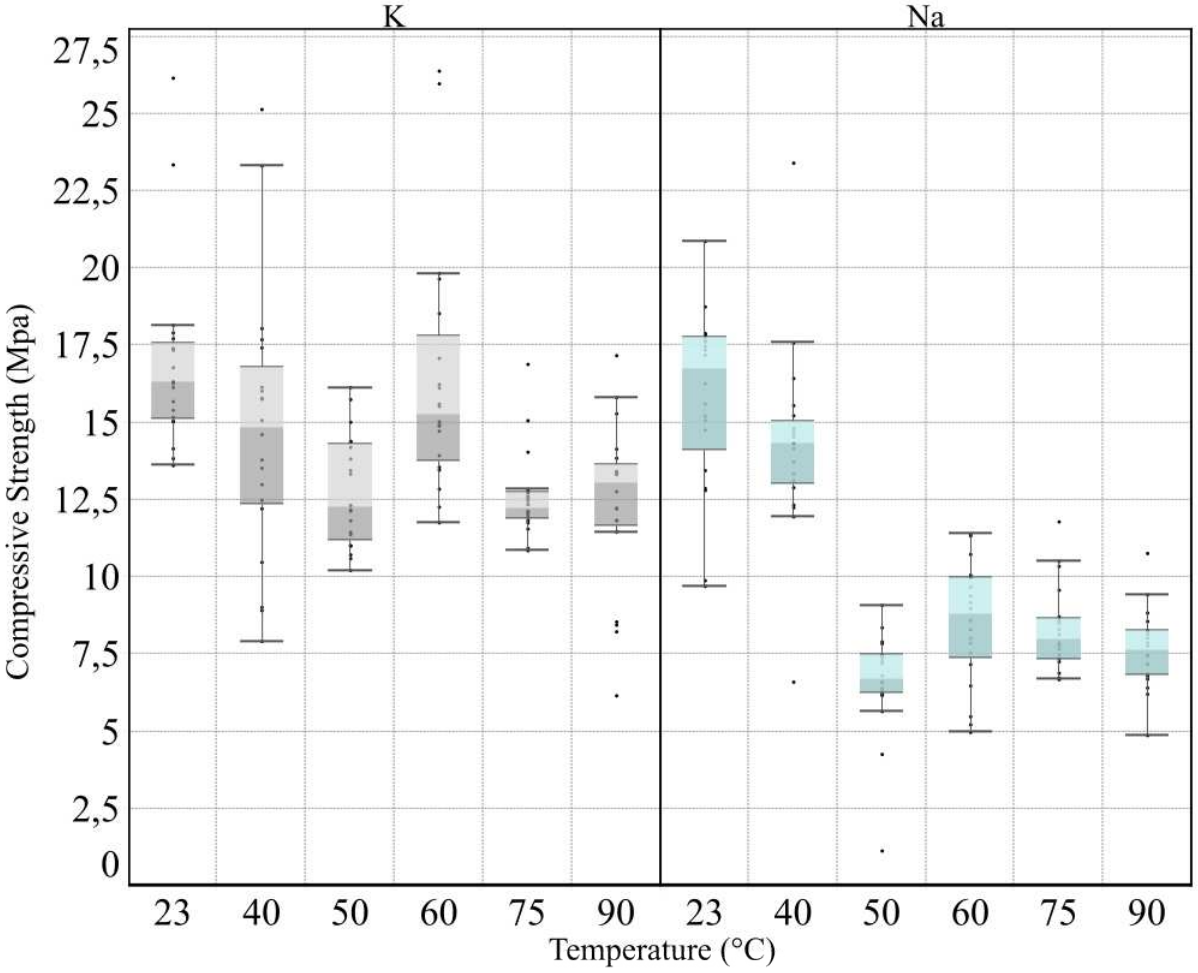

Figure 4.6: *Empirical distribution of compressive strength vs curing temperature.*

Temperature seems to negatively affect the average compressive strength of samples, yet up to some threshold. Above such value, the trend changes, getting less clear. This suggests modeling the data as specified in the following:

$$E(\sigma) = \begin{cases} \beta_0 + \beta_1 T + \beta_2 I_{T>60}\ Alkaline\ Cation\ K \\ (\beta_0 + \gamma_0) + (\beta_1 + \gamma_1) T + \gamma_2 I_{T>40}\ Alkaline\ Cation\ Na \end{cases} \tag{4.5}$$

where T is the temperature and I_A is dummy variable taking value 1 when event A occurs, and value 0 otherwise. In this case, event A refers to the temperature exceeding a certain threshold. The estimated parameters, along with their standard errors and significance are summarized in Table 4.3. Some main remarks are discussed in the following.

Table 4.3: *Estimates, standard errors and level of significance of parameters in Eq. 4.5; F statistics, R2, DF (Degree of Freedom). Significance levels: 0 '***', 0.001 '**', '× ' 1*

Parameter	Estimate (standard error)	Significance
β_0	16.04 (1.22)	***
γ_0	-0.17 (1.72)	
β_1	-0.005 (0.04)	
γ_1	-0.02 (0.05)	.
β_2	-1.99 (1.17)	
γ_2	-6.87 (1.05)	***
$R^2 = 0.59$; F-statistic: 48.16 on 5 and 239 DF ***		

The model does not prove any evidence of a linear relationship between the expected compressive strength and the curing temperature, neither before nor after the

selected thresholds, and for none of the cations (the associated parameter β_1 and γ_1 are indeed not significant) With low curing temperature, there is no evidence of a different expected compressive strength between the two cations (the γ_0 is also not significant). In both types of geopolymers there is evidence of a threshold curing temperature that shifts the expected compressive strength toward lower values, especially in sodium-based geopolymers. The expected shift is estimated to amount to about -1.99 MPa for potassium-based geopolymers when the temperature exceeds a threshold of 60°C, and to about -6.87 MPa for sodium-based geopolymers when the temperature exceeds a threshold of 40°C. These patterns demonstrate consistency with preceding scholarly research (Ghanbari et al, 2017). Nevertheless, at this stage of the investigation, the reason behind this behavior is still unclear. Systematic NMR structural investigations of the samples should be carried out to assess any diversity in the developed network, but this is beyond the scope of the present work. An overall negative impact of the curing temperature on the compressive strength could be explained by the fact that the rate of polycondensation and water evaporation in the geopolymer both increase with increasing curing temperature; the latter promotes the formation of larger, macropores, which are believed to be more interconnected than micro and mesopores (Ramón et al., 2011). Consequently, the presence of macropores can decrease mechanical strength (Rovnaník and Pavel, 2010). Similar trends have been found in other works under similar conditions (Bakria et al., 2011; Lee et al., 2016) The model is overall informative (F test is significant) and the R^2 suggests that the temperature can explain almost 60% of the total variability. Nevertheless, residual analysis (reported in Figure 5) indicates some weak deviations from the model assumptions, especially with reference to the hypothesis of normal errors. While this is likely to be due to the presence of some outliers (see also Figure 4.6), these results warn to use some caution in considering reliable the inference associated to such model.

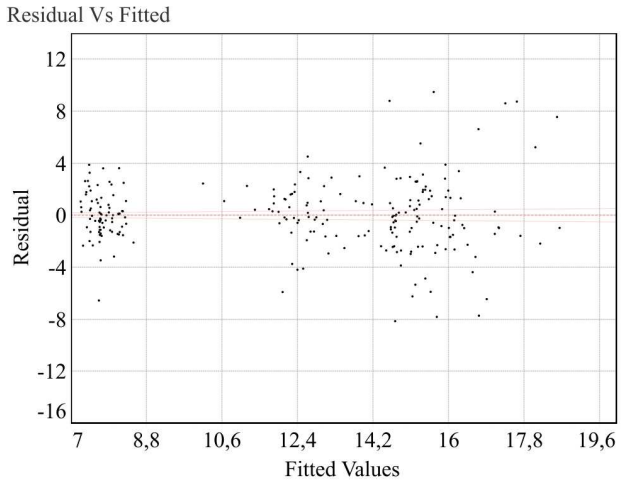

(a)

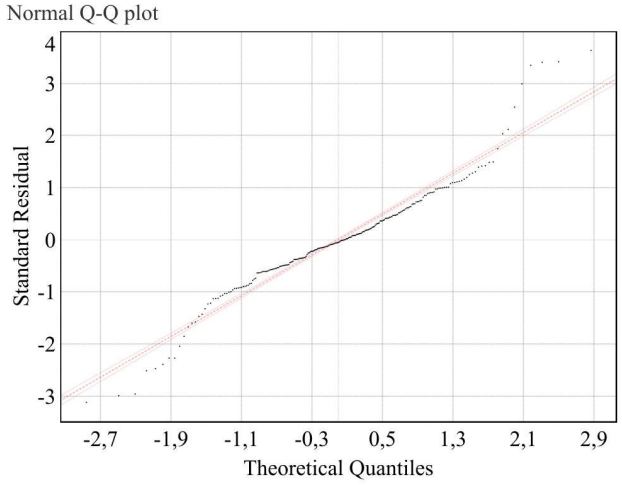

(b)

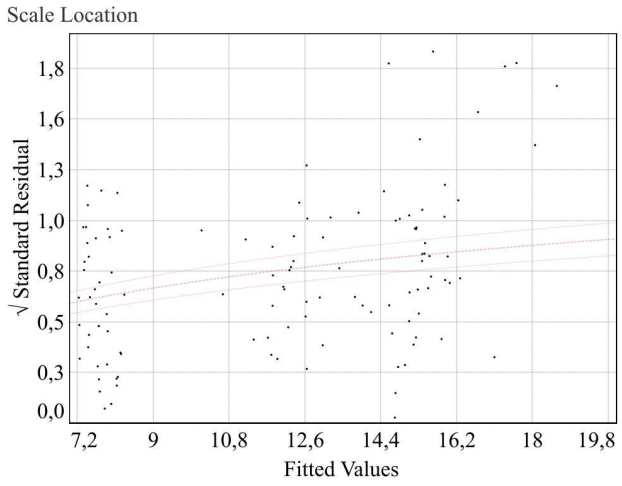

(c)

Figure 4.7: *Residual analysis of the estimated model in Eq.4.5*

4.3.3 Effect of the SiO_2/Al_2O_3 molar ratio

Fig. 4.8 shows the empirical distribution of the compressive strength and silica to alumina ratio and clearly shows a quadratic trend for both types of geopolymers.

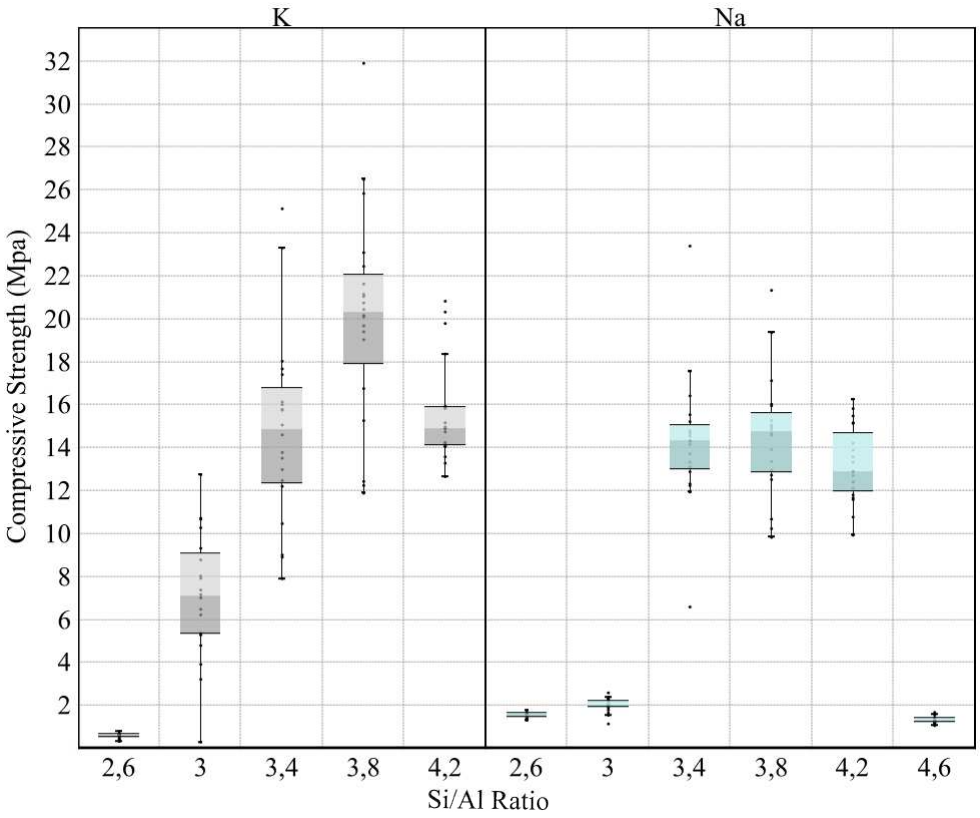

Figure 4.8: *Empirical distribution of compressive strength vs SiO_2/Al_2O_3 ratio.*

The following model is thus adopted:

$$E(\sigma) = \begin{cases} \beta_0 + \beta_1 \frac{SiO_2}{Al_2O_3} + \beta_2 (\frac{SiO_2}{Al_2O_3})^2 \; Alkaline\; Cation\; K \\ (\beta_0 + \gamma_0) + (\beta_1 + \gamma_1) \frac{SiO_2}{Al_2O_3} + (\gamma_2 + \beta_2)(\frac{SiO_2}{Al_2O_3})^2 \; Alkaline\; Cation\; Na \end{cases} \tag{4.6}$$

The estimated parameters, along with their standard errors and significance are summarized in Table 4.4. Some main remarks are discussed in the following.

Table 4.4: *Estimates, standard errors and level of significance of parameters in Eq. 4.6; F statistics, R2, DF (Degree of Freedom). Significance levels: 0 '***', 0.001 '**', '× ' 1*

Parameter	Estimate (standard error)	Significance
β_0	-148.99 (15.84)	***
γ_0	-13.67 (19.05)	
β_1	85.71 (9.5)	***
γ_1	10.02 (11.23)	
β_2	-11.01 (1.39)	***
γ_2	-1.96 (1.61)	
$R^2 = 0.75$; F-statistic: 130.6 on 5 and 212 DF ***		

The estimated model confirms a significant quadratic, concave trend linking the expected compressive strength and the silica to alumina ratio. Knowing that the Al component of metakaolin tends to dissolve more easily than the Si component (Weng et al., 2002), we can assume that more $Al(OH)_4^-$ species are readily available for condensation with respect to $Si(OH)_4$ ones. This is particularly true for the systems with low values of the SiO_2 / Al_2O_3 ratio: condensation is likely to have occurred between aluminate and silicate species, producing poly(sialate) polymer structures. With increasing Si content, the overall higher amount of silicate species promotes the reaction between them, resulting in oligomeric silicates; the dominance of the latter leads to better mechanical properties with increasing SiO_2 / Al_2O_3 ratio. Above a certain threshold for the SiO_2 / Al_2O_3 ratio (3.8 for both potassium and sodium-based geopolymers) the mechanical strength drops significantly. This decrease could be linked to the fact that, for higher concentration of SiO_2, the dissolution of metakaolin becomes more difficult, resulting in the permanence of unreacted metakaolin in the final material acting as a point of defect. Data trends are in good agreement with data present in the literature (Duxson et al., 2005); however, the compressive strength values, on average, are lower

than those generally reported in the literature. It is worth noticing that the amount of water in the formulations is relatively high compared to the literature (H_2O/Al_2O_3 = 18, whereas generally a range of 11– 13 is employed), leading to a generally more porous structure and hence limited strength. On average, the silica to alumina ratio explains the expected variation of the compressive strengths with no difference between the two types of geopolymers (γ parameters result all not to be significant).

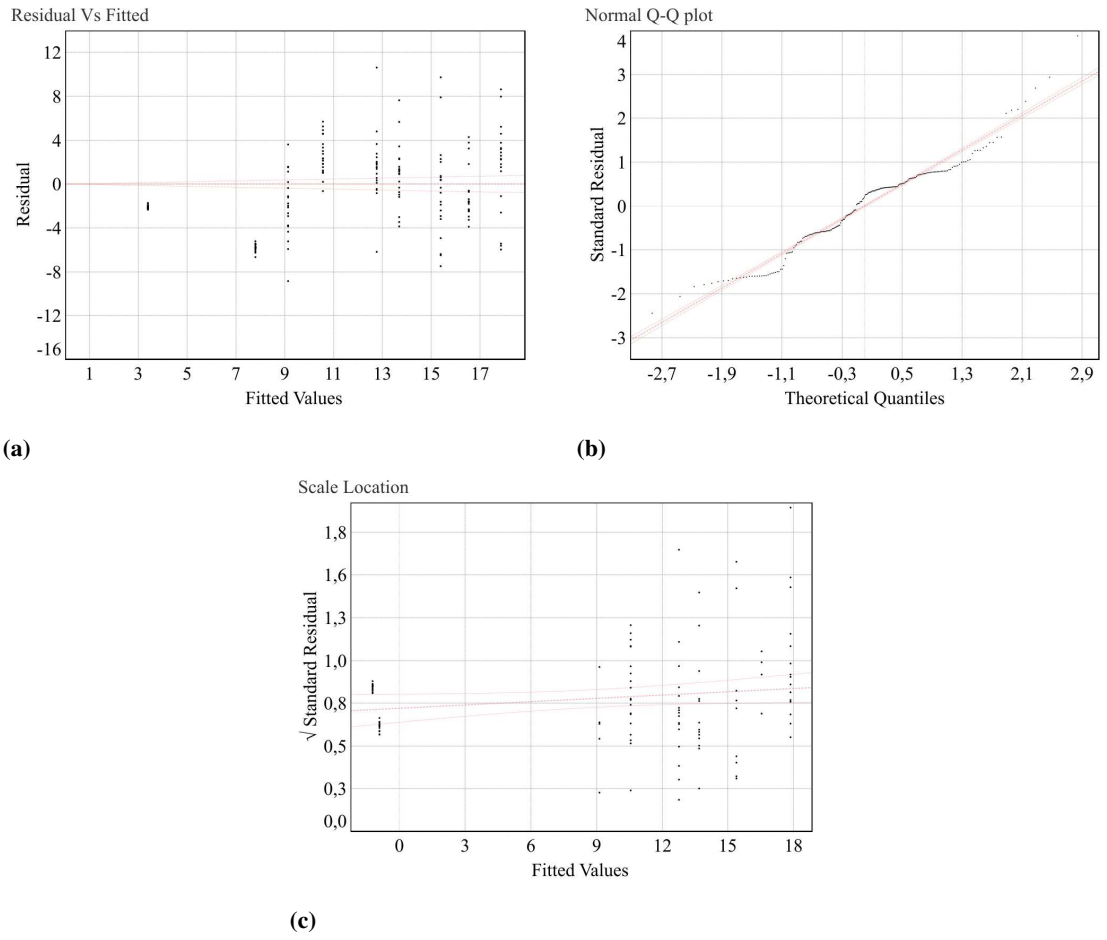

Figure 4.9: *Residual analysis of the estimated model in Eq.4.6*

The residual analysis suggests that (Fig. 4.9) model does not show evident violation of the hypotheses and is consequently to be considered reliable. It also shows a very good fit of the data, with the silica to alumina ratio showing to be a major responsible for explaining the variability of the compressive strength ($R^2 = 0.75$).

4.3.4 Effect of the H_2O/Al_2O_3 molar ratio

Fig.4.10 shows the empirical distribution of the compressive strength and H_2O/Al_2O_3 molar ratio.

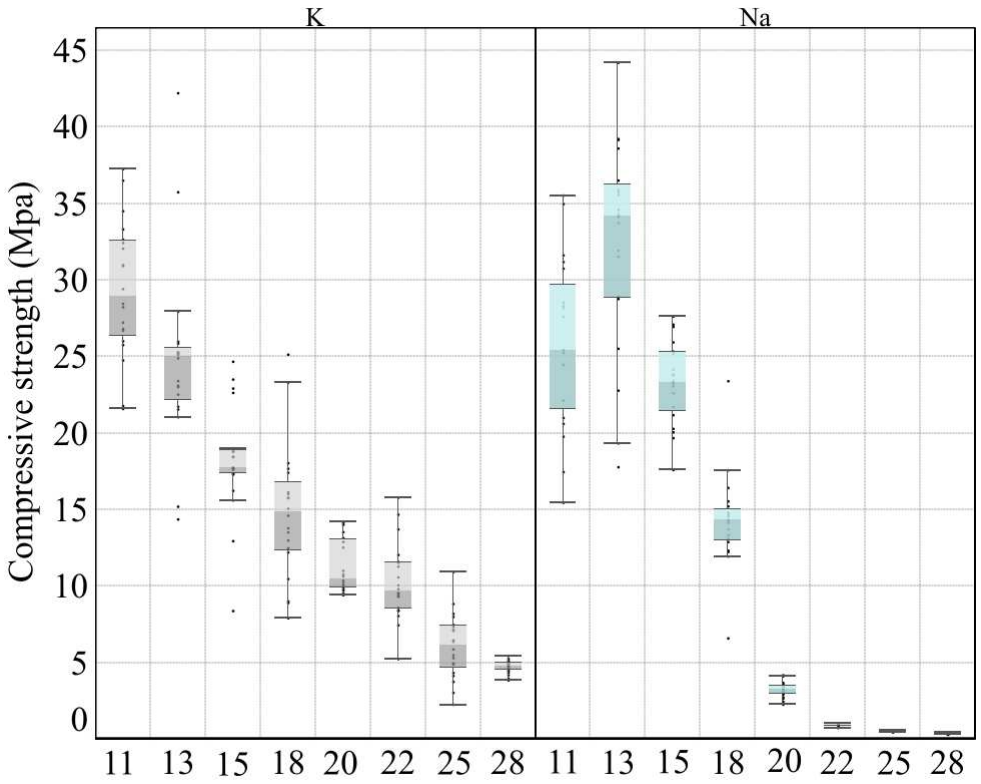

Figure 4.10: *Empirical distribution of compressive strength vs H_2O/Al_2O_3 ratio.*

This ratio seems to negatively affect the average compressive strength of the samples. Potassium-based geopolymer samples show a clearly visible decreasing trend, while sodium-based ones show at the beginning (from H_2O/Al_2O_3 = 11 to 13) an increase in the compressive strength. Exceeding H_2O/Al_2O_3 = 13 results in a decrease of the compressive strength, but with a higher slope than for the potassium-based geopolymer system until H_2O/Al_2O_3 = 22, where a plateau is reached.

The statistical model is the following:

$$E(\sigma) = \begin{cases} \beta_0 + \beta_1 \frac{H_2O}{Al_2O_3} + \beta_2 (\frac{H_2O}{Al_2O_3})^2 \; Alkaline\; Cation\; K \\ (\beta_0 + \gamma_0) + (\beta_1 + \gamma_1) \frac{H_2O}{Al_2O_3} + (\gamma_2 + \beta_2) (\frac{H_2O}{Al_2O_3})^2 \; Alkaline\; Cation\; Na \end{cases} \tag{4.7}$$

The estimated parameters, along with their standard errors and significance are summarized in Table 4.5. Some main remarks are discussed in the following.

Table 4.5: *Estimates, standard errors and level of significance of parameters in Eq. 4.7; F statistics, R2, DF (Degree of Freedom). Significance levels: 0 '***', 0.001 '**', '× ' 1*

Parameter	Estimate (standard error)	Significance
β_0	64.89 (4,76)	***
γ_0	18.48 (0.52)	***
β_1	-3.99 (0.52)	**
γ_1	-1.65 (0.73)	*
β_2	0.07 (0.01)	***
γ_2	0.09 (0.01)	***
$R^2 = 0.75$; F-statistic: 130.6 on 5 and 212 DF ***		

The estimated model confirms a significant quadratic decrease in the compressive strength value linked to an increase on the H_2O/Al_2O_3 molar ratio. This trend is in accordance with the literature (Ismail et al., 2011; Xie and Kayali, 2014) As previously mentioned, increasing the water content (increasing the H_2O/Al_2O_3 molar ratio) increases the porosity of the final structure (Khale and Chaudhary, 2007). Pores act as a defect point and therefore a higher porosity significantly lowers the compression strength of the final product.

The model shows a very good fit of the data (high R^2 and low residual reported in

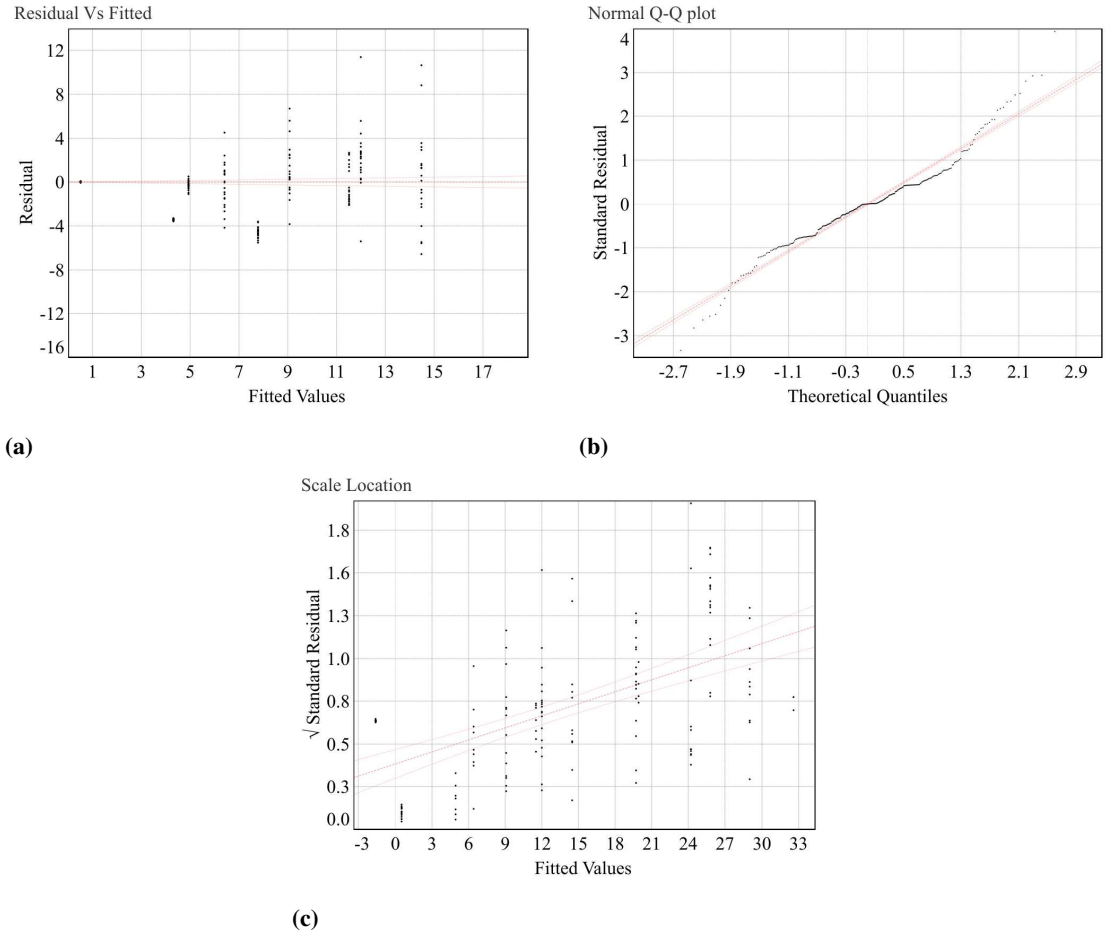

Figure 4.11: *Residual analysis of the estimated model in Eq 4.7*

Fig. 4.11). The fitting of the data could be improved even more using a polynomial with a higher degree (from 2 to 3). However, some of the hypotheses underlying the model are not fully satisfied (slightly heteroskedasticity in Fig.4.11c) and so for this reason the estimates are not completely reliable.

4.3.5 Comprehensive Model

To separate the possible effect of each condition all other things being equal, a full factorial design of experiments should be conducted. Nevertheless, in the experimental unfeasibility of varying so many conditions, a comprehensive model has been estimated. The model attempts the ambitious aim of explaining the variability of the compressive strength of metakaolin-based geopolymers by accounting for all the factors

considered so far, namely curing and aging time, curing temperature and composition (SiO_2/Al_2O_3 and H_2O/Al_2O_3 molar ratios). Among several alternative formulations, the best model has been selected, specified as follows:

$$\mathrm{E}(\sigma) = \begin{cases} \beta_0 + \beta_1 C + \beta_2 A + \beta_3 T + \beta_4 I_{T>60} + \beta_5 \frac{SiO_2}{Al_2O_3} + \beta_6 \frac{SiO_2}{Al_2O_3}^2 + \\ \beta_7 \frac{H_2O}{Al_2O_3} + \beta_8 (\frac{H_2O}{Al_2O_3})^2 \; Alkaline\; Cation\; K \\ \\ (\beta_0 + \gamma_0) + (\beta_1 + \gamma_1) C + (\beta_2 + \gamma_2) A + (\beta_3 + \gamma_3) T + \gamma_4 I_{T>40} + \\ (\beta_5 + \gamma_5) \frac{SiO_2}{Al_2O_3} + (\beta_6 + \gamma_6) \frac{SiO_2}{Al_2O_3}^2 + \\ (\beta_7 + \gamma_7) \frac{H_2O}{Al_2O_3} + (\beta_8 + \gamma_8) (\frac{H_2O}{Al_2O_3})^2 \; Alkaline\; Cation\; Na \end{cases} \tag{4.8}$$

The estimated parameters, along with their standard errors and significance are summarized in Table 4.6.

The model is essentially consistent with the results emerging from the marginal models discussed above, yet some further significance has arisen when accounting for all the factors involved.

Curing time is confirmed to positively affect the expected compressive strength in both types of geopolymers, with a larger effect on sodium-based cations. Aging time is also confirmed to have a moderate positive effect on the compressive strength of sodium-based geopolymers only. Same goes for the H_2O/Al_2O_3 molar ratio, negatively affecting the compressive strengths with a quadratic trend.

Table 4.6: *Estimates, standard errors and level of significance of parameters in Eq. 4.3.5; F statistics, R2, DF (Degree of Freedom). Significance levels: 0 '***', 0.001 '**', '× ' 1*

β_0	-95.45 (13.68)	***	γ_0	1.90	
β_1	0.06 (0.02)	***	γ_1	0.05 (0.02)	.
β_2	-0.007 (0.01)		γ_2	0.04 (0.01)	**
β_3	-0.06 (0.02)	*	γ_3	0.03 (0.04)	
β_4	0.38 (0.90)		γ_4	-4.51 (1.27)	***
β_5	83.43 (7.23)	***	γ_5	11.18 (8.79)	
β_6	-10.67 (1.05)	***	γ_6	-2.14 (1.25)	.
β_7	-3.66 (0.36)	***	γ_7	-1.46 (0.50)	**
β_8	0.06 (0.008)	***	γ_8	0.02 (0.01)	.
$R^2 = 0.73$, F-statistic: 199.1 on 17 and 1236 DF ***					

The silica to alumina ratio also maintains the expected quadratic effect on both types of geopolymer, yet accounting for all the involved factors allows for a significant difference between the trends of the two cations to arise. Sodium-based geopolymers show a larger parabolic curvature, suggesting both a slower increase and a slower decrease after the maximum is reached.

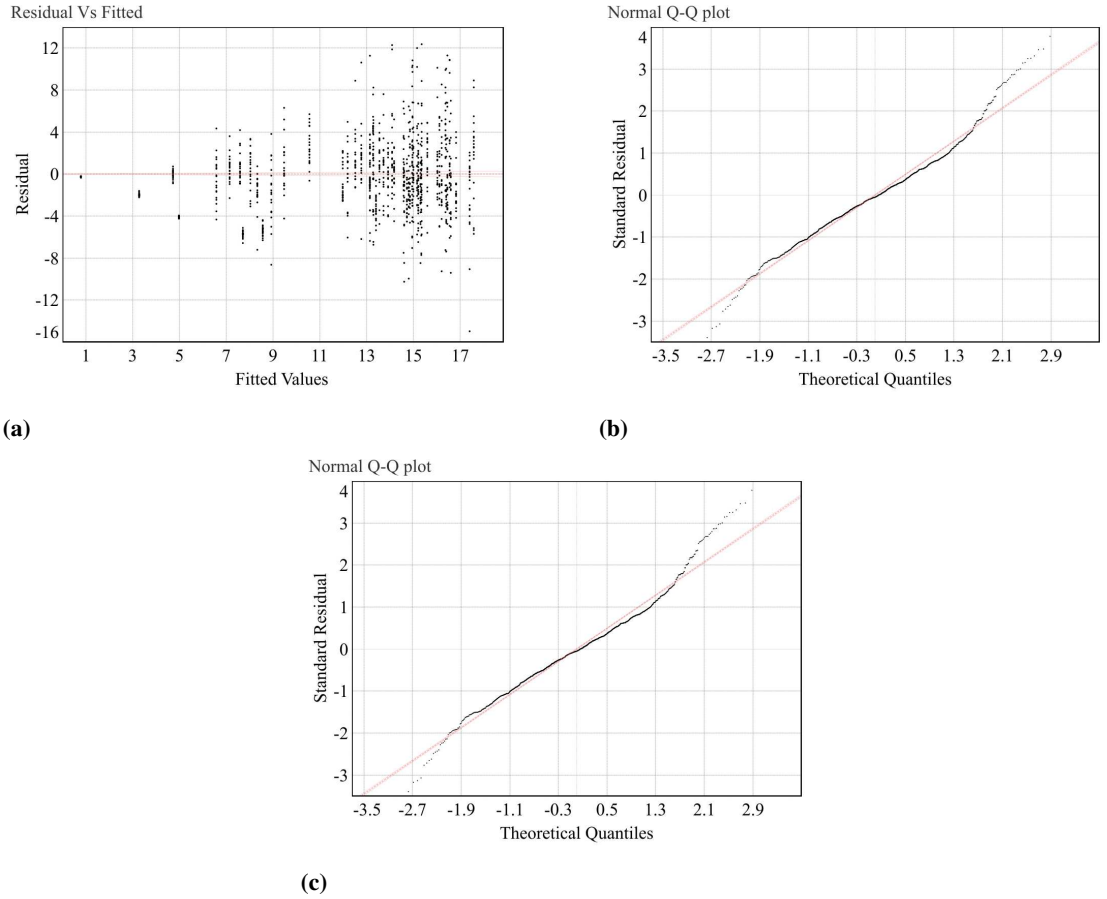

Figure 4.12: *Residual analysis of the global model*

Variation of all the involved experimental condition is globally able to explain about 73% of the total variability of the compressive strength. Residual analysis (reported in Fig. 4.12) is overall satisfactory: slight evidence of the violation of the hypothesis of normality is evident at the tails of the distribution only. We posit that this is due to either small changes in the experimental conditions (beyond our control), or to some measurement errors, leading to a few outlier values of the compressive strength. Also, a limited trend in the scale location plot suggests a moderate heteroskedasticity of the errors, which might reduce the efficiency of the estimates. Nevertheless, the standard errors are overall rather small with respect to the estimates, hence their possible increase because of the loss of efficiency can be considered tolerable and does not undermine the whole reliability of the model.

4.3.6 Model Limitations

It's important to note that the current model is strictly limited to describing the compressive strength within the boundaries set by the conditions chosen for this study. As such, the results may not be directly extrapolated to different processing conditions. This presents a potential area for future development, where the model could be refined and validated across a broader set of conditions. At this juncture, the model is most reliable for small sample sizes. One of the key challenges we've identified is the introduction of a size effect factor to consider samples with varying dimensions. Size effects can significantly influence material properties, particularly in the case of geopolymers where the microstructure plays a key role in determining performance. Therefore, future work will focus on developing and validating a size effect factor to ensure that our model can accurately predict the behavior of geopolymers regardless of sample size.

4.3.7 Conclusions

Three different statistical models have been proposed to account for the experimental relationship between the compressive strength of potassium and sodium-based geopolymer samples and different process parameters and their composition. For all models, the errors have been computed and analyzed to assess their statistical reliability. We can conclude that:

- Curing time shows a positive relationship with compressive strength.
- Aging time has a slight positive effect on sodium geopolymers, and it does not significantly affect potassium-based geopolymers.
- Curing temperature negatively affects compressive strength. In fact, increasing the curing temperature led to a decrease in the compressive strength values.
- The SiO_2/Al_2O_3 ratio shows a significant quadratic concave trend with compressive strength. Increasing this ratio provides an increase in the compressive

strength up to a certain threshold which is different for potassium and sodium-based geopolymers. Above the threshold, increasing SiO_2/Al_2O_3 led to a decrease in the mechanical properties.

- The potassium-based geopolymer system shows an almost linearly inverse proportionality between compressive strength and the H_2O/Al_2O_3 molar ratio. The sodium-based geopolymer system displays an increase of compressive strength at the beginning (from H_2O/Al_2O_3 = 11 to 13). Above H_2O/Al_2O_33 = 13, a linear decrease can be observed until H_2O/Al_2O_3 = 20, while after this threshold a plateau is reached.

A final comprehensive statistical model has been proposed that is able to predict the compressive strength of both potassium and sodium based geopolymers as a function of some process variables (curing and aging time, curing temperature) and the geopolymer formulation (SiO_2/Al_2O_3 and H_2O/Al_2O_3 molar ratios). The observed differences in the mechanical strength of the samples as a function of the different parameters considered can be attributed, according to the literature, to variations in the characteristics of the geopolymer network developed under the different processing conditions.

Further work will aim to add greater variability to the model in order to achieve a better description capability of the compressive strength dependencies on the processing condition; moreover, more efforts will be devoted to the further validation of the proposed model for different starting raw materials (e.g., fly ash) and for composite materials using a geopolymer phase as matrix. Moreover, the model is strictly limited to describing the compressive strength inside the boundaries set by the conditions chosen to design the entire work. At this stage, the model is reliable for small samples; more work is ongoing to introduce a size effect factor to consider samples with different dimensions.

Nevertheless, the fact that the model is based on the testing of more than 1200 samples all prepared in a consistent way and provides a reasonable fitting of data, lends appropriate consistency to the statistical model proposed.

Conclusions

This thesis encapsulates a comprehensive exploration into the innovative applications and advancements in geopolymer technology, underpinned by four pivotal studies carried out throughout the doctoral journey. The initial investigation unveiled a novel methodology of enhancing carbon dioxide (CO_2) adsorption via high-shear wet granulation of potassium-based geopolymer, with a notable enhancement in adsorption capacities achieved through zeolite 13x incorporation and APTES functionalization. This lays a solid foundation for future research to delve into other functionalization techniques, propelling the development of efficient and sustainable solutions for CO_2 capture.

Transitioning from granulation to additive manufacturing, the second study employed the Direct Ink Writing (DIW) method to fabricate geopolymer and geopolymer-zeolite structures, revealing a significant influence of geometry on adsorption performance. The exceptional adsorption capacities showcased, especially in the context of clenbuterol adsorption, affirm the potential of geopolymers in environmental remediation, setting a promising trajectory for the commercialization of such products once the scaling-up challenges of the DIW process are surmounted.

The third study ventured into a novel application of geopolymer membranes, demonstrating the successful production of these membranes using the warm pressing technique. The findings from this study not only pave the way for ongoing cut-off experiments but also serve as a precursor for employing geopolymer membranes in combating water pollution, a critical environmental challenge.

Lastly, the fourth study embarked on a rigorous statistical analysis to model the compressive strength behavior of potassium and sodium-based geopolymers. The comprehensive statistical model proposed, underpinned by the testing of over 1200 samples, holds promise in predicting the compressive strength based on various process variables and geopolymer formulations. This model serves as a stepping stone for future work aimed at enhancing its descriptive capability and validating it across different raw materials and composite materials with a geopolymer matrix.

In summary, the collective findings from these four studies underscore the versatility and potential of geopolymer technology in addressing a spectrum of environmental challenges. The innovative methodologies employed, the novel applications explored, and the promising results obtained, collectively contribute to the burgeoning body of knowledge in geopolymer research. The journey traversed in this thesis not only sheds light on the multifaceted benefits of geopolymers but also propels the discourse towards more sustainable and efficient solutions for environmental remediation and beyond.

Bibliography

[1] Twin screw granulation using conveying screws: Effects of viscosity of granulation liquids and flow of powders. *Powder Technology*, 238:77–90, 2013.

[2] Effect of initial water content and curing moisture conditions on the development of fly ash-based geopolymers in heat and ambient temperature. *Construction and Building Materials*, 67:20–28, 2014.

[3] Ceyhun Akarsu, Halil Kumbur, and Ahmet Erkan Kideys. Removal of microplastics from wastewater through electrocoagulation-electroflotation and membrane filtration processes. *Water Science and Technology*, 84:1648–1662, 2021.

[4] Galip Akay and Kui Zhang. Process intensification in ammonia synthesis using novel coassembled supported microporous catalysts promoted by nonthermal plasma. *Industrial & Engineering Chemistry Research*, 56:457–468, 2017.

[5] G D Akpen, M I Aho, and M H Mamwan. Equilibrium and kinetics of colour adsorption from textile wastewater by a novel adsorbent. *Global Journal of Pure and Applied Sciences*, 24:61–67, 2018.

[6] Isil Akpinar, Riki J Drout, Timur Islamoglu, Satoshi Kato, Jiafei Lyu, and Omar K Farha. Exploiting $\pi - \pi$ interactions to design an efficient sorbent for atrazine removal from water. *ACS applied materials & interfaces*, 11:6097–6103, 2019.

[7] Imran Ali, Tengda Ding, Changsheng Peng, Iffat Naz, Huibin Sun, Juying Li, and Jingfu Liu. Micro-and nanoplastics in wastewater treatment plants: occurrence, removal, fate, impacts and remediation technologies–a critical review. *Chemical Engineering Journal*, 423:130205, 2021.

[8] Ian J Allan, Kirk T Semple, Rina Hare, and Brian J Reid. Cyclodextrin enhanced biodegradation of polycyclic aromatic hydrocarbons and phenols in contaminated soil slurries. *Environmental science & technology*, 41:5498–5504, 2007.

[9] Ali Alloul, Mouhamadou Amar, Mahfoud Benzerzour, and Nor-Edine Abriak. Geopolymer mortar with flash-calcined sediments cured under ambient conditions. *Construction and Building Materials*, 391:131809, 2023.

[10] Byeong-Kwan An. Adsorption kinetic study of ruthenium complex dyes onto tio 2 anodes for dye-sensitized solar cells (dsscs). *Journal of the Korean Institute of Electrical and Electronic Material Engineers*, 24:929–934, 2011.

[11] Julien Archez, Ameni Gharzouni, I Sobrados, A Piancastelli, J F Caron, N Texier-Mandoki, X Bourbon, and S Rossignol. Geopolymer local network evolution under time and temperature. *Journal of Non-Crystalline Solids*, 566:120870, 2021.

[12] Nurliyana Ariffin, Mohd Mustafa Al Bakri Abdullah, Mohd Remy Rozainy Mohd Arif Zainol, Mohd Fared Murshed, Meor Ahmad Faris, and Ridho Bayuaji. Review on adsorption of heavy metal in wastewater by using geopolymer. volume 97, page 01023. EDP Sciences, 2017.

[13] Chengying Bai, Giorgia Franchin, Hamada Elsayed, Alessandro Zaggia, Lino Conte, Hongqiang Li, and Paolo Colombo. High-porosity geopolymer foams with tailored porosity for thermal insulation and wastewater treatment. *Journal of Materials Research*, 32:3251–3259, 2017.

[14] A M Mustafa Al Bakria, H Kamarudin, M BinHussain, I Khairul Nizar, Y Zarina, and A R Rafiza. The effect of curing temperature on physical and chemical properties of geopolymers. *Physics Procedia*, 22:286–291, 2011.

[15] Arvind K Bansal, Garima Balwani, and Sneha Sheokand. *Chapter 12 - Critical Material Attributes in Wet Granulation*, pages 421–453. Academic Press, 2019.

[16] Francisco Belzagui, Martí Crespi, Antonio Álvarez, Carmen Gutiérrez-Bouzán, and Mercedes Vilaseca. Microplastics' emissions: Microfibers' detachment from textile garments. *Environmental Pollution*, 248:1028–1035, 2019.

[17] Francisco Belzagui, Carmen Gutiérrez-Bouzán, Antonio Álvarez Sánchez, and Mercedes Vilaseca. Textile microfibers reaching aquatic environments: A new estimation approach. *Environmental Pollution*, 265:114889, 2020.

[18] Vera Bolis, Claudia Busco, and Piero Ugliengo. Thermodynamic study of water adsorption in high-silica zeolites. *The Journal of Physical Chemistry B*, 110:14849–14859, 2006.

[19] M Boscherini, F Miccio, E Papa, V Medri, E Landi, F Doghieri, and M Minelli. The relevance of thermal effects during co2 adsorption and regeneration in a geopolymer-zeolite composite: Experimental and modelling insights. *Chemical Engineering Journal*, 408:127315, 2021.

[20] Mattia Boscherini, Francesco Miccio, Elettra Papa, Valentina Medri, Elena Landi, Ferruccio Doghieri, and Matteo Minelli. Co2 adsorption in a geopolymer-zeolite composite: Experimental dynamic tests and modelling insights on related thermal effects. *Chemical Engineering Transactions*, 86:1069–1074, 2021.

[21] R F Botti, M D M Innocentini, T A Faleiros, M F Mello, D L Flumignan, L K Santos, G Franchin, and P Colombo. Additively manufactured geopolymer structured heterogeneous catalysts for biodiesel production. *Applied Materials Today*, 23:101022, 2021.

[22] Andreas Börger, Peter Supancic, and Robert Danzer. The ball on three balls test for strength testing of brittle discs: stress distribution in the disc. *Journal of the European Ceramic Society*, 22:1425–1436, 2002.

[23] Andreas Börger, Peter Supancic, and Robert Danzer. The ball on three balls test for strength testing of brittle discs: stress distribution in the disc. *Journal of the European Ceramic Society*, 22:1425–1436, 2002.

[24] Sebastiano Candamano, Alfonso Policicchio, Anastasia Macario, G Conte, R G Agostino, Patrizia Frontera, and Fortunato Crea. Co2 adsorption investigation on an innovative nanocomposite material with hierarchical porosity. *Journal of Nanoscience and Nanotechnology*, 19:3223–3231, 2019.

[25] Massimiliano Caramia, Paolo Dell'Olmo, Massimiliano Caramia, and Paolo Dell'Olmo. Multi-objective optimization. *Multi-objective Management in Freight Logistics: Increasing Capacity, Service Level, Sustainability, and Safety with Optimization Algorithms*, pages 21–51, 2020.

[26] Minju Cha, Chanhee Boo, and Chanhyuk Park. Simultaneous retention of organic and inorganic contaminants by a ceramic nanofiltration membrane for the treatment of semiconductor wastewater. *Process Safety and Environmental Protection*, 159:525–533, 2022.

[27] Minju Cha, Chanhee Boo, In-Hyuck Song, and Chanhyuk Park. Investigating the potential of ammonium retention by graphene oxide ceramic nanofiltration membranes for the treatment of semiconductor wastewater. *Chemosphere*, 286:131745, 2022.

[28] Minju Cha, Soyoun Kim, and Chanhyuk Park. Recent advances and future potential of anaerobic ceramic membrane bioreactors for wastewater treatment: A review. *Membrane Water Treatment*, 11:31, 2020.

[29] T W Cheng, M L Lee, M S Ko, T H Ueng, and S F Yang. The heavy metal adsorption characteristics on metakaolin-based geopolymer. *Applied Clay Science*, 56:90–96, 2012.

[30] Pui Kwan Cheung and Lincoln Fok. Characterisation of plastic microbeads in facial scrubs and their estimated emissions in mainland china. *Water research*, 122:53–61, 2017.

[31] Emilie Chevalier, Marylène Viana, Sophie Cazalbou, and Dominique Chulia. Comparison of low-shear and high-shear granulation processes: effect on implantable calcium phosphate granule properties. *Drug development and industrial pharmacy*, 35:1255–1263, 2009.

[32] Arti Chouksey, Manvendra Verma, Nirendra Dev, Ibadur Rahman, and Kamal Upreti. An investigation on the effect of curing conditions on the mechanical and microstructural properties of the geopolymer concrete. *Materials Research Express*, 9:055003, 2022.

[33] Philippe Colomban. Sol-gel control of the micro/nanostructure of functional ceramic-ceramic and metal-ceramic composites. *Journal of materials research*, 13:803–811, 1998.

[34] J Davidovits. Geopolymer chemistry and applications, saint-quentin, 2011.

[35] Joseph Davidovits. Geopolymers and geopolymeric materials. *Journal of thermal analysis*, 35:429–441, 1989.

[36] Joseph Davidovits. Geopolymers: inorganic polymeric new materials. *Journal of Thermal Analysis and calorimetry*, 37:1633–1656, 1991.

[37] Joseph Davidovits. Geopolymer cement. *A review. Geopolymer Institute, Technical papers*, 21:1–11, 2013.

[38] Kalyanmoy Deb, Karthik Sindhya, and Jussi Hakanen. *Multi-objective optimization*, pages 161–200. CRC Press, 2016.

[39] Guy. Degand, Anne. Bernes-Duyckaerts, and Guy. Maghuin-Rogister. Determination of clenbuterol in bovine tissues and urine by enzyme immunoassay. *Journal of Agricultural and Food Chemistry*, 40:70–75, 1 1992. doi: 10.1021/jf00013a014.

[40] Haojie Ding, Jian Zhang, Huan He, Ying Zhu, Dionysios D Dionysiou, Zhen Liu, and Chun Zhao. Do membrane filtration systems in drinking water treatment plants release nano/microplastics? *Science of the Total Environment*, 755:142658, 2021.

[41] P Duxson, A Fernández-Jiménez, J L Provis, G C Lukey, A Palomo, and J S J van Deventer. Geopolymer technology: the current state of the art. *Journal of Materials Science*, 42:2917–2933, 2007.

[42] Peter Duxson, John L Provis, Grant C Lukey, Seth W Mallicoat, Waltraud M Kriven, and Jannie S J Van Deventer. Understanding the relationship between geopolymer composition, microstructure and mechanical properties. *Colloids and Surfaces A: Physicochemical and Engineering Aspects*, 269:47–58, 2005.

[43] Z Emdadi, N Asim, M A Yarmo, R Shamsudin, M Mohammad, and K Sopian. The study of naoh and aging time effects on green geopolymer's compressive strength. *Advances in Environmental Biology*, 10:119–125, 2016.

[44] Aleksandar Erić, Dragoljub Dakić, Stevan Nemoda, Mirko Komatina, and Branislav Repić. Experimental method for determining forchheimer equation coefficients related to flow of air through the bales of soy straw. *International Journal of heat and mass transfer*, 54:4300–4306, 2011.

[45] Alireza Esparham and Amir Bahador Moradikhou. Factors influencing compressive strength of fly ash-based geopolymer concrete. *Amirkabir Journal of Civil Engineering*, 53:21–31, 2021.

[46] A Faure, P York, and R C Rowe. Process control and scale-up of pharmaceutical wet granulation processes: a review. *European Journal of Pharmaceutics and Biopharmaceutics*, 52:269–277, 2001.

[47] Lisa S Fendall and Mary A Sewell. Contributing to marine pollution by washing your face: microplastics in facial cleansers. *Marine pollution bulletin*, 58:1225–1228, 2009.

[48] Giorgia Franchin, Janne Pesonen, Tero Luukkonen, Chengying Bai, Paolo Scanferla, Renata Botti, Sara Carturan, Murilo Innocentini, and Paolo Colombo. Removal of ammonium from wastewater with geopolymer sorbents fabricated via additive manufacturing. *Materials & Design*, 195:109006, 2020.

[49] Giorgia Franchin, Paolo Scanferla, Luca Zeffiro, Hamada Elsayed, Andrea Baliello, Giovanni Giacomello, Marco Pasetto, and Paolo Colombo. Direct ink writing of geopolymeric inks. *Journal of the European Ceramic Society*, 37:2481–2489, 2017.

[50] João P G L Frias and Roisin Nash. Microplastics: Finding a consensus on the definition. *Marine pollution bulletin*, 138:145–147, 2019.

[51] Ana Galvão, Margarida Aleixo, Hilda De Pablo, Clara Lopes, and Joana Raimundo. Microplastics in wastewater: microfiber emissions from common household laundry. *Environmental Science and Pollution Research*, 27:26643–26649, 2020.

[52] J Ramón Gasca-Tirado, José Carlos Rubio-Ávalos, M S Muñiz-Villarreal, Alejandro Manzano-Ramírez, José Luis Reyes-Araiza, S Sampieri-Bulbarela, Carlos Villaseñor-Mora, J J Pérez-Bueno, L M Apatiga, and Vicente Amigó Borrás. Effect of porosity on the absorbed, reemitted and transmitted light by a geopolymer metakaolin base. *Materials Letters*, 65:880–883, 2011.

[53] Jenna Gavigan, Timnit Kefela, Ilan Macadam-Somer, Sangwon Suh, and Roland Geyer. Synthetic microfiber emissions to land rival those to waterbodies and are growing. *PLoS One*, 15:e0237839, 2020.

[54] M Ghanbari, A M Hadian, A A Nourbakhsh, and K J D MacKenzie. Modeling and optimization of compressive strength and bulk density of metakaolin-based geopolymer using central composite design: A numerical and experimental study. *Ceramics International*, 43:324–335, 2017.

[55] R Girimonte, B Formisani, and F Testa. Adsorption of co2 on a confined fluidized bed of pelletized 13x zeolite. *Powder Technology*, 311:9–17, 2017.

[56] D J Godfrey and S John. Disc flexure tests for the evaluation of ceramic strength. *Ceramic materials and components for engines*, pages 657–665, 1986.

[57] Jong Kwon Han, Beom Soo Shin, and Du Hyung Choi. Comprehensive study of intermediate and critical quality attributes for process control of high-shear wet granulation using multivariate analysis and the quality by design approach. *Pharmaceutics*, 11, 2019.

[58] Le Han, Xiaodong Wang, Boqiang Wu, Shibin Zhu, Jixiang Wang, and Yuehong Zhang. In-situ synthesis of zeolite x in foam geopolymer as a co2 adsorbent. *Journal of Cleaner Production*, 372:133591, 2022.

[59] Djwantoro Hardjito, Steenie E Wallah, Dody M J Sumajouw, and B Vijaya Rangan. Factors influencing the compressive strength of fly ash-based geopolymer concrete. *Civil engineering dimension*, 6:88–93, 2004.

[60] Amer Hassan, Mohammed Arif, and Mohd Shariq. Use of geopolymer concrete for a cleaner and sustainable environment–a review of mechanical properties and microstructure. *Journal of cleaner production*, 223:704–728, 2019.

[61] Peter Dybdahl Hede. Fluid bed particle processing-ebooks and textbooks from bookboon. com, 2013.

[62] Michael G Herting and Peter Kleinebudde. Roll compaction/dry granulation: Effect of raw material particle size on granule and tablet properties. *International journal of pharmaceutics*, 338:110–118, 2007.

[63] Yoshio Hiramatsu and Yukitoshi Oka. Determination of the tensile strength of rock by a compression test of an irregular test piece. volume 3, pages 89–90. Elsevier, 1966.

[64] Jiachen Huang, Jianquan Luo, Xiangrong Chen, Shichao Feng, and Yinhua Wan. How do chemical cleaning agents act on polyamide nanofiltration membrane and fouling layer? *Industrial & Engineering Chemistry Research*, 59:17653–17670, 2020.

[65] Martin A Hubbe, Saeid Azizian, and Sigrid Douven. Implications of apparent pseudo-second-order adsorption kinetics onto cellulosic materials: A review. *BioResources*, 14, 2019.

[66] Bing hui Mo, He Zhu, Xue min Cui, Yan He, and Si yu Gong. Effect of curing temperature on geopolymerization of metakaolin-based geopolymers. *Applied clay science*, 99:144–148, 2014.

[67] Joseph Cesarano III and P D Calvert. Freeforming objects with low-binder slurry. 2000.

[68] I Ismail, John Provis, Jannie Van Deventer, and Sinin Hamdan. The effect of water content on compressive strength of geopolymer mortars. *AES-ATEMA International Conference Series - Advances and Trends in Engineering Materials and their Applications*, pages 49–56, 1 2011.

[69] J C Jaeger. Failure of rocks under tensile conditions. volume 4, pages 219–227. Elsevier, 1967.

[70] Yeongmi Jeong, Slawomir W Hermanowicz, and Chanhyuk Park. Treatment of food waste recycling wastewater using anaerobic ceramic membrane bioreactor for biogas production in mainstream treatment process of domestic wastewater. *Water research*, 123:86–95, 2017.

[71] BHWS De Jong and Gordon E Brown Jr. Polymerization of silicate and aluminate tetrahedra in glasses, melts, and aqueous solutions—i. electronic structure of h6si2o7, h6alsio71-, and h6al2o72-. *Geochimica et Cosmochimica Acta*, 44:491–511, 1980.

[72] J Jänchen, D Ackermann, H Stach, and W Brösicke. Studies of the water adsorption on zeolites and modified mesoporous materials for seasonal storage of solar heat. *Solar energy*, 76:339–344, 2004.

[73] Jingyan Kang, Yujie Zhang, Xing Li, Lijing Miao, and Aiguo Wu. A rapid colorimetric sensor of clenbuterol based on cysteamine-modified gold nanoparticles. *ACS applied materials & interfaces*, 8:1–5, 2016.

[74] Divya Khale and Rubina Chaudhary. Mechanism of geopolymerization and factors influencing its development: a review. *Journal of materials science*, 42:729–746, 2007.

[75] Soyoun Kim and Chanhyuk Park. Fouling behavior and cleaning strategies of ceramic ultrafiltration membranes for the treatment and reuse of laundry wastewater. *Journal of Water Process Engineering*, 48:102840, 2022.

[76] Naveen Konduru, Peter Lindner, and Nada Marie Assaf-Anid. Curbing the greenhouse effect by carbon dioxide adsorption with zeolite 13x. *AIChE journal*, 53:3137–3143, 2007.

[77] H Gjelstrup Kristensen and T Schaefer. Granulation: a review on pharmaceutical wet-granulation. *Drug development and industrial pharmacy*, 13:803–872, 1987.

[78] C Kuenzel, T P Neville, S Donatello, L Vandeperre, A R Boccaccini, and C R Cheeseman. Influence of metakaolin characteristics on the mechanical properties of geopolymers. *Applied Clay Science*, 83:308–314, 2013.

[79] Mukund Lahoti, Pratik Narang, Kang Hai Tan, and En-Hua Yang. Mix design factors and strength prediction of metakaolin-based geopolymer. *Ceramics international*, 43:11433–11441, 2017.

[80] Mukund Lahoti, En-Hua Yang, and Kang Hai Tan. Influence of mix design parameters on geopolymer mechanical properties and microstructure. *Developments in Strategic Ceramic Materials II: Ceramic Engineering and Science Proceedings Volume 37, Issue 7*, 37:21–33, 2017.

[81] DKPK Lavanya, P K Kulkarni, Mudit Dixit, Prudhvi Kanth Raavi, and L Naga Vamsi Krishna. Sources of cellulose and their applications—a review. *International Journal of Drug Formulation and Research*, 2:19–38, 2011.

[82] Chadon Lee, Songhee Lee, and Ngocchien Nguyen. Modeling of compressive strength development of high-early-strength-concrete at different curing temperatures. *International Journal of Concrete Structures and Materials*, 10:205–219, 2016.

[83] Yoojin Lee, Minju Cha, Yeon So, In-Hyuck Song, and Chanhyuk Park. Functionalized boron nitride ceramic nanofiltration membranes for semiconductor wastewater treatment. *Separation and Purification Technology*, 300:121945, 2022.

[84] Jingyi Li, Huihui Liu, and J Paul Chen. Microplastics in freshwater systems: A review on occurrence, environmental effects, and methods for microplastics detection. *Water research*, 137:362–374, 2018.

[85] Binbin Liu, Jiamiao Wang, Jia Zeng, Lijie Zhao, Youjie Wang, Yi Feng, and Ruofei Du. A review of high shear wet granulation for better process understanding, control and product development. *Powder Technology*, 381:204–223, 2021.

[86] Maricela Lizcano, Hyun Soo Kim, Sandip Basu, and Miladin Radovic. Mechanical properties of sodium and potassium activated metakaolin-based geopolymers. *Journal of Materials Science*, 47:2607–2616, 2012.

[87] Linyu Long, Fenfen Li, Mengying Shu, Caili Zhang, and Yunxuan Weng. Fabrication and application of carboxymethyl cellulose-carbon nanotube aerogels. *Materials*, 12:1867, 2019.

[88] Márlon A Longhi, Zuhua Zhang, Erich D Rodríguez, Ana Paula Kirchheim, and Hao Wang. Efflorescence of alkali-activated cements (geopolymers) and the impacts on material structures: A critical analysis. *Frontiers in Materials*, 6:89, 2019.

[89] Tero Luukkonen, Kateřina Věžníková, Emma-Tuulia Tolonen, Hanna Runtti, Juho Yliniemi, Tao Hu, Kimmo Kemppainen, and Ulla Lassi. Removal of ammonium from municipal wastewater with powdered and granulated metakaolin geopolymer. *Environmental Technology*, 39:414–423, 2018.

[90] Tero Luukkonen, Juho Yliniemi, Harisankar Sreenivasan, Katja Ohenoja, Mikko Finnilä, Giorgia Franchin, and Paolo Colombo. Ag-or cu-modified geopolymer filters for water treatment manufactured by 3d printing, direct foaming, or granulation. *Scientific Reports*, 10:1–14, 2020.

[91] Xuemin Lv, Qian Dong, Zhiqiang Zuo, Yanchen Liu, Xia Huang, and Wei-Min Wu. Microplastics in a municipal wastewater treatment plant: Fate, dynamic distribution, removal efficiencies, and control strategies. *Journal of Cleaner Production*, 225:579–586, 2019.

[92] Nader Mahinpey, Davood Karami, and Babak Labbaf. Zeolites and their composites for co2 adsorption. *CO2-philic Polymers, Nanocomposites and Chemical Solvents*, pages 271–288, 2023.

[93] J F Martinez-Navarro. Food poisoning related to consumption of illicit beta-agonist in liver. *Lancet (British Edition)*, 336, 1990.

[94] Faris Matalkah, Parviz Soroushian, Anagi Balchandra, and Amirpasha Peyvandi. Characterization of alkali-activated nonwood biomass ash–based geopolymer concrete. *Journal of Materials in Civil Engineering*, 29:04016270, 2017.

[95] Hayley K McIlwraith, Jack Lin, Lisa M Erdle, Nicholas Mallos, Miriam L Diamond, and Chelsea M Rochman. Capturing microfibers–marketed technologies reduce microfiber emissions from washing machines. *Marine pollution bulletin*, 139:40–45, 2019.

[96] M Minelli, E Papa, V Medri, F Miccio, P Benito, F Doghieri, and E Landi. Characterization of novel geopolymer–zeolite composites as solid adsorbents for co2 capture. *Chemical Engineering Journal*, 341:505–515, 2018.

[97] Matteo Minelli, Valentina Medri, Elettra Papa, Francesco Miccio, Elena Landi, and Ferruccio Doghieri. Geopolymers as solid adsorbent for co2 capture. *Chemical Engineering Science*, 148:267–274, 2016.

[98] Adelaide Miranda, Lidia Martínez, and Pieter A A De Beule. Facile synthesis of an aminopropylsilane layer on si/sio2 substrates using ethanol as aptes solvent. *MethodsX*, 7:100931, 2020.

[99] M Muracchioli, G Menardi, M D' Agostini, G Franchin, and P Colombo. Modeling the compressive strength of metakaolin-based geopolymers based on the statistical analysis of experimental data. *Applied Clay Science*, 242:107020, 2023.

[100] Fionn Murphy, Ciaran Ewins, Frederic Carbonnier, and Brian Quinn. Wastewater treatment works (wwtw) as a source of microplastics in the aquatic environment. *Environmental science & technology*, 50:5800–5808, 2016.

[101] M S Muñiz-Villarreal, A Manzano-Ramírez, S Sampieri-Bulbarela, J Ramón Gasca-Tirado, J L Reyes-Araiza, J C Rubio-Ávalos, J J Pérez-Bueno, L M Apatiga, A Zaldivar-Cadena, and V Amigó-Borrás. The effect of

temperature on the geopolymerization process of a metakaolin-based geopolymer. *Materials Letters*, 65:995–998, 2011.

[102] Imogen E Napper, Aaron C Barrett, and Richard C Thompson. The efficiency of devices intended to reduce microfibre release during clothes washing. *Science of the Total Environment*, 738:140412, 2020.

[103] Imogen E Napper and Richard C Thompson. Release of synthetic microplastic plastic fibres from domestic washing machines: Effects of fabric type and washing conditions. *Marine pollution bulletin*, 112:39–45, 2016.

[104] Donald A Nield, Adrian Bejan, Donald A Nield, and Adrian Bejan. Mass transfer in a porous medium: multicomponent and multiphase flows. *Convection in porous media*, pages 57–84, 2017.

[105] Rui M Novais, Robert.C. Pullar, and João A Labrincha. Geopolymer foams: An overview of recent advancements. *Progress in Materials Science*, 109:100621, 2020.

[106] Muhd Fadhil Nurruddin, Haruna Sani, Bashar S Mohammed, and Ibrahim Shaaban. Methods of curing geopolymer concrete: A review. *International Journal of Advanced and Applied Sciences*, 5:31–36, 2018.

[107] Biranchi Panda, Suvash Chandra Paul, Lim Jian Hui, Yi Wei Daniel Tay, and Ming Jen Tan. Additive manufacturing of geopolymer for sustainable built environment. *Journal of cleaner production*, 167:281–288, 2017.

[108] E Papa, E Landi, A Natali Murri, F Miccio, A Vaccari, and V Medri. Co2 adsorption at intermediate and low temperature by geopolymer-hydrotalcite composites. *Open Ceramics*, 5:100048, 2021.

[109] E Papa, V Medri, C Paillard, B Contri, A Natali Murri, A Vaccari, and E Landi. Geopolymer-hydrotalcite composites for co2 capture. *Journal of Cleaner Production*, 237:117738, 2019.

[110] Elettra Papa, Matteo Minelli, Maria Chiara Marchioni, Elena Landi, Francesco Miccio, Annalisa Natali Murri, Patricia Benito, Angelo Vaccari, and Valentina Medri. Metakaolin-based geopolymer – zeolite naa composites as co2 adsorbents. *Applied Clay Science*, 237:106900, 2023.

[111] Jeong Hoon Park, Sun Hyung Kim, and Kyung Hyun Ahn. Role of carboxymethyl cellulose binder and its effect on the preparation process of anode slurries for li-ion batteries. *Colloids and Surfaces A: Physicochemical and Engineering Aspects*, 664:131130, 2023.

[112] Jeewan Pokhrel, Nidhika Bhoria, Stavroula Anastasiou, Theodoros Tsoufis, Dimitrios Gournis, George Romanos, and Georgios N Karanikolos. Co2 adsorption behavior of amine-functionalized zif-8, graphene oxide, and zif-8/graphene oxide composites under dry and wet conditions. *Microporous and Mesoporous Materials*, 267:53–67, 2018.

[113] Joana Correia Prata. Microplastics in wastewater: State of the knowledge on sources, fate and solutions. *Marine pollution bulletin*, 129:262–265, 2018.

[114] B Vijaya Rangan. Fly ash-based geopolymer concrete. 2008.

[115] Navid Ranjbar, Amin Kashefi, and Mahmoud R Maheri. Hot-pressed geopolymer: Dual effects of heat and curing time. *Cement and Concrete Composites*, 86:1–8, 2018.

[116] Navid Ranjbar, Amin Kashefi, Guang Ye, and Mehdi Mehrali. Effects of heat and pressure on hot-pressed geopolymer. *Construction and Building Materials*, 231:117106, 2020.

[117] Navid Ranjbar, Mohammad Mehrali, Mahmoud R Maheri, and Mehdi Mehrali. Hot-pressed geopolymer. *Cement and Concrete Research*, 100:14–22, 2017.

[118] Marcello Romagnoli, Cristina Leonelli, Elie Kamse, and Magdalena Lassinantti Gualtieri. Rheology of geopolymer by doe approach. *Construction and Building Materials*, 36:251–258, 2012.

[119] Carlos A Rosas-Casarez, Susana P Arredondo-Rea, José M Gómez-Soberón, Jorge L Alamaral-Sánchez, Ramón Corral-Higuera, Manuel de Jesús Chinchillas-Chinchillas, and Octavio H Acuña-Agüero. Experimental study of xrd, ftir and tga techniques in geopolymeric materials. *Int. J. Adv. Comput. Sci. Appl*, 4(4):221–226, 2014.

[120] Pavel Rovnaník. Effect of curing temperature on the development of hard structure of metakaolin-based geopolymer. *Construction and building materials*, 24:1176–1183, 2010.

[121] Pavel Rovnaník, Pavla Rovnanikova, Martin Vyšvařil, Stefania Grzeszczyk, and Elżbieta Janowska-Renkas. Rheological properties and microstructure of binary waste red brick powder/metakaolin geopolymer. *Construction and Building Materials*, 188:924–933, 2018.

[122] Shengqian Ruan, Shikun Chen, Jiayu Lu, Qiang Zeng, Yi Liu, and Dongming Yan. Waterproof geopolymer composites modified by hydrophobic particles and polydimethylsiloxane. *Composites Part B: Engineering*, 237:109865, 2022.

[123] K Sagoe-Crentsil and L Weng. Dissolution processes, hydrolysis and condensation reactions during geopolymer synthesis: Part ii. high si/al ratio systems. *Journal of materials science*, 42:3007–3014, 2007.

[124] Arunkumar Samanta, An Zhao, George K. H. Shimizu, Partha Sarkar, and Rajender Gupta. Post-combustion co2 capture using solid sorbents: A review. *Industrial & Engineering Chemistry Research*, 51:1438–1463, 2011.

[125] Nur Sani, Zakaria Man, Rashid Shamsuddin, Azizli Khairun Azizi, and ku zilati ku shaari. Determination of excess sodium hydroxide in geopolymer by volumetric analysis. *Procedia Engineering*, 148:298–301, 12 2016.

[126] T Seiffarth, M Hohmann, K Posern, and Ch Kaps. Effect of thermal pre-treatment conditions of common clays on the performance of clay-based geopolymeric binders. *Applied Clay Science*, 73:35–41, 2013.

[127] Srinivasan Shanmugam. Granulation techniques and technologies: recent progresses. *BioImpacts: BI*, 5:55, 2015.

[128] L Simão, E Fernandes, D Hotza, M J Ribeiro, O R K Montedo, and F Raupp-Pereira. Controlling efflorescence in geopolymers: A new approach. *Case Studies in Construction Materials*, 15:e00740, 2021.

[129] Kenneth Sing. The use of nitrogen adsorption for the characterisation of porous materials. *Colloids and Surfaces A: Physicochemical and Engineering Aspects*, 187:3–9, 2001.

[130] Prune Steins, Arnaud Poulesquen, Fabien Frizon, Olivier Diat, Jacques Jestin, Jérémy Causse, David Lambertin, and Sylvie Rossignol. Effect of aging and alkali activator on the porous structure of a geopolymer. *Journal of Applied Crystallography*, 47:316–324, 2014.

[131] Y Suleiman, H Ibrahim, N V Anyakora, F Mohammed, A Abubakar, B O Aderemi, and P C Okonkwo. Design and fabrication of fluidized-bed reactor. *International Journal of Engineering and Computer Science*, 2:1595–1605, 2013.

[132] Jing Sun, Xiaohu Dai, Qilin Wang, Mark C M Van Loosdrecht, and Bing-Jie Ni. Microplastics in wastewater treatment plants: Detection, occurrence and removal. *Water research*, 152:21–37, 2019.

[133] Julia Talvitie, Anna Mikola, Arto Koistinen, and Outi Setälä. Solutions to microplastic pollution–removal of microplastics from wastewater effluent with advanced wastewater treatment technologies. *Water research*, 123:401–407, 2017.

[134] Yih Horng Tan, Jason A Davis, Kohki Fujikawa, N Vijaya Ganesh, Alexei V Demchenko, and Keith J Stine. Surface area and pore size characteristics of nanoporous gold subjected to thermal, mechanical, or surface modification studied using gas adsorption isotherms, cyclic voltammetry, thermogravimetric analysis, and scanning electron microscopy. *Journal of materials chemistry*, 22:6733–6745, 2012.

[135] E Teunou and D Poncelet. Batch and continuous fluid bed coating – review and state of the art. *Journal of Food Engineering*, 53:325–340, 2002.

[136] Ravindra N Thakur and Somnath Ghosh. Effect of mix composition on compressive strength and microstructure of fly ash based geopolymer composites. *ARPN J. Eng. Appl. Sci*, 4:68–74, 2009.

[137] Patthamaporn Timakul, Kanyarat Thanaphatwetphisit, and Pavadee Aungkavattana. Effect of silica to alumina ratio on the compressive strength of class c fly ash-based geopolymers. *Key engineering materials*, 659:80–84, 2015.

[138] Anish Mathai Varghese and Georgios N Karanikolos. Co2 capture adsorbents functionalized by amine – bearing polymers: A review. *International Journal of Greenhouse Gas Control*, 96:103005, 2020.

[139] N K Verma, M C Rao, and S Kumar. Effect of curing regime on compressive strength of geopolymer concrete. volume 982, page 012031. IOP Publishing, 2022.

[140] Prakash R Vora and Urmil V Dave. Parametric studies on compressive strength of geopolymer concrete. *Procedia Engineering*, 51:210–219, 2013.

[141] Cheng Wang, Shaozheng Leng, Huidong Guo, Liyun Cao, and Jianfeng Huang. Acid and alkali treatments for regulation of hydrophilicity/hydrophobicity of natural zeolite. *Applied Surface Science*, 478:319–326, 2019.

[142] Hongling Wang, Haihong Li, and Fengyuan Yan. Synthesis and mechanical properties of metakaolinite-based geopolymer. *Colloids and Surfaces A: Physicochemical and Engineering Aspects*, 268:1–6, 2005.

[143] Qiang Wang, Jizhong Luo, Ziyi Zhong, and Armando Borgna. Co2 capture by solid adsorbents and their applications: current status and new trends. *Energy & Environmental Science*, 4:42–55, 2011.

[144] E J Wellham, L Elber, and D S Yan. The role of carboxy methyl cellulose in the flotation of a nickel sulphide transition ore. *Minerals Engineering*, 5:381–395, 1992.

[145] L Weng, K Sagoe-Crentsil, and T Brown. Speciation and hydrolysis kinetics of aluminates in inorganic polymer systems. 2002.

[146] Luqian Weng and K Sagoe-Crentsil. Dissolution processes, hydrolysis and condensation reactions during geopolymer synthesis: Part i—low si/al ratio systems. *Journal of materials science*, 42:2997–3006, 2007.

[147] Paul S Wheatley, Pavla Chlubná-Eliášová, Heather Greer, Wuzong Zhou, Valerie R Seymour, Daniel M Dawson, Sharon E Ashbrook, Ana B Pinar, Lynne B McCusker, Maksym Opanasenko, Jiří Čejka, and Russell E Morris. Zeolites with continuously tuneable porosity. *Angewandte Chemie International Edition*, 53:13210–13214, 11 2014. https://doi.org/10.1002/anie.201407676.

[148] Ross P Williams and Arie Van Riessen. Determination of the reactive component of fly ashes for geopolymer production using xrf and xrd. *Fuel*, 89:3683–3692, 2010.

[149] Mengjie Wu, Wenchang Tang, Shaohua Wu, Hongyu Liu, and Chunping Yang. Fate and effects of microplastics in wastewater treatment processes. *Science of the Total Environment*, 757:143902, 2021.

[150] Yongni Wu, Mengfan Yu, Yanju Li, Yue Wu, Ziqiang Shao, and Yanhua Liu. Film properties, water retention, and growth promotion of derivative carboxymethyl cellulose materials from cotton straw. *Advances in Polymer Technology*, 2021:1–10, 2021.

[151] Xuelian Yu, Alexey Shavel, Xiaoqiang An, Zhishan Luo, Maria Ibáñez, and Andreu Cabot. Cu2znsns4-pt and cu2znsns4-au heterostructured nanoparticles for photocatalytic water splitting and pollutant degradation. *Journal of the American Chemical Society*, 136:9236–9239, 2014.

[152] Wei Zhang, Jiang shan Li, Xiao Huang, Zhen Chen, Lei Lang, and Kang Huang. Unraveling the cation adsorption of geopolymer binder: A molecular dynamics study. *Chemosphere*, page 139118, 2023.

[153] Zuhua Zhang, John Provis, Andrew Reid, and Hao Wang. Fly ash-based geopolymers: The relationship between composition, pore structure and efflorescence. *Cement and Concrete Research*, 64:30–41, 10 2014.

[154] Jing Zhong, Guo-Xiang Zhou, Pei-Gang He, Zhi-Hua Yang, and De-Chang Jia. 3d printing strong and conductive geo-polymer nanocomposite structures modified by graphene oxide. *Carbon*, 117:421–426, 2017.

[155] Shima Ziajahromi, Peta A Neale, Llew Rintoul, and Frederic D L Leusch. Wastewater treatment plants as a pathway for microplastics: development of a new approach to sample wastewater-based microplastics. *Water research*, 112:93–99, 2017.

[156] Andrea Zocca, Paolo Colombo, Cynthia M Gomes, and Jens Günster. Additive manufacturing of ceramics: issues, potentialities, and opportunities. *Journal of the American Ceramic Society*, 98:1983–2001, 2015.

[157] Vladimír Živica, Svetozar Balkovic, and Milan Drabik. Properties of metakaolin geopolymer hardened paste prepared by high-pressure compaction. *Construction and Building Materials*, 25:2206–2213, 2011.